Veronika Seidl, BSc.

Quality control and evaluation for atmospheric profiles from GNSS radio occultation reference processing

Master's Thesis
to achieve the university degree of
Diplom-Ingenieurin
Master's degree programme: Technical Physics

submitted to

Graz University of Technology

Supervisor
Univ.-Prof. Mag. Dr.rer.nat. Gottfried Kirchengast

Co-Supervisor
Dipl.-Ing. Dr.rer.nat. Veronika Proschek

Wegener Center for Climate and Global Change (WEGC) and Institute of Physics
University of Graz

Graz, December 2018

AFFIDAVIT

I declare that I have authored this thesis independently, that I have not used other than the declared sources/resources, and that I have explicitly indicated all material which has been quoted either literally or by content from the sources used. The text document uploaded to TUGRAZonline is identical to the present master‘s thesis.

Date

Signature

Abstract

In times of climate change it is more important than ever to observe essential climatological variables not only on Earth's surface but also in the free atmosphere. The usage of the Global Positioning System (GPS) to perform Radio Occultation (RO) measurements provides data of high accuracy, long-term stability and global coverage at altitudes over the Upper Troposphere–Lower Stratosphere (UTLS).
This thesis introduces an innovative Quality Control (QC) algorithm system that contributes to the new Reference Occultation Processing System (rOPS) of the Wegener Center for Climate and Global Change. The new QC validates the near-raw level RO excess phase data and has, on one hand, the power to reject measurements completely, if criteria of high importance are not fulfilled. On the other hand, informative QC flags are set when the data are not passing a certain check, or they are truncated at reliable top and bottom altitude levels. The basis of the QC system is the evaluation of the observed excess phase data against independent forward-model data.
A robust algorithm chain was found, which effectively quality-controls RO data sources, for multiple different RO satellite missions and all climate regions globally. The RO data are in general of high quality, since the rate of discarded measurements is commonly below 10 %, for the best-quality RO data (MetOp mission) even near zero.
Furthermore the disparities among climate regions are evident. By inspecting the process step-wise, it is clearly traceable how the controlled measurements rise in accuracy, by discarding bad-quality parts. The result is a set of data, which provides thermodynamic profiles of temperature, density and pressure of high quality for climate monitoring and research.

Zusammenfassung

In Zeiten des Klimawandels ist es wichtiger denn je, klimatologisch essentielle Variablen nicht nur auf der Erdoberfläche sondern auch in der freien Atmosphäre zu beobachten. Die Verwendung des Globalen Positioning System (GPS) zur Durchführung von Radio-Okkultationsmessungen (RO) liefert Daten von hoher Exaktheit, Langzeitstabilität und globaler Abdeckung in Höhen der oberen Troposphäre und unteren Stratosphäre (UTLS).
Diese Arbeit stellt ein innovatives Algorithmus-System zur Qualitätskontrolle (QC) vor, welches zu dem neuen Reference Occultation Processing System (rOPS) des Wegener Centers für Klima und globalen Wandel beiträgt. Die neue QC überprüft die RO Exzess-Phasen und hat zum einen die Fähigkeit Messungen völlig zu verwerfen, wenn Kriterien von höchster Wichtigkeit nicht erfüllt sind. Zum anderen werden informative QC Flags gesetzt, wenn Daten einen bestimmten Check nicht bestehen oder an zuverlässigen Höhenober- und Höhenuntergrenzen gekürzt werden. Die Basis des QC Systems ist die Bewertung der Exzess-Phasen Daten im Vergleich mit unabhängigen vorwärts-modellierten Daten.
Eine robuste Abfolge von Algorithmen wurde gefunden, welche die RO Datenquellen effektiv, für mehrere verschiedene RO Satellitenmissionen und alle Klimaregionen weltweit, auf ihre Qualität überprüft. Die RO Daten sind generell von hoher Qualität, da die Rate der verworfenen Messungen allgemein unter 10 % liegt. Für das Set von RO Daten mit der höchsten Qualität (MetOp Mission) belief sich die Rate sogar auf nahezu 0 %.
Weiters werden die Unterschiede zwischen den diversen Klimaregionen aufgezeigt. Bei schrittweisem Untersuchen des Prozesses ist eindeutig nachvollziehbar, dass die Zusammensetzung der Daten in ihrer Genauigkeit steigt, indem Teile der Messungen verworfen werden. Das Ergebnis ist ein Datenset, dass thermodynamische Profile von Temperatur, Dichte und Druck mit hoher Qualität für Klimamonitoring und -forschung liefert.

Acknowledgments

In the first place, I would like to express my sincere thanks to my supervisor Univ.-Prof. Mag. Dr.rer.nat. Gottfried Kirchengast for the opportunity to write my thesis at the Wegener Center for Climate and Global Change. His support, expert knowledge and valuable advice from the very beginning as well as during the work has been inestimable.
I am particularly grateful to my co-supervisor Dipl.-Ing. Dr.rer.nat. Veronika Proschek, who gave her assistance whenever needed, and irrespective of wether it was a question related to programming, theoretical nature, or just a trivial issue. Furthermore I would like to thank her for co-reviewing my thesis.
I would like to thank all members of the ARSCliSys research group as well as the Wegener Center administrative team for their assistance and great entertainment during lunch breaks. In general, the entire team of the Wegener Center provided an comfortable environment and served a productive place to work.
I would like to thank Anna Hadley for her longstanding friendship and for proof-reading my thesis.
Most of all, I would like to thank my family for their emotional support and inexhaustible patience especially during my studies but throughout my entire life. Thank you for encouraging me in all of my interest, no matter if academic or personal.
Last but not least I want to dedicate this thesis to Daniel, who always reassures me in times of stress and encourages me steadily to surpass myself.

Contents

1 Introduction

Today global climate change is a undeniable fact. Since the beginning of recording in 1880, the 2000s have been the decade with the highest mean surface temperatures and $C0_2$ concentrations (Trenberth and Fasullo 2013).
Climate change is mainly caused by the enormous rise of greenhouses gases in the Earth's atmosphere, due the industrial-,population- and economic growth. Certainly, natural factors, (e.q. solar cycles or volcanic activity), influence climate too, but it is most likely that more than the half of the increase of mean global surface temperature is due to anthropogenic influence. Furthermore it is strongly assumed that the consisting climate extrema (e.g. hot spells and heavy precipitations) and risks, that go along with, will intensify.
These statements and numerous other reasons express the importance of further research in long time observations, modelling and process studies of the future climate, to give Earth the opportunity to prepare for future climate changes and implement required policy measures to reduce the magnitudes (IPCC 2013).

With the implementation of Radio Occultation (RO) using the Global Navigation Satellite System (GNSS) it is possible to have a global observing system with high accuracy, high vertical resolution and a long-term stability of climate variables.
The Global Positioning System (GPS) RO technique provides profiles of refractivity, temperature, pressure and water vapor in the neutral atmosphere as well as electron density in the ionosphere. The measurements are performed when an electromagnetic signal, transmitted by a GPS satellite, travels through Earth's atmosphere and get tracked by an GPS receiver mounted on a Low Earth Orbit (LEO) satellite. Due to the relative motion of the satellites, the atmosphere can be scanned from top to bottom (setting event) or bottom to top (rising event). The waves, when travelling through the atmosphere, obtain a phase delay by refractive bending and slowing of the signal. Depending on it's refractive properties, arises a specific bending angle which leads to the atmospheric parameters (Kuo et al. 2004; Hajj et al. 2002; Kursinski et al. 1997; Melbourne et al. 1994).
RO data have a very high accuracy (e.g. temperature deviations $<1\,\mathrm{K}$) and a high spartial resolution (0.1 km near the surface and 1 km in the stratosphere) (Anthes 2011). According to that, it is important to secure that the raw measurement data fulfill these high standards to derive thermodynamic profiles with a sufficient high quality along the used data length.
In this master thesis, a careful evaluation of the raw measurement data (phase delay) will be done, leading to a Quality Control (QC) at the very beginning of the algorithm chain of the Wegener Center for Climate and Global Change (WEGC)

Reference Occultation Processing System (rOPS) (Kirchengast et al. 2017).
Chapter 2 provides a short introduction into the theoretical background of the RO measurement as well as an overview of the rOPS, where the QC is embedded, and the examined data sets.
In Chapter 3 the general structure and detail procedure of the QC is introduced. The main steps with their certain limitations are explained, as well as the evaluated results for the several boundaries. In addition, the analysis of the data sets will be shown.
The results of the different tasks are presented in Chapter 4, revealing deviations between the various satellite missions and climate regions. The conclusion presents a summary of the defined boundary limits and an outlook for further studies.

2 Background

2.1 Principle of Radio Occultation Measurements

The origin of RO lies in the early 1960's, where a group of scientists from Stanford University and Jet Propulsion Labratory (JPL) used radio connection between earth and the spacecrafts Mariner 3 and 4 to explore the atmosphere of Mars (Yunck et al. (2000)). In 1995 an experiment called GPS/MET (Global Positioning System/Meteorology) launched supplied the evidence, that with RO by using GPS satellite and a LEO satellite carrying a GPS receiver, it is possible to have global soundings of Earth atmosphere with high quality (Ware et al. (1996)).
The RO method is a remote and active limb sounding technique, where artificial radio waves, transmitted by GNSS satellites, penetrate the earth's atmosphere and due to its density field get refracted. Each of the 24 consisting GPS satellites constantly transmit two right-handed polarized signals at the frequencies: f_1= 1575.42 MHZ and f_2= 1227.60 MHZ, which equates wavelenghts of λ_1= 0.190 m and λ_2= 0.244 m. The two signals are also called L1- and L2-signal, because their frequencies correspond to the L-band frequency domain between 1 and 2 GHz (Pirscher 2010). The satellites orbiting on six different planes in a distance of about 20200 km away from Earth's surface. An occultation event occurs, whenever a LEO satellite (distance to Earth's surface about 500-2000 km (Syndergaard 1999)) receives a ray path that passes through Earth's atmosphere. Figure 2.1 illustrates the geometrical optic approximation thereto.

According to Snell's law, the signal received at LEO satellite has been bent with a bending angle (α) due to the vertical gradient of density and hence it's changing refractive index. This atmosphere characterizing bending angle can not be measured directly, but derived by applying an inversion technique.

The measured observable is the difference in phase delay, the so-called excess phase, between initially transmitted signal and the refracted and bent incoming signal as a function of time (Rocken et al. 1997). Assuming that the signal would travel through vacuum only, the phase delay only depends on the relative velocities of the satellites (Doppler Shift). By passing through atmosphere an additional term, the excess phase, due to vertical density gradient arise (more precise description of excess phase, follows in subsequent Section 2.2).
Because of the relative motions of GPS and LEO satellite the radio rays pass the atmosphere at diverse tangent heights which result in a near vertical profile of phase and amplitude measurements as a function of time.
With the Doppler shift profiles and the occcultation geometry (space- and velocity-vectors of the LEO and GPS satellites) the bending angle profiles ($\alpha(a)$) as a

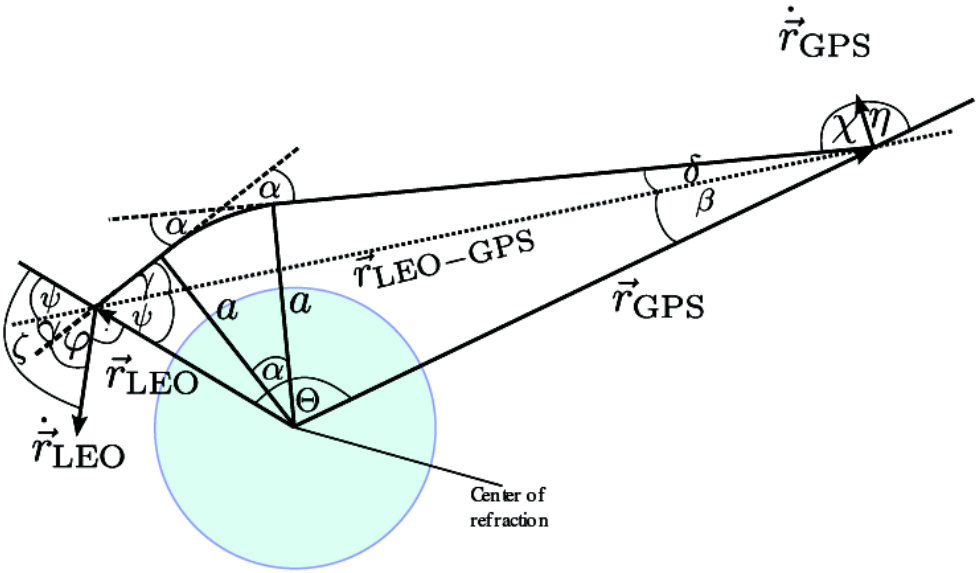

Figure 2.1: Geometrical approximation of a setting RO occultation event. The GPS satellite, travelling with a velocity $\dot{\vec{r}}_{\mathrm{GPS}}$ transmits a signal, which is refracted by the neutral atmosphere and the ionosphere before it gets received by LEO satellite (orbiting with a velocity $\dot{\vec{r}}_{\mathrm{LEO}}$. The dotted line $\vec{r}_{\mathrm{LEO-GPS}}$ is vacuum path between LEO and GPS satellite, a the impact parameter (the perpendicular distance between either of the ray asymptotes and the center of refraction), α the bending angle, $\vec{r}_{\mathrm{GPS}}$ and $\vec{r}_{\mathrm{LEO}}$ the position vectors of the GPS and the LEO satellite,as well as several other angles, that are needed to calculate the bending angle α (respectively after Pirscher (2010)).

function of impact paramater (a) (representing the perpendicular distance between ray path and center of refraction) can be derived. It can be calculated as following:

$$a = |\vec{r}_{\mathrm{LEO}}| \sin(\gamma + \psi) = |\vec{r}_{\mathrm{GPS}}| \sin(\delta + \beta) \tag{2.1}$$

with $\vec{r}_{\mathrm{LEO}}$ and $\vec{r}_{\mathrm{GPS}}$ are the position vectors of LEO and GPS satellite and the paired angles give the total angle between those position vectors and the ray directions (see Figure 2.1).
Hence the angles φ and χ can be derived with (Pirscher 2010; Syndergaard 1999):

$$\varphi(a) = \zeta - \arcsin\left(\frac{a}{|\vec{r}_{\mathrm{LEO}}|}\right) \tag{2.2}$$

$$\chi(a) = (\pi - \eta) - \arcsin\left(\frac{a}{|\vec{r}_{\mathrm{GPS}}|}\right) \tag{2.3}$$

The bending angle $\alpha(a)$ is then given by:

$$\alpha(a) = \Theta - \arccos\left(\frac{a}{|\vec{r}_{\mathrm{LEO}}|}\right) - \arccos\left(\frac{a}{|\vec{r}_{\mathrm{GPS}}|}\right) \tag{2.4}$$

Subsequently an inversion of the Abel integral of the bending angle profile leads to a refractive index profile as a function of impact altitude (Steiner 1998):

$$n(a_i) = \exp\left[-\frac{1}{\pi}\int_{a_i}^{\infty}\frac{\alpha(a)}{\sqrt{a^2 - a_t^2}}\mathrm{d}a\right] \tag{2.5}$$

with $a_i = n(a_i) \cdot r_i$ is the impact parameter for a specific ray and $r_i = r_t$ is the radius of the corresponding tangent point. Then the atmospheric refractivity (N) is defined by:

$$N(h) = (n(h) - 1) \cdot 10^6 \tag{2.6}$$

with

$$h = \frac{a}{n(a)} - r_\mathrm{c} \tag{2.7}$$

where h is the height above the Earth's ellipsoid and r_c is the radius of the ellipsoidal Earth at the location of the occultation event (Kirchengast et al. 2017). The refractivity (N) of the waves get mainly affected by the dry neutral atmosphere, moist atmosphere and free electrons in the ionosphere, which can be expressed in first order by Kursinski et al. (1997):

$$N(h) = 77.6\frac{p(h)}{T(h)} + 3.73 \cdot 10^5\frac{p_w(h)}{T(h)^2} + 4.03 \cdot 10^7\frac{n_e(h)}{f^2} + 1.4W(h) \tag{2.8}$$

where p is the atmospheric pressure in hPa, T is the atmospheric temperature in K, p_w is the partial water vapor pressure in hPa, and n_e is the electron density in m^{-3}, f the transmitter frequency in Hz and W is the mass density of condensed water in the atmosphere in $\mathrm{g/m}^3$.
Based on Equation 2.8 and the assumption of 'dry temperature', profiles of dry density, dry pressure and dry temperature can be derived as a function of height.

2.2 GPS Signal Structure and Determination of the Excess Phase

In the following section the construction of the transmitted electromagnetic waves of the Global Positioning System (GPS) satellites as well as the investigation of the excess phase is explained in detail, since the thesis is entirely based on this key variable. The subsequent description is deduced from Dixon (1991) and Pirscher (2010).
The two transmitted GPS Signals L1 and L2 are modulated by two Pseudo-Random Noise (PRN) codes, which make it possible to uniquely identify each of the 24 GPS satellites. Both signals are modulated by the Precision (P) code. On the L1-signal a lower frequency Coarse/Acquisition (C/A) code is additionally modulated with a phase shift of 90°. By modulating the signals with a low bit rate data stream

(50 Hz), the signals carry navigation and transmitter clock information (Steiner et al. 2011). The signals have the following structure:

$$S_{\mathrm{L1}} = A_{\mathrm{P}} P(t) D(t) \cos(\omega_1 t) + A_{\mathrm{C}} C(t) D(t) \sin(\omega_1 t) \tag{2.9}$$

$$S_{\mathrm{L2}} = A_{\mathrm{P}} P(t) D(t) \cos(\omega_2 t) \tag{2.10}$$

where A_{P} and A_{C} are the amplitudes and $P(t)$ and $C(t)$ the sequences of the P-code and C/A-code. $D(t)$ labels the sequence of the modulation that contains the navigation information.

Excess Phase

In principle, the RO acgps measurement is based on obtaining the distance between the transmitter and the receiver. This difference is referred as phase pseudorange, due to the different system times of the receiver and the transmitter. In addition to this, there is also a code pseudorange, which determines the time delay between transmission and the reception of the signal. To derive those pseudoranges, it is necessary to measure the time or phase delay, relative to transmitted GPS signal, which are majorly caused by the relative motion of GPS and LEO satellite (kinematic Doppler shift), as well as the influence of the signal transmitting media (Earth's atmosphere). For RO measurements the determination of phase difference (phase pseudorange) is used, because the evaluation is more precise than the time delay.

The GPS receiver on the LEO satellite is able to replicate the PRN-code of a satellite signal. By comparing the received GPS signal with the self-generated signal from the receiver, a phase delay $\Delta\phi$ (in cycles) proportional to the range difference $\Delta\rho$ (in m) is measurable:

$$-\Delta\phi = -\int_{t_0}^{t'} \Delta f \mathrm{d}t = \frac{1}{\lambda} \int_{t_0}^{t'} \dot{\rho} \mathrm{d}t = \frac{1}{\lambda} \Delta\rho \tag{2.11}$$

with the Doppler shift $\Delta f = -\frac{\dot{\rho}}{\lambda}$ (in Hz), the differentiated range $\dot{\rho}$ (in $\frac{\mathrm{m}}{\mathrm{s}}$) and the signal's wavelength $\lambda = c/f$ (in m). With the initial time t_0 and time t', the start of transmitting an the reception of the signal are defined. The phase pseudorange Φ is then expressed as following:

$$\Phi = -\Delta\phi_{\mathrm{LEO}}^{\mathrm{GPS}} = \frac{1}{\lambda}\rho + \frac{c}{\lambda}\delta_{\mathrm{LEO}} + + \frac{c}{\lambda}\delta_{\mathrm{GPS}} + N \tag{2.12}$$

with $-\Delta\phi_{\mathrm{LEO}}^{\mathrm{GPS}}$ is the phase difference between generated and received signal, ρ is the distance between GPS at initial time t_0 and LEO satellite at time $t' = t_0 + \delta t$, c is the speed of light in vaccum, δ_{LEO} and δ_{GPS} are the differences from receiver and transmitter clocks to a known time system, and N is the number of cycles between transmitter and receiver at the beginning.

By multiplying the Equation 2.12 with the wavelength λ leads to the range L (in m), which is later referred as excess phase:

$$L = \lambda\Phi = \rho + c\delta_{\mathrm{LEO}} + c\delta_{\mathrm{GPS}} + \lambda N \tag{2.13}$$

The here introduced phase delay (L) is mainly influenced by the relative motion of transmitter and receiver, the neutral atmosphere induced Doppler shift (which is for RO measurement the main interest), the ionosphere induced Doppler shift and other error sources (satellite-related, propagation-medium-related and receiver-related) affecting the phase delay. For a detailed discussion of the range errors see Hofmann-Wellenhof et al. (2008).

Ionosphere Corrected Excess Phase

As mentioned above, the phase delay contains a Doppler shift term, due to the propagation through the ionosphere. When the solar ultraviolet radiation propagates through the atmosphere, the radiation gets absorbed by gaseous molecules in the atmosphere, which causes the emission of outer shell electrons. These free electrons highly interact with the transmitted radio-waves from the GPS satellite by negative refraction of the signal.
As the focus of interest lies only on the impact of neutral atmosphere, it is necessary to correct or reduce the ionospheric influence. Ignoring third- and higher order therms, the ionospheric group delay can be corrected by a linear combination of the excess phases L1 and L2 as a function of time (Blewitt 1989), leading to the ionosphere corrected excess phase:

$$L_{\mathrm{c}}(t) = \frac{f_1^2 L_1(t) - f_2^2 L_2(t)}{f_1^2 - f_2^2} \tag{2.14}$$

with f_1 is the carrier frequency and L_1 the excess phase of Signal S_{L1}, f_2 is the carrier frequencyand L_2 the excess phase of Signal S_{L2}. The underlying assumption is that the two signals travel along identical ray paths, which is not exact due to the dispersive nature of the ionosphere (Syndergaard 2000).

2.3 The Reference Occultation Processing System

Following section briefly introduces the main components of the new RO measurement retrieval at the WEGC, the Reference Occultation Processing System (rOPS), that uses raw RO measurement data of phase delay profiles and precise orbit information to derive phase delay and atmospheric parameters i.e. refractivity, (dry-)temperature, (dry-)pressure, water vapor and electron density of the ionosphere. The renewals when compared to the older version are the baseband approach (explained later in detail), an even more accurate retrieval with residual relative numerical uncertainties below 10^{-4} and the integration of a complete uncertainty propagation chain from the fundamental-time uncertainty and relevant

side influences from the raw RO data and high-accuracy GNSS orbit data through four processors to the atmospheric variables (Gorbunov and Kirchengast 2015; Schwarz et al. 2018; Gorbunov and Kirchengast 2018; Innerkofler et al. 2018). Figure 2.2 gives an insight in the complex structure of the rOPS, with it's three main components, the Daily System Modeling (DSM), the Event System Modeling (ESM) and the Occultation Data Processing (ODP).

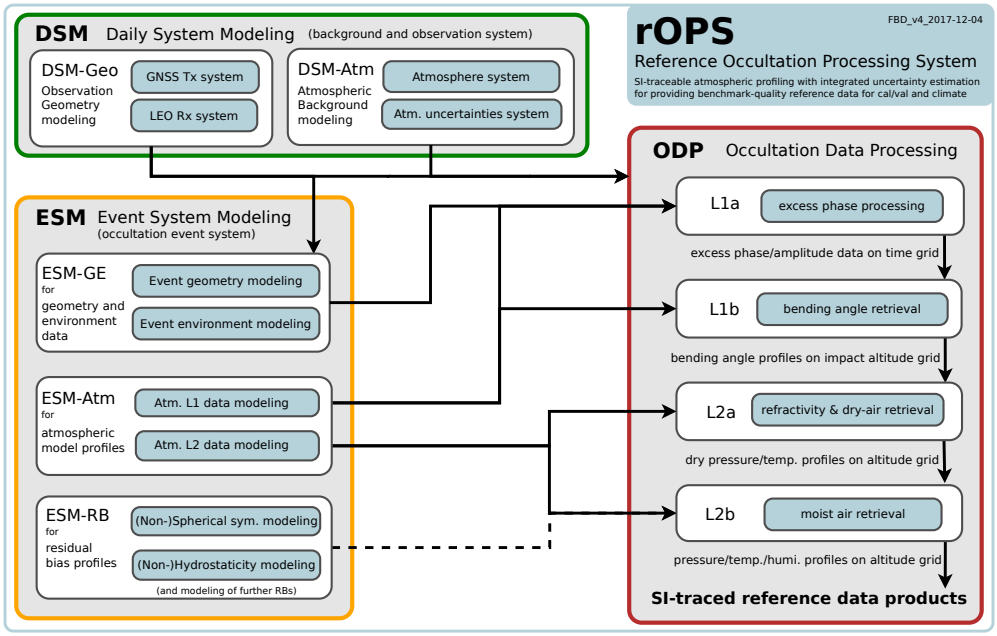

Figure 2.2: Overview of the rOPS, illustrating the design and flow of the system modeling and data analysis approach, indicating its main systems and subsystems as well as its core, the occultation data processing system (taken from Kirchengast et al. (2017)).

The core of the rOPS is the ODP, which is divided in four processors:

- Level 1a (L1a) processor
- Level 1b (L1b) processor
- Level 2b (L2b) processor
- Level 2a (L2a) processor

The initial step at the ODP of the rOPS retrieval starts with raw orbit and occultation data (termed as Level 0 (L0) data), to derive excess phase profiles (L1a data) of the two GNSS transmitted signals.
The profiles are provided on a time grid with a sampling rate of 50 Hz. Prospectively these L1a data will be evaluated via the quality control (QC), that is introduced in this thesis, in order to further improve the quality of the final thermodynamic

profiles.
In the L1b processor, the excess phase profiles are further processed to obtain the Doppler shift and furthermore the Geometric Optic (GO) and Wave Optic (WO) bending angle profiles, which will be assembled afterwards. The combination of the two bending angle profiles (from L1- and L2-signal) serves the correction of ionospheric effects, which leads to the neutral bending angle profile as a function of impact altitude.
The L2a processor integrates the neutral atmosphere bending angle profiles which are dynamically statistically optimized via the Abel transform, to obtain the refractivity profiles. This yields to the determination of the dry pressure, by assuming a hydrostatic pressure integral, and dry temperature profiles, both relative to a Mean Sea Level (MSL) altitude grid.
Finally, the L2b processor performs a moist air retrieval, by combining the derived dry air parameters with background information to temperature and humidity. For detailed informations see Kirchengast et al. (2017).

2.4 Input Data Sets

All RO excess phase data used in this thesis are provided by University Corporation for Atmospheric Research (UCAR). The collocated background excess phase profile are provided by a forward simulation of European Centre for Medium-Range Weather Forecasts (ECMWF) forcast T42 fields with the experimental rOPS system.
The L1a processed dataset is from the specific test day 15 July 2008, and contains measurements from four different LEO satellites receiver missions:

- CHAllenging Mini- Satellite Payload (CHAMP)
- Constellation Observing System for Meteorology, Ionosphere, and Climate (FORMOSAT-3/COSMIC)
- Meteorological Operational Satellite (MetOp)
- Gravity Recovery And Climate Experiment (GRACE)

Table 2.1 lists the missions, including their date of launch, as well as the status of the mission, and the name of the satellite, whose data contributed to the evaluation.

Table 2.1: List of RO satellite missions from where RO data are used for this thesis

Mission	Launch	Status (October 2018)	Receiver satellite	No. of used L1a profiles
CHAMP	July 2000	decomissioned	CHAMP	77
FORMOSAT-3/ COSMIC	April 2006	active	FM-1	169
MetOp	October 2006	active	METOP-A	577
GRACE	March 2002	decomissioned	GRACE-A	124

3 Method

This chapter provides a detailed description of the Quality Control (QC), that follows to the L1a process, where raw measurement data yield to the derivation of the raw excess phase profiles. The new QC validates the very untreated signals and has on the one side the power to reject excess phase profiles completely, if a criteria of high importance is not fulfilled or the data length is not sufficiently long enough to get further processed.
On the other side, bad QC flags are set at profile's area, where the data are not passing a certain check and then truncated, by defining new top and bottom levels. The following Figures 3.1 and 3.2 should give a shematic overview, by introducing the main components of the QC (the corresponding explanations of used abbreviations can be find in Table 3.1).
The initial step (purple box in Figure 3.1) is providing and a rough physical bound check of of L1a processed data. Additional steps needed to be done for University Corporation for Atmospheric Research (UCAR) processed data. Afterwards an outlier detection and correction is performed (red box in Figure 3.1), to neglect and replace the values with strong deviation. Subsequently the ionosphere corrected excess phase (excess phase Lc) can be derived.
The third part (yellow box in Figure 3.1) has the assignment to crop the profiles, by assigning new top and bottom levels.
Subsequently the actual quality check, which insist of two parts, bounds and smoothness check, is done (top green box in Figure 3.2).
Both of these checks are performed on the previously determined ionosphere corrected excess phase (excess phase Lc), and are able to update the top and bottom levels of the excess phases. Since the signal-to-noise ratio is in general higher for L2-signal, the updated levels from Lc in the quality checks get directly adopted for L2.
The excess phase (ex.phase) L1 runs through a separate process to check and set the bottom level independently (bottom box in Figure 3.2).

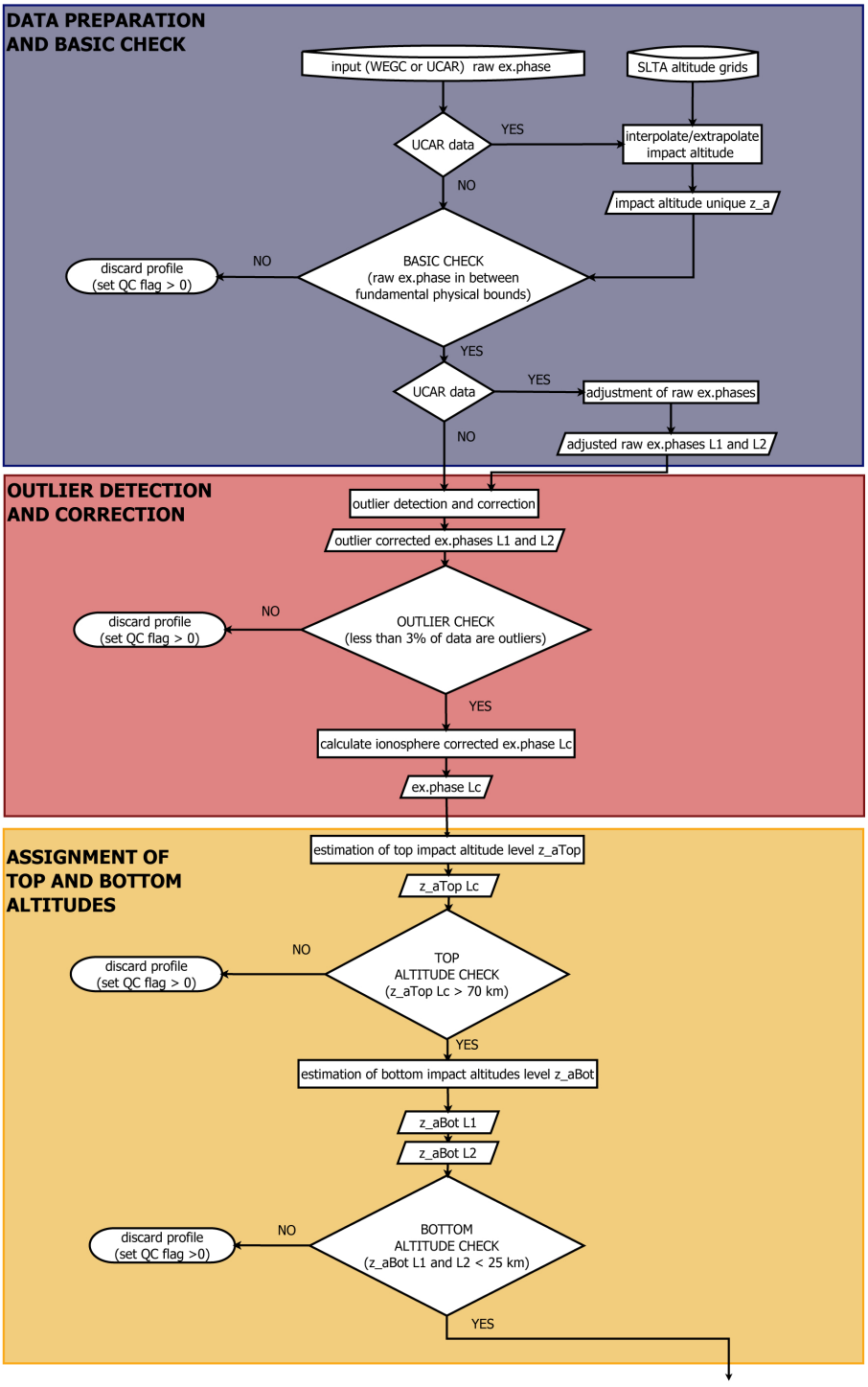

Figure 3.1: Schematic workflow of the QC (Tasks 1-3), list of used abbreviations can be seen at table 3.1

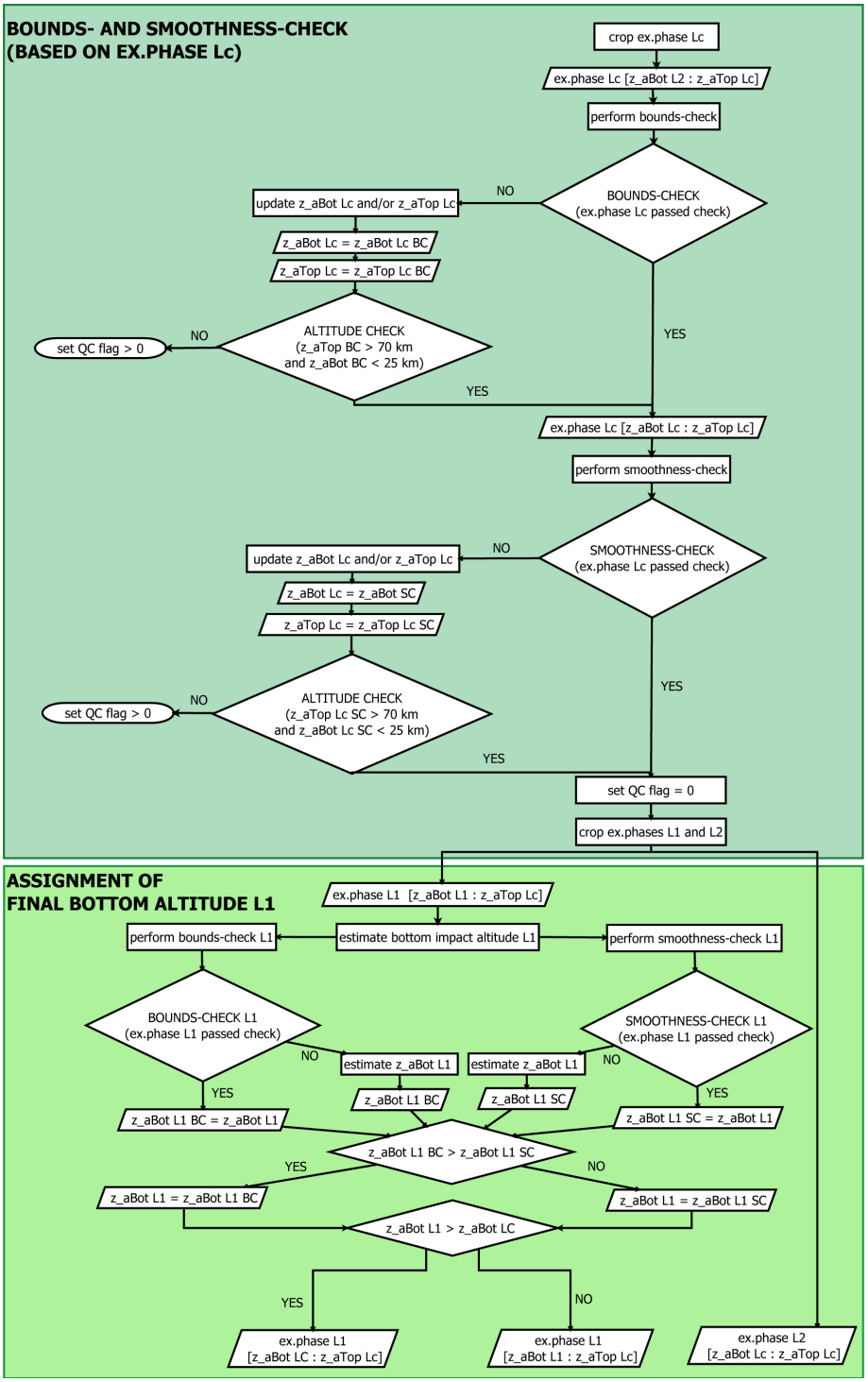

Figure 3.2: Schematic workflow of the QC (Tasks 4-5), list of used abbreviations can be seen at table 3.1

The aim of the QC after the L1a processor is to ensure, to have continuous excess phase profiles with a quality, that is accurate enough to get further processed, by removing (or at least flagging) parts which are not sufficient accurate or have a nonphysical behavior, to achieve in the end of the Reference Occultation Processing System (rOPS) thermodynamic profiles with high precision.

Table 3.1: Overview of used variables and related Symbols

Variable Name	Symbol	Symbol (Flowchart)
ex.phase of signal L1	L1	ex.phase L1
ex.phase of signal L2	L2	ex.phase L2
ionosphere corrected ex.phase	Lc	ex.phase Lc
impact altitude	z_a	z_a
top impact altitude level for ex.phase L1	$z_{a\mathrm{Top}}^{\mathrm{L1}}$	z_aTop L1
top impact altitude level for ex.phase L2	$z_{a\mathrm{Top}}^{\mathrm{L2}}$	z_aTop L2
top impact altitude level for ex.phase Lc	$z_{a\mathrm{Top}}^{\mathrm{Lc}}$	z_aTop Lc
bottom impact altitude level for ex.phase L1	$z_{a\mathrm{Bot}}^{\mathrm{L1}}$	z_aBot L1
bottom impact altitude level for ex.phase L2	$z_{a\mathrm{Bot}}^{\mathrm{L2}}$	z_aBot L2
bottom impact altitude level for ex.phase Lc	$z_{a\mathrm{Bot}}^{\mathrm{Lc}}$	z_aBot Lc
bounds check	BC	BC
smoothness check	SC	SC

3.1 Key Variables

The Quality Control (QC) is completely based on the raw ex.phases L1 and L2 and their derived components. Furthermore an approximated information of the impact altitude along the profile and a forward (background) model excess profile are needed, to relate the profiles with each other.

3.1.1 Excess Phase

The excess phase describes the difference in phase delay between the two initially transmitted radio signals and the refracted and bent incoming signal as a function of time.
The GNSS RO measurements provide data from an altitude of about 120 km (Lower Thermosphere) down to the Earth's surface (Troposphere). In the highest impact altitudes, the excess phase profiles have small values in the range of several centimeters; but when reaching the lower Stratosphere and Troposphere, the excess phase can achieve values up to kilometer range.
The magnitude of excess phase not only changes with impact altitude, but also when comparing occultation events at different latitudes. For example implies a region with high temperatures or humidity a greater excess phase than in ones

where temperature is low and air is dry. Therefore, the excess phase are divided in various climate regions for the analysis:

Table 3.2: Classification of climate regions, depending on latitude (for July)

Climate Region	Latitude Range [°]
Global atmosphere	[90,90]
Sub-arctic summer	[55,90]
Mid-latitude summer	[20,55]
Tropical	[-20,20]
Mid-latitude winter	[-55,-20]
Sub-arctic winter	[-90,-55]

Due to the distinct wavelengths and the different modulation of the two signals S_{L1} and S_{L2} (explained in Section 2.2), the excess phase L2 is of minor quality compared with excess phase L1. Particularly in lower impact altitudes the increase of excess phase L2's noise is in general very significant.
This matter of fact is of secondary priority by now, since the two excess phases get treated separately, but later in the rOPS bending angle retrieval, the angles of both signals get linear combined to correct the ionosphere influence.
To sustain high quality and ionospheric correction in lower heights too, the excess phase L2 will be extrapolated from a specific point (i.e. in QC determined bottom level) to the lower lying bottom level of L1.

3.1.2 Ionosphere Corrected Excess Phase

The linear combination of the excess phase L1 and L2 is an effortless way to correct the ionospheric influence in first order (see Section 2.2 Equation 2.14).
By using data at daytime and during the maximum of the solar cycle, the ionospheric effect becomes important above 30 km (Kursinski et al. 1997). As it can be seen in the bottom panel of Figure 3.3, the offset to the forward-modeled excess phase (excess phase Lm) almost vanishes for the excess phase Lc.

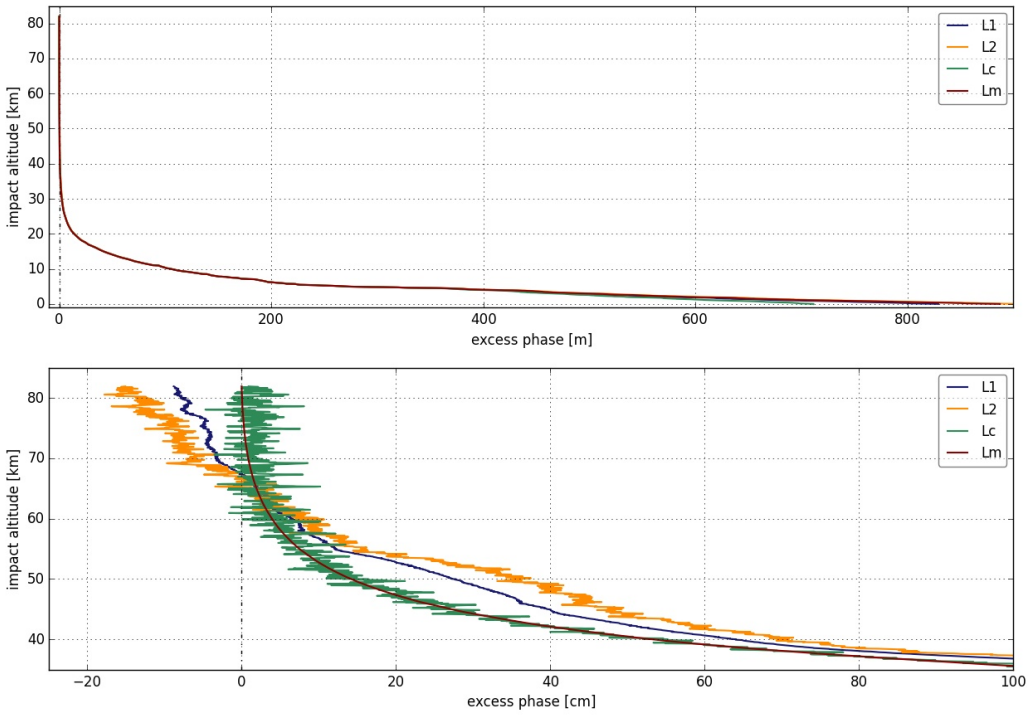

Figure 3.3: Illustration of the difference between the excess phases L1, L2, Lc and the excess phase Lm . The top panel maps the profiles in the total range, the bottom panel illustrates, the difference of the phases by zooming in higher impact altitudes. (CHAMP-RO event, 15 July 2008, 00:28:50 UTC)

3.1.3 Baseband Excess Phase

Processing data on delta-profiles, the so-called 'baseband approach' is one of the most important renewals in the rOPS. By subtracting a zero order profile (excess phase) from a excess phase Lm, the dynamic range of these delta-profiles (BB excess phase profiles) is reduced, as well as the bias (left panel in Figure 3.4). This leads to simplified operators and a decrease in residual numerical errors. (Kirchengast et al. 2016a). The baseband excess phase (BB excess phase) is defined after Kirchengast et al. (2016b) as:

$$\delta L_{\mathrm{om}} = L_{\mathrm{o}} - L_{\mathrm{m}} \tag{3.1}$$

with L_{o} is the observed excess phase, L_{m} is the excess phase Lm and δL_{om} is the resulting BB excess phase.

3.1.4 Lowpass-filtered Baseband Excess Phase

For further calculations a signal with suppressed high-frequency noise is needed. Therefore, proceeding from the BB excess phase, a Blackman-Windowed-Sinc

(BWS) lowpass-filter $\mathbf{F}^{\mathrm{BWS}}$ with a cutoff frequency f_c at 0.5 Hz is applied.
The relative cutoff frequency $f_\mathrm{r} = f_\mathrm{c}/f_\mathrm{s}$ is consequential 0.01 (for a sampling rate of f_s= 50 Hz) and the Blackman window size M is set to $M = 2 \cdot f_\mathrm{s}/f_\mathrm{c} + 1 = 201$ data points, which correspond to a effective window size of 101 datapoints or 2 s (or in high altitudes a length of 5 km).
After setting the cutoff frequency and the window size, the weights w_m (with $0 \leq m \leq M$) for $\mathbf{F}^{\mathrm{BWS}}$ are calcuated as follows (with a special value at $m = M/2$, not separately shown):

$$w_m = \mathrm{K}\frac{\sin(2\pi) \cdot f_\mathrm{r}(m - M/2)}{m - M/2}\left[0.42 - 0.5\cos\left(2\pi\frac{m}{M}\right) + 0.08\cos\left(\pi\frac{m}{M}\right)\right] \quad (3.2)$$

with the normalization $\mathrm{K} = 1/\sum w_m$ to provide unity gain, the sinc function, supplying a 'perfect' lowpass-filter and the Blackman window (Smith 1999).
The BWS filter obtains a better smoothing effect, by keeping a higher resolution when i.e. compared to a simple moving average Boxcar filter (Schwarz et al. 2018).
The lowpass-filtered baseband excess phase (LFBB excess phase) δL_{Fom} (middle panel in Figure 3.4) is then defined as follows:

$$\delta L_{\mathrm{Fom}} = \mathbf{F}^{\mathrm{BWS}}\delta L_{\mathrm{om}} \quad (3.3)$$

where δL_{om} is the baseband excess phase of the observed excess phase L_o.

3.1.5 Highpass-filtered Baseband Excess Phase

The highpass-filtered baseband excess phase (HFBB excess phase) is commonly known as double-delta profile. Here the BB excess phase (a single-delta profile) is subtracted from the BWS filtered LFBB excess phase:

$$\delta L_{\mathrm{oHF}} = L_{\mathrm{om}} - L_{\mathrm{Fom}} \quad (3.4)$$

with L_{oHF} is the HFBB excess phase, L_{om} is the BB excess phase, L_{Fom} is the LFBB excess phase of the observed excess phase L_o.
The result is a sort of noise level profile, since the low-frequency parts are canceled out by subtracting the BB excess phase from the LFBB excess phase. The big advantages of this output are, that the data is unbiased until lowest altitudes and the focus is only on the noise ratio, which lighten the detection of an arise of it.
In Figure 3.4 the discussed signals are shown. The BB excess phase in the left panel is thoroughly unbiased except for the part below 20 km. The LFBB excess phase in the middle panel exhibits a copy of BB excess phase without noise and smaller variations and represents the large scale effects of the atmosphere. The HFBB excess phase instead is total unbiased and contains almost only information about the noise level.

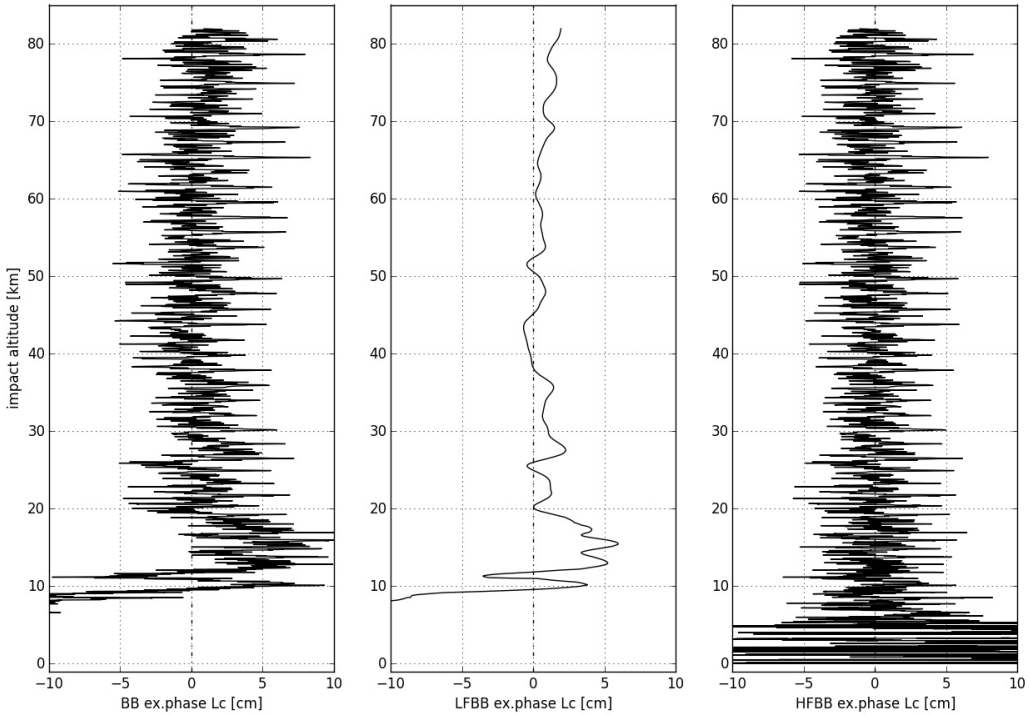

Figure 3.4: Illustration of the BB excess phase (left panel), the LFBB excess phase (middle panel) and the HFBB excess phase (right panel). (CHAMP-RO event, 15 July 2008, 00:28:50 UTC)

3.2 Border Handling

The QC strongly depends on filter applications, such as runnning median or running standard deviation. The formulas for deriving the moving mean $\bar{x}_i$, moving standard deviation (stdev) σ_i and moving percentile p_{j,x_i} are as follows:

$$\bar{x}_i = \frac{1}{M} \sum_{n=i-M/2}^{i+M/2} x_n \tag{3.5}$$

$$\sigma_i = + \sqrt{\frac{1}{M} \sum_{n=i-M/2}^{i+M/2} (x_n - \bar{x}_i)^2} \tag{3.6}$$

$$p_{j,x_i} = x_{\uparrow} (n = m) \tag{3.7}$$

with M is the window size. The j-th percentile of data point x_i is p_{j,x_i} and $x_{\uparrow}(n)$ is a list of ascending values of $x(n)$, where $n \in [i - M/2, i + M/2]$ and $m = \frac{j}{100} \cdot M$. Corresponding to these formulas, the data points, where $i \in \{< M/2, > N - M/2\}$, with N is the total amount of data points, do not have enough data points on one side to derive a symmetrical median.
It would be possible to decrease the window size when reaching endpoints of the data, but this potentially can cause unwanted biases. Therefore, depending on the certain type of profile (e.g. single- or double-delta profile), different border handlings are used to ensure useful data at data's edges. By artificially continuing the signal at the beginning and end for $M/2$ data points, the issue is attempt to be circumvented. Following border handles are used:

- **Nearest**
  Extending the signal by replicating the value which is nearest to the edge for all added values
  (Example: 1111|12345|5555)

- **Constant**
  Not extending the signal and setting the border determined values to a constant value (k)
  (Example: kkkk|12345|kkkk)

- **Mirror**
  Extending the signal by mirroring the $M/2$ input next to nearest data point to the edge for all
  (Example: 5432|12345|4321)

- **Extrapolation** Extending the signal by extrapolating the signal via a spline function
  (Example: -3-2-10|12345|6789)

Depending on certain input, different methods are used:

BB excess phase

- Outlier detection and correction:
  For the derivation of the boundary of outlier detectio the moving percentile is needed. To correct the detected outliers, the usage of the moving stdev is necessary.
  Therefore, the first and last $M/2$ values of the running calculations of BB excess phases L1 and L2 are set to a constant value, which is the percentile of these $M/2$ values.

- Calculation of moving standard deviation:
  In this case, the BB excess phase will be extended on both edges. After correcting outliers, the BB excess phase consist almost entirely of unbiased random noise in the highest altitudes. Hence, the BB excess phase is extended in highest ranges by mirroring.
  At impact altitudes close to bottom, the values of the BB excess phases arises approximately linear, leading to an extrapolation of the signal by a linear spline function.

- Calculation of LFBB excess phase:
  The applied BWS filter on BB excess phase, takes for data point x_i instead of the $n = i \pm M/2$ elements, the following $n = i + M$ elements. Therefore, the top of the profile has not to be extended. The bottom values, will be extrapolated by a linear spline function.

HFBB excess phase

- Calculation of moving standard deviation:
  In contrast to BB excess phase, both borders will be treated equal. Consindering that, HFBB excess phases represent in general the noise of the excess phase, that is random distributed, leads to a mirroring border handling.

3.2.1 Window Size

The in the outlier detection and correction (see Section 3.4) defined window size $M = 101$ data points is adopted for all other filter applications.

3.3 System Setup and Fundamental Plausibility Check

The here introduced QC evaluates the quality of the output of Level 1a processor (raw excess phase profiles). Possible sources are rOPS processed L1a data from WEGC itself or provided by other data centers. For this thesis, the entire used data were preprocessed by UCAR.
As an initial task, a rough check is performed, to proof the physical plausibility of the data:
The near-raw excess phase L1 and L2 need to be within the specific range:

$$(L_\mathrm{m} - 50\,\mathrm{m}) \leq L'_\mathrm{o} \leq (L_\mathrm{m} + 50\,\mathrm{m}) \tag{3.8}$$

with L_m is the excess phase Lm, L'_o and $\mathrm{o} = \{1, 2\}$ representing raw excess phase L1 and L2.
For UCAR preprocessed profiles a range of $L_\mathrm{m} \pm 500\,\mathrm{m}$ is chosen, due to the profiles' offset (see further information below). If some profile does not full fill this criteria, $\mathrm{QC}_\mathrm{rough}$ flag $\neq 0$, and the processing for this profile will not be continued. It is need to be said that the number of profiles, that fail this basic check is in general very low (≈ 1 ‰).
Afterwards an important circumstance comes into account by using UCAR data: In several profiles the impact altitude (perpendicular distance between Earth's surface and ray) is not (in the whole range) existent. But several checks at the QC are in between specific impact altitude ranges, which makes the information of impact altitude essential. (This part will not be executed in WEGC rOPS since the forward model is done in advance to the retrieval down to phases as a function of time.)
The only constantly available variable is the Straight Line Tangent Point (SLTP) altitude, that presents the distance between LEO satellite and center of refraction. Estimating the impact altitude follows with the SLTP altitude variable of the measurement and two altitude grids (SLTP- and impact altitude).
Both grids are based on an altitude grid with 100 m spacing, a top value of 120 km and a bottom of 100 m. For the derivation an inter- and extrapolation of those grids onto the SLTP variable as a function of time is done.
In higher impact altitudes the fit suits fairly good, but for lower ones (impact altitude below 20 km), deviations could possible came up. This leads to some unphysical values of impact altitude underneath 0 m, which can be sometimes seen in further figures.
As a next step, a from UCAR artificially added bias for raw ex.phases L1 and L2 will be corrected. The 50 m-offset in the UCAR processed profiles is included to secure, that in further calculations, complications with negative values do not arise. But to perform the baseband approach, this offset would aggravate the benefits of the baseband calculation.
Therefore the ex.phases L1 and L2 get shifted somehow, that their medians match in a specific impact altitude range with the excess phase Lm's median:

$$L_{\mathrm{o}} = L'_{\mathrm{o}} - \Delta L \tag{3.9}$$

with

$$\Delta L = \tilde{L}_{\mathrm{o}}(z_a) - \tilde{L}_{\mathrm{m}}(z_a) \tag{3.10}$$

where L'_o is the observed raw excess phase, $\tilde{L}_{\mathrm{o}}(z_a)$ and $\tilde{L}_{\mathrm{m}}(z_a)$ are the median of the raw excess phase and excess phase Lm in the impact altitude range of 60 km$\leq z_a \leq$ 70 km and $o \in \{1, 2\}$ for the L1- and L2-signal, respectively.

3.4 Outlier Detection and Correction

The outlier detection, correction and check is another highly important part of the QC, as further calculation respond very sensitively on outliers (by executing calculations that include averages and standard deviations).
An outlier is defined as a data point, that is significantly further apart than the median of the values around it (see Figure 3.5).

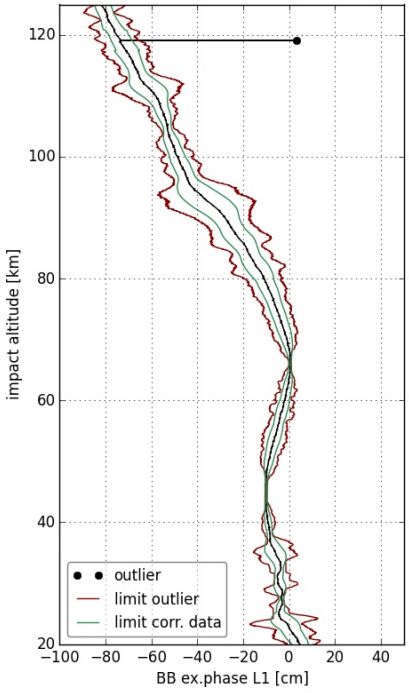

Figure 3.5: Example of an outlier, including the limits for the data (dark red line) as well as the boundary within the corrected data point needs to be (dark green line). (CHAMP-RO event, 15 July 2008, 02:38:08 UTC)

Per profile only a certain amount (3 %) of outliers are allowed, to ensure that a bias is not artificially generated. The outlier correction will be separately performed on the BB excess phases L1 and L2, providing to have signals that are already more

or less unbiased and independent of the atmosphere influences, which simplifies to focus on the distribution of the data values itself.
The performance is a moving median-referenced percentile-based rejection and correction using robust statistics. There are several steps necessary to receive an outlier free data profile:

Box 3.1: The outlier detection and correction algorithm

1. Calculation of moving 16th, 84th and 50th (i.e. median) percentiles (p_{16}, p_{84}, p_{50}) of the BB excess phase (δL_{om}) over a window size of M=101 data points.

2. Defining low and high boundaries:
   The 16th and 84th percentiles correspond to
   an estimated standard deviation ($\pm\sigma$) and a data point is (here) defined as an outlier when its value is greater than the five-fold of the corresponding percentile-based boundary. This leads to the bounds:
   $\Delta L_{\downarrow}^{\mathrm{out}}$: $p_{50} - 5 \cdot (p_{50} - p_{16})$
   $\Delta L_{\uparrow}^{\mathrm{out}}$: $p_{50} + 5 \cdot (p_{84} - p_{50})$

3. Check if datapoints of the BB excess phase (δL_{om}) are in between the boundaries:
   $\Delta L_{\downarrow}^{\mathrm{out}} < \delta L_{\mathrm{om}} < \Delta L_{\uparrow}^{\mathrm{out}}$

4. In case of an outlier detection, replacing value:
   - Determine a new data point value (x_{new}) by generating a random number (via normal distributed random number generator) and the standard deviation $\tilde{\sigma} = \frac{1}{2}(p_{84} - p_{16})$, with p_{16} and p_{84} being the moving 16th and 84th percentile value of the data point.
     $x_{\mathrm{new}} = x_{\mathrm{rand},\tilde{\sigma}}$
   - Check if the new generated data point is valid:
     $-3\tilde{\sigma} < x_{\mathrm{new}} < +3\tilde{\sigma}$
     (if not valid, calculate new data point value (x_{new}) and repeat check)
   - Replace the value: $x_{\mathrm{out}} = x_{\mathrm{new}}$

5. Outlier check:
   Verify that less than 3 % of data points got corrected
   - Pass $\rightarrow$ $\mathrm{QC}_{\mathrm{out}}$ flag $= 0$
   - Fail $\rightarrow$ $\mathrm{QC}_{\mathrm{out}}$ flag $\neq 0$ and discard profile

6. Back transformation of corrected data (BB excess phases L1 and L2) to ex.phases L1 and L2:
   $L_{\mathrm{o,corr}} = \delta L_{\mathrm{om,corr}} + L_{\mathrm{m}}$
   with $\mathrm{o} \in \{1, 2\}$ for excess phase L1 and L2 and L_{m} the model ex.phase

Using a moving percentile-based detection instead of a moving average-based, provides that outlier do not affect the calculation as much as they would by a

moving average.
Furthermore, it has to be taken into account, that the values of the BB excess phase are not symmetrically distributed around its median, which makes it important to define a proper window size for the calculation of the moving statistics.
By increasing the set of data points, also the probability rises that an outlier might not be detected. But when decreasing the range, the facilitation of an artificially bias gains, which leads to the detection of a rather okay value as an outlier.
The chosen window size of $M = 101$ data points, for calculating the moving variables, arises as a result of evaluating statistics, that counted the amount of profiles with at least one detected outlier by using various window sizes.
As it can be seen in Figure 3.6, decreases the number of detected outliers and so the number of profiles with increasing window size.

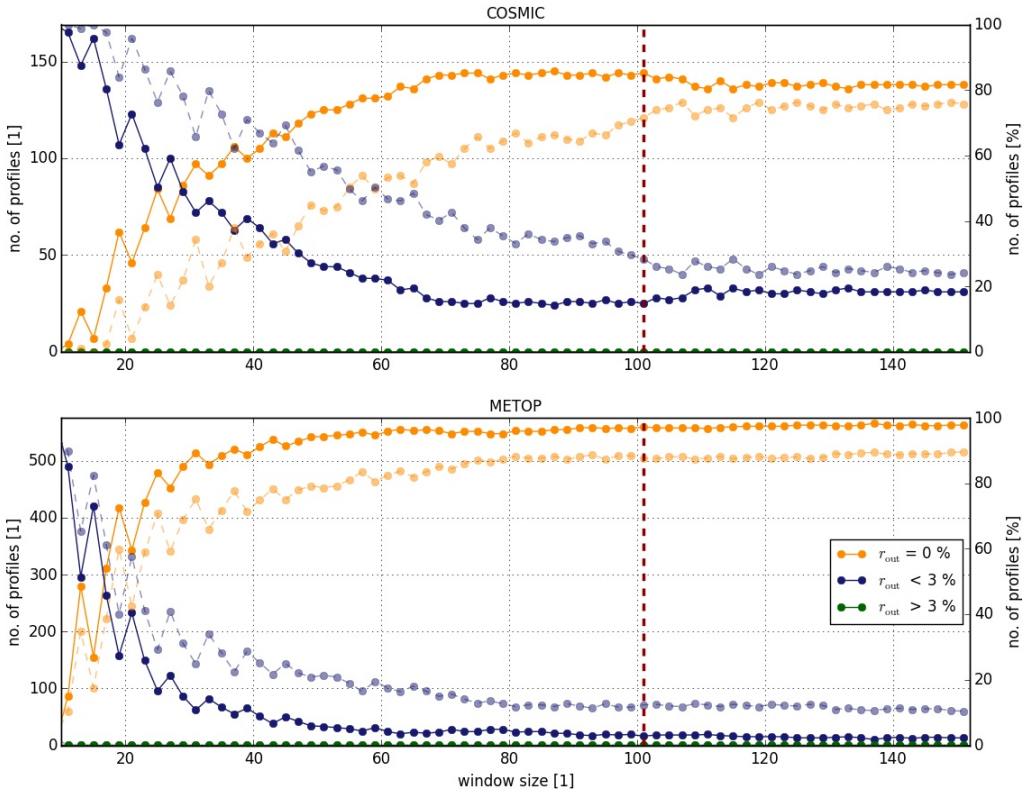

Figure 3.6: Relation between the profiles with detected outliers and the window size, that was used for outlier detection, for satellite COSMIC (top panel) and METOP (bottom panel). The yellow points represent the profiles with an outlierrate $r_{\text{out}} = 0\,\%$, the blue ones $r_{\text{out}} < 3\,\%$ and the green points with an outlierrate $r_{\text{out}} > 3\,\%$. The darker points exhibit the evaluation for the excess phase L1, the brighter ones for excess phase L2.

Even if the slope of counts with an outlier rate $r_{\text{out}} < 3\,\%$ for satellite METOP (bottom panel), declines significant faster than the one for satellite COSMIC, the number of counted outlier stays quite constant after passing the window size

$M = 100$ data points mark.
The outlierrate for excess phase L2 (marked in Figure 3.6 as brighter dots) takes longer to reach an almost constant level and has a higher outlierrate than L1, which confirms the expectation of the minor quality of excess phase L2 data.
It is remarkable, that for the satellite METOP almost all data profiles have a outlierrate of 0 %. The number of files with an outlierrate $r_{\text{out}} > 3\,\%$ is for all profiles zero (including the results for satellite CHAMP and GRACE), which means that irrespective the window size, all profiles would have passed the outlier check.

After the elimination of outliers, the very important auxiliary variable, the ionosphere corrected excess phase (excess phase Lc), is calculated via Equation 2.14. Since the already mentioned benefits of the usage of the excess phase Lc (see Section 2.2), most of the following checks are based on the excess phase Lc instead on the original phase delays L1 and L2.

3.5 Assignment of Impact Altitude Range

The estimation of an impact altitude range serves to screen the profiles in the highest and lowest impact altitudes and takes a first guess, in which area the quality of the profile is sufficient accurate to receive precise physical parameters. Estimating the top impact altitude level ($z_{a\text{Top}}$) and bottom impact altitude level ($z_{a\text{Bot}}$) is performed separately and based on the moving standard deviation of the BB excess phase Lc (for top impact altitude level) and HFBB excess phases L1 and L2 (for bottom impact altitude levels). The signals will be cut above/underneath these estimated top/bottom level and when a certain height criteria for the top and bottom impact altitudes is not reached, the whole profile will be discarded.

3.5.1 Assignment of Top Impact Altitude Level

To obtain the top impact altitude level for the ex.phases L1 and L2, the moving standard deviation of the BB excess phase Lc is used. The negligible offset of the BB excess phase Lc to the excess phase Lm provides a reasonable determination of the top level, by analyzing the moving standard deviation of an unbiased signal.

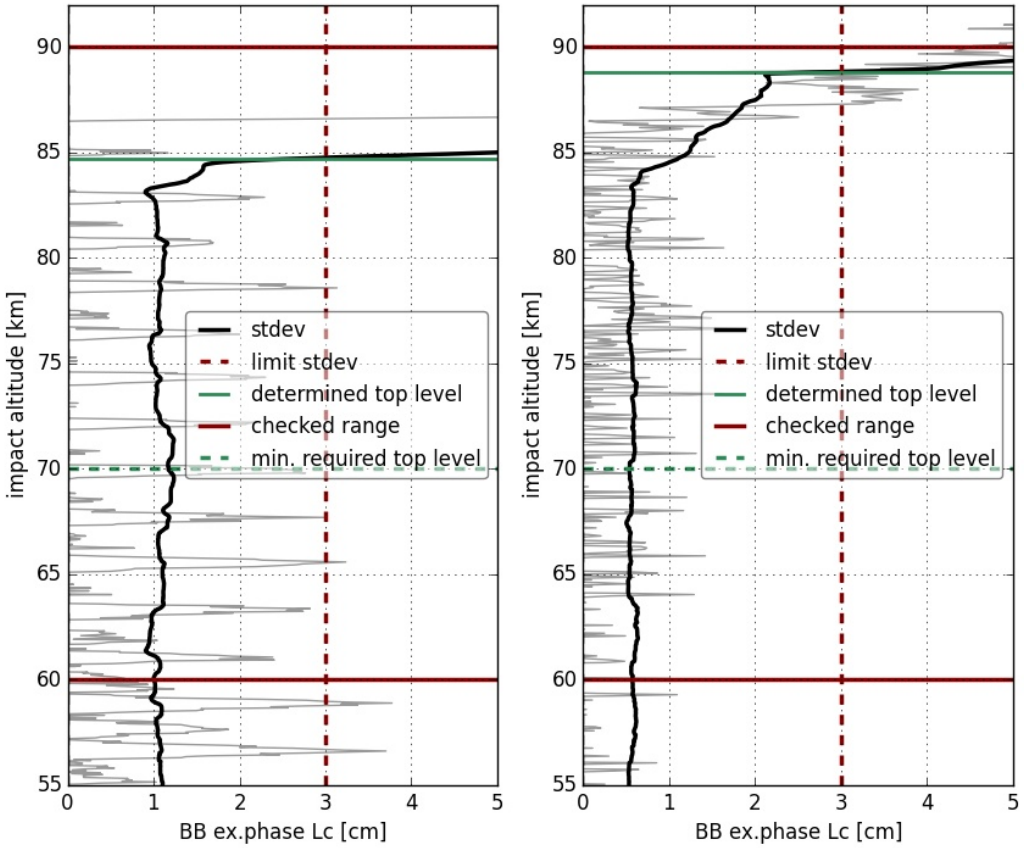

Figure 3.7: Illustration of the assignment of the top impact altitude level of the excess phase Lc for a CHAMP-RO event (left) and a COSMIC-RO event (right). The black line represents the moving stdev of the BB excess phase Lc (grey line), the dashed red line displays the boundary for the stdev, the solid red lines limit the checked impact altitude range, the solid green line indicates the resulting determined top level and the dashed green line displays the minimum required top level. (CHAMP-RO event, 15 July 2008, 03:20:32 UTC; COSMIC-RO event, 15 July 2008, 02:45:54 UTC)

Figure 3.7 shows the estimation of the top impact altitude level for a CHAMP-RO event (left panel) and a COSMIC-RO event (right panel). By reviewing the profile from bottom to top (of a specific height impact altitude range between 60 km and 90 km) the top impact altitude level is set as soon as one data point exceeds the boundary limit.
Here the assignment of the top impact altitude level steps in detail:

Box 3.2: The assignment of top impact altitude level algorithm

1. Calculate the BB excess phase Lc:

$$\delta L_{\mathrm{cm}} = L_{\mathrm{c}} - L_{\mathrm{m}} \tag{3.11}$$

   with L_{c} is the ionosphere corrected excess phase and L_{m} is the forward-modeled excess phase.

2. Determine the moving standard deviation of the BB excess phase Lc, as an indicator for the dispersion of data values.

3. Checking the standard deviation in the range of impact altitudes $z_a \in [60, 90]$ km from bottom to top and set the top impact altitude level ($z_{a\mathrm{Top}}$), when standard deviation exceeds the top impact altitude bound value (ΔL^{Top}= 3 cm) for the first time (see Figure 3.7).
   The later retrieval only processes profiles in an impact altitude range z_a <90 km. For this reason, profile's data with impact altitudes beyond 90 km will be not considered. When the standard deviation does not exceed the bound, the top level is set at the highest possible position (i.e. at z_a =90 km).

4. Altitude check and set of the QC flag:
   Verify if the determined top impact altitude level ($z^{\mathrm{Lc}}_{a\mathrm{Top}}$) is higher located than the minimum required top impact altitude level ($z^{\mathrm{min}}_{a\mathrm{Top}}$=70 km).
   - Pass $\rightarrow$ $\mathrm{QC}_{\mathrm{Top}} = 0$
   - Fail $\rightarrow$ $\mathrm{QC}_{\mathrm{Top}} \neq 0$ and discard whole profile

The most important issue at this part of estimating the top impact altitude level, is defining the appropriate limit for the moving standard deviation.
It is the key to find a value that is neither too strict, because the assigned level will be re-checked at bounds and smoothness check, nor too gentle, since atmospheric density is still quite low in this part of the atmosphere (compared to lower impact altitudes), which leads commonly to fairly minimal differences between excess phase Lc and excess phase Lm.
The excess phase Lc limit value for the top impact altitude level determination comes along with the results that are represented in Figure 3.8.
Here the y-axes displays the number of profiles, with exceeding standard deviation (in impact altitudes between 60 km and 90 km), corresponding to a certain limit value (x-axes).
The number of profiles, with a standard deviation exceeding the limit, decreases for the excess phase Lc much faster than for the excess phases L1 and L2, which demonstrates that the ionospheric influence is still remarkably high in lower

thermosphere and higher mesosphere and affects the standard deviation of the excess phases L1 and L2.
At the chosen limit value $\Delta L^{\mathrm{Top}} = 3\,\mathrm{cm}$, the amount of excess phase Lc profiles stays fairly constant for all satellites, and pictures a good balance between a tight and loose bound.

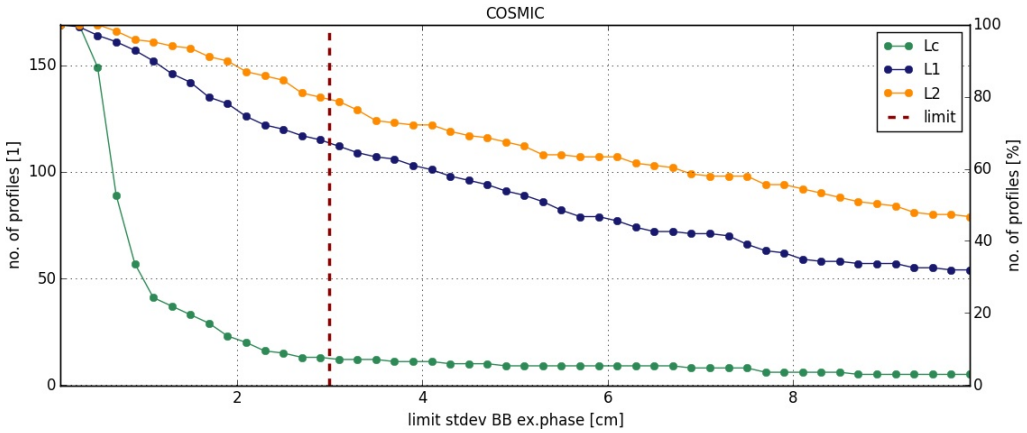

Figure 3.8: Relation between the bound value and the number of profiles that do not pass the altitude check, because the standard deviation of the BB excess phase exceeds the bound value at impact altitudes between 60 km and 90 km for satellite COSMIC. The green points points exhibit the evaluation for excess phase Lc, the blue ones for excess phase L1 and the yellow points for L2.

3.5.2 Assignment of Bottom Impact Altitude Levels

To obtain the bottom impact altitude level, the ex.phases L1 and L2 itself are taken, instead of the former used excess phase Lc. One reason is, that in altitudes closer to the Earth's surface (lower stratosphere and the troposphere), the ionospheric influence is almost negligible for solar non-extreme activity, and the major reason is, downward from lower stratosphere, the difference in quality between L1 and L2 increases significantly.
But for the calculation of the bending angle (in the L1b processor), both ex.phases are needed to correct the ionospheric effect by their linear combination. When the qualitative poorer excess phase L2 would be used completely downward to the bottom impact altitude level of L1, the quality of the determined atmospheric properties could be potentially negatively affected. In avoidance of this, both phases are treated independently from each other. Later the data of excess phase L2 will be extrapolated from its bottom level down to the bottom level of L1.

At this point the highpass-filtered baseband (HFBB) excess phase is used for the first time. As with decreasing impact altitude, the atmospheric density and pressure gets higher, which leads to increasing ex.phases (in impact altitudes around 80 km the phase delay leads to some centimeters, but close to the surface it arises up to roughly a kilometer).

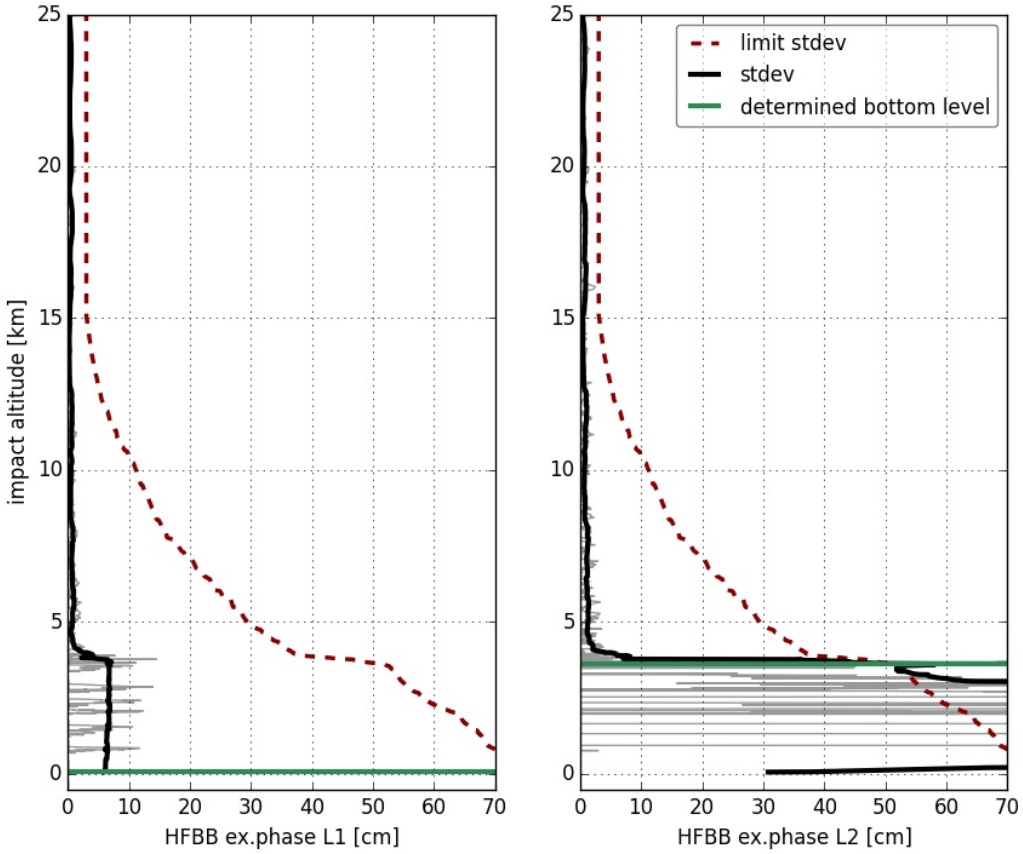

Figure 3.9: Illustration of the assignment of the bottom impact altitude levels for excess phase L1 (left panel) and L2 (right panel). The black lines represent the moving standard deviation of the HFBB excess phases (grey line), the dashed red line displays the boundary for the standard deviation and the solid green lines indicate the resulting determined impact altitude levels for excess phase L1 and L2. (CHAMP-RO event, 15 July 2008, 0:58:27 UTC)

Figure 3.9 illustrates the method of defining the bottom impact altitude levels. It is well observable that excess phase L1 has a significant smaller deflection as the excess phase L2, leading to a lower bottom impact altitude level.
The estimation of bottom impact altitude levels ($z^{\mathrm{L1}}_{a\mathrm{Bot}}$ and $z^{\mathrm{L2}}_{a\mathrm{Bot}}$) is based on the standard deviation of the highpass-filtered baseband excess phases L1 and L2 and is done separately for the two signals. The boundary is in contrast to Section 3.5.1

a combination of a fix value and a relative one, depending on the forward-modeled excess phase (see Figure 3.9). Here the algorithm steps to define the bottom impact altitude level in detail:

Box 3.3: The assignment of bottom impact altitude level algorithm

1. Calculation of the HFBB excess phase, by building the difference between BB excess phase and the LFBB excess phase (after Section 3.1.5):

$$\delta L_{\mathrm{oHF}} = L_{\mathrm{om}} - L_{\mathrm{Fom}} \tag{3.12}$$

   with δL_{oHF} is the HFBB excess phase, L_{om} is the BB excess phase, $L_{\mathrm{Fom}} = \mathbf{F}^{\mathrm{BWS}}\, \delta L_{\mathrm{om}}$ is the LFBB excess phase of the observed excess phase L_{o}, where $\mathrm{o} \in \{1, 2\}$.

2. Computation of the moving standard deviation of the HFBB excess phase ($\sigma_{\delta L_{\mathrm{oHF}}}$), as an indicator of the dispersion of data values.

3. Defining the boundary for the bottom impact altitude levels:
   - Combination of an absolute bound value ($\Delta L^{\mathrm{Bot}}_{\mathrm{abs}} = 3\,\mathrm{cm}$) and a relative bound value ($\Delta L^{\mathrm{Bot}}_{\mathrm{rel}} = 0.001 \mathrel{\widehat{=}} 0.1\,\%$).
   - Calculating the boundary profile (ΔL^{Bot}) via a maximum function:

$$\Delta L_{\mathrm{Bot}} = \mathrm{Max}[\Delta L^{\mathrm{Bot}}_{\mathrm{abs}}, \Delta L^{\mathrm{Bot}}_{\mathrm{rel}} \cdot L_{\mathrm{m}}] \tag{3.13}$$

     where L_{m} is the excess phase Lm

4. Checking the standard deviation in an impact altitude range ($z_a < 30\,\mathrm{km}$) from top to bottom and set the bottom impact altitude level ($z^{L_{\mathrm{o}}}_{a\mathrm{Bot}}$), when standard deviation exceeds the boundary (ΔL^{Bot}) for the first time.

5. Altitude check and set of the QC flag:
   Verify if the determined altitude level ($z^{L_{\mathrm{o}}}_{a\mathrm{Bot}}$) is lower than the minimum required bottom level ($z^{\mathrm{min}}_{a\mathrm{Bot}} = 25\,\mathrm{km}$).
   - Pass $\rightarrow \mathrm{QC}_{\mathrm{Bot}} = 0$
   - Fail $\rightarrow \mathrm{QC}_{\mathrm{Bot}} \neq 0$ and discard whole profile (no matter, if only one or both excess phases failed).

The definition of the bottom boundary depends on the moving standard deviation manner of the HFBB excess phase L1 and L2. By looking at Figure 3.10, one can see the absolute values of the moving standard deviation for HFBB excess phase L1 (left panel), compared to the HFBB excess phase L1's standard deviation in

relation to the excess phase Lm (right panel).
It is fairly significant that absolute standard deviation stays quite constant down to an impact altitude of 15 km. The relative standard deviation instead starts to shrink and behaves more invariable beneath an impact altitude of 15 km. The boundary for the bottom impact altitude level (ΔL^{Bot}) is composed of an absolute bound value and an relative bound value, which will be multiplied by the excess phase Lm.
Same as for the assignment of the top impact altitude limit, the determination of those two bound values is defined, by comparing the number of profiles, with exceeding standard deviation over changing boundary values. The statistic analysis for the two bound values is done separately; for the absolute boundary value, only the moving standard deviation of HFBB excess phase within an impact altitude range of 15 km to 30 km is taken into account, and for the relative boundary value the data below this range exclusively. The exact impact altitude level on which the transition between absolute and relative boundary value takes place, correspond to the climate region (see Table 3.2 in Section 3.1). In areas with high humidity or high pressure is the excess phase in general greater than in other climate region regions. Therefore the forward-modeled excess phase varies too.

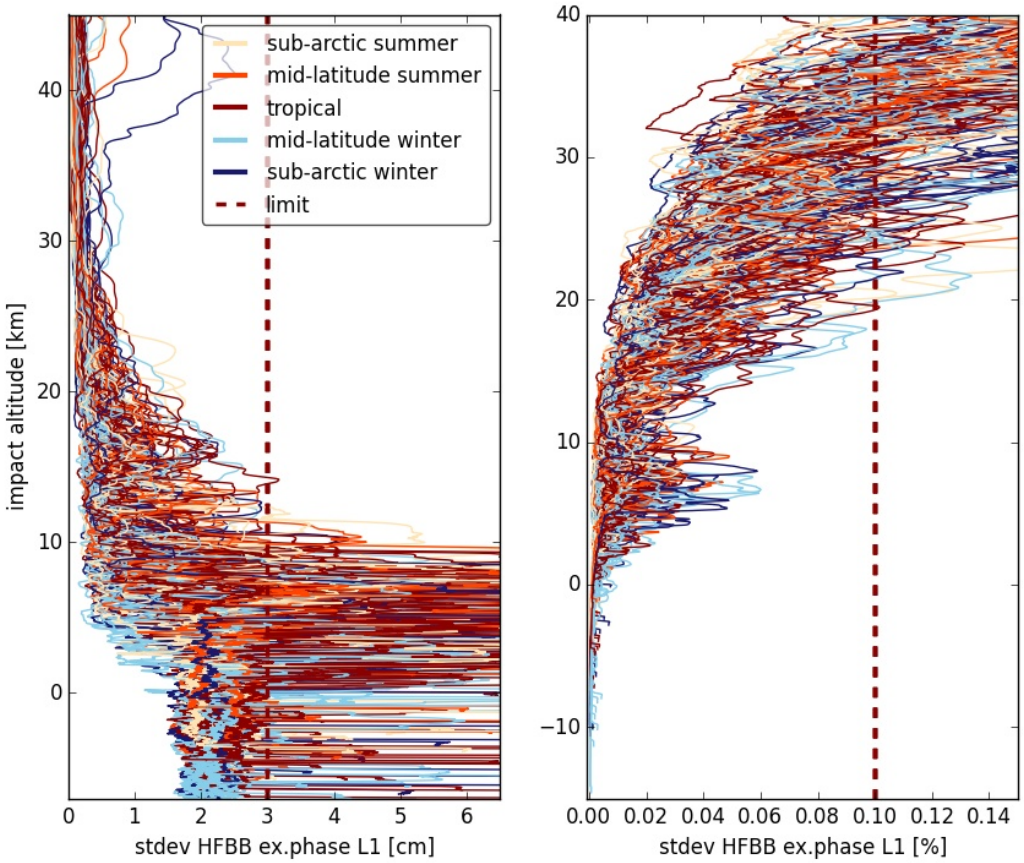

Figure 3.10: Illustration of the moving standard deviation's behavior of HFBB ex.phase L1, demonstrated by the data of satellite GRACE. The right panel shows the absolute standard deviation; the left panel illustrates the relative behavior of standard deviation to the excess phase Lm. The different colors demonstrate the various climate regions, the dashed red line represents the chosen boundary for the standard deviation.[1]

[1] The impact altitudes lower 0 km occur due to the inter- and extrapolation to obtain the impact altitude variable (mentioned in Section 3.3)

In Figure 3.11 the evaluation in an impact altitude range between 15 km and 30 km is observable. Here the y-axes exhibit the number of profiles, with exceeding standard deviation of HFBB excess phase in an impact altitude range between 15 km and 30 km corresponding to a certain limit value (x-axes). In contrast to the results for the top impact altitude boundary assignment, the standard deviation of the HFBB excess phase L1 and L2 (blue and yellow points) are already lower as for the HFBB excess phase Lc (green points). Same as for the standard deviation of the BB excess phase Lc in higher impact altitudes, the amount of profiles with an exceeding standard deviation stays largely constant above an limit value of 3 cm. The number of profiles with stdevs greater than 3 cm is also for HFBB excess phase Lc quite low.

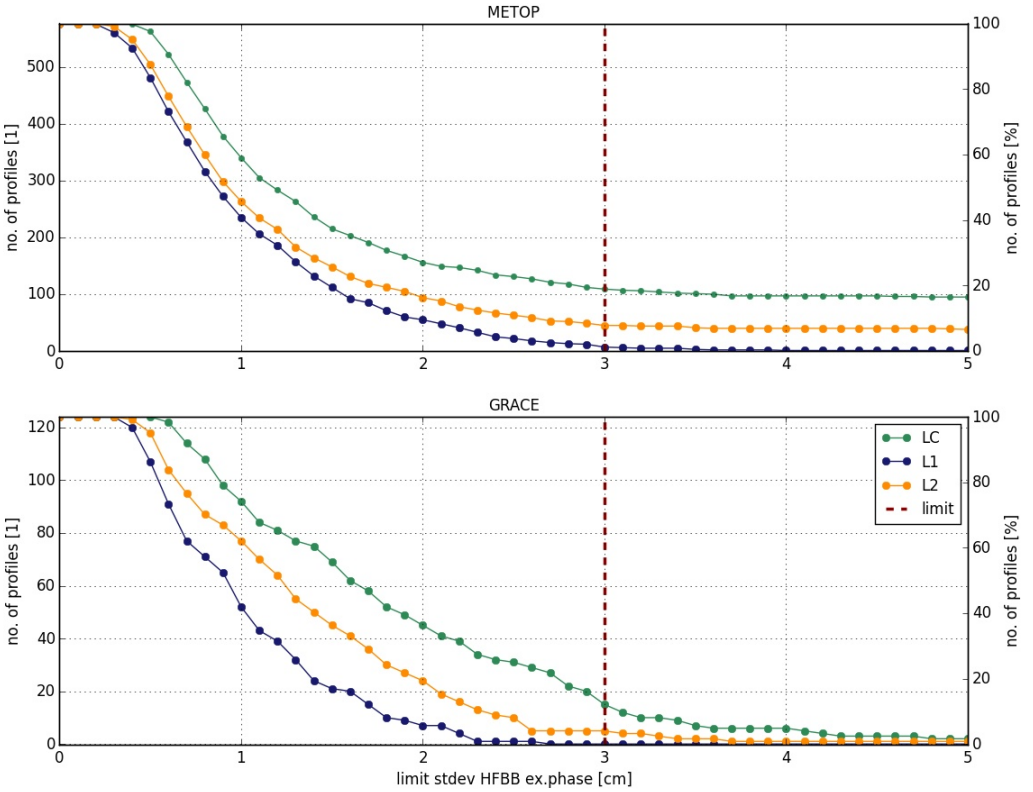

Figure 3.11: Relation between the bound value for the standard deviation of HFBB excess phase and the number of profiles that do not pass the altitude check, because the standard deviation of BB excess phase exceeds the bound value at impact altitudes between 15 km and 30 km for satellite METOP (top panel) and GRACE (bottom panel). The blue and yellow points exhibit the evaluation for the excess phase L1 and L2, the green ones for excess phase Lc and the dashed red line displays the chosen limit value for the boundary.

In Figure 3.12 the evaluation in an impact altitude range lower 15 km is observable. Here the y-axes exhibit the number of profiles, with exceeding standard deviation

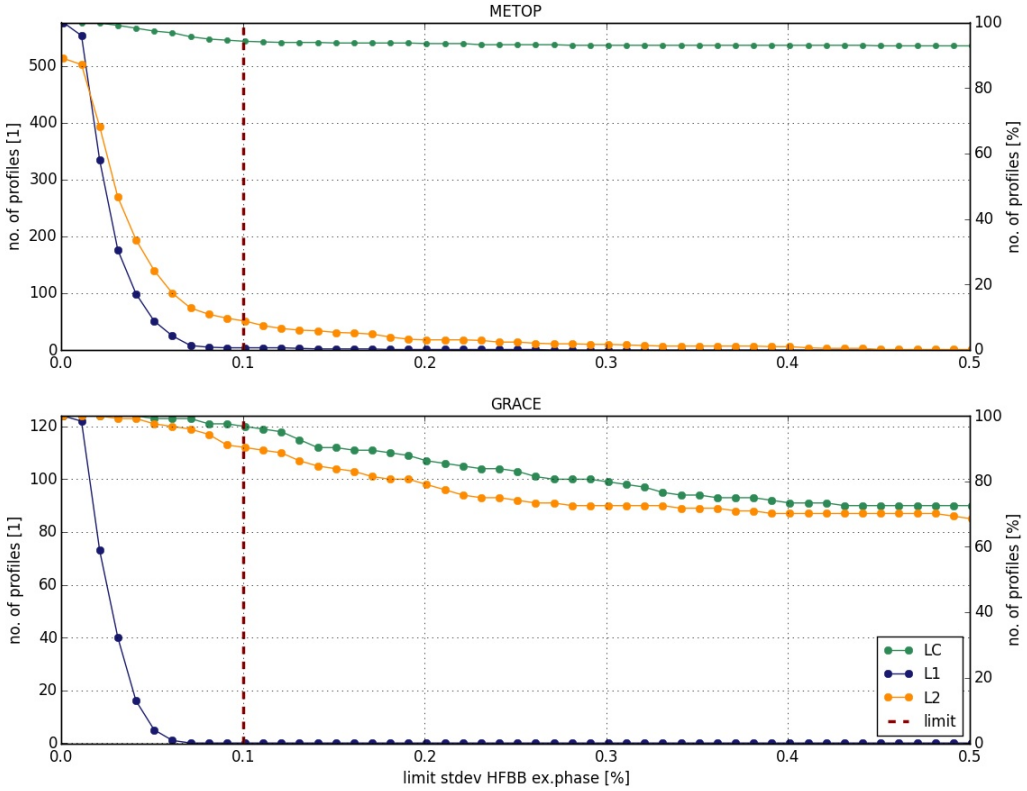

Figure 3.12: Relation between the relative bound value for the standard deviation of HFBB excess phase and the number of profiles that do not pass the altitude check, because the standard deviation of HFBB excess phase exceeds the bound value at impact altitudes below 15 km for satellite METOP (top panel) and GRACE (bottom panel). The blue and yellow points exhibit the evaluation for the excess phase L1 and L2, the green ones for excess phase Lc and the dashed red line displays the chosen limit value for the boundary.

in an impact altitude range lower 15 km, corresponding to a certain bound value (x-axes). For the selected relative bound value ($\Delta L_{\mathrm{rel}}^{\mathrm{Bot}} = 0.1\,\%$), almost all ex.phases L1 pass, for excess phase L2 it strongly depends on the satellite, whether they have a high or low standard deviation. The standard deviation of excess phase Lc is in these low impact altitudes definitely higher than for excess phase L1 and L2 due to noise summation, which strengthen the decision to use excess phase L1 and L2 instead of excess phase Lc.
The relative bound value ($\Delta L_{\mathrm{rel}}^{\mathrm{Bot}}$) seems to be chosen fairly loose. In particular when looking at Figure 3.10, but the data recording changes for some LEO satellites in low impact altitudes to a different processing (from closed- to open-loop processing), which causes a jump in the signal-to-noise ratio. Furthermore phase shifts caused by local multipath occur, which arises when multiple signals of different paths arrive simultaneously at the receiver, due to the reflection and scattering close to receiver's antenna (Kursinski et al. 1997). Moreover ex.phases reach almost values

between hundreds of meters and a kilometer.

3.6 Quality Check of Data Values

The actually QC reviews the profiles in between the previously estimated top impact altitude level ($z^{\mathrm{Lc}}_{a\mathrm{Top}}$) and bottom impact altitude level ($z^{\mathrm{L2}}_{a\mathrm{Bot}}$).
Since checks are based on the linear combined excess phase Lc, the bottom impact altitude from L2 instead of L1 is used (the quality of the lower part of excess phase L1 will be controlled in an extra task, see following Section 3.7).
In this section two consecutive tests are presented, termed bounds check and smoothness check, both applied on a derived quantity of the excess phase Lc e.g. BB excess phase Lc and the derivative of the HFBB excess phase Lc, respectively.

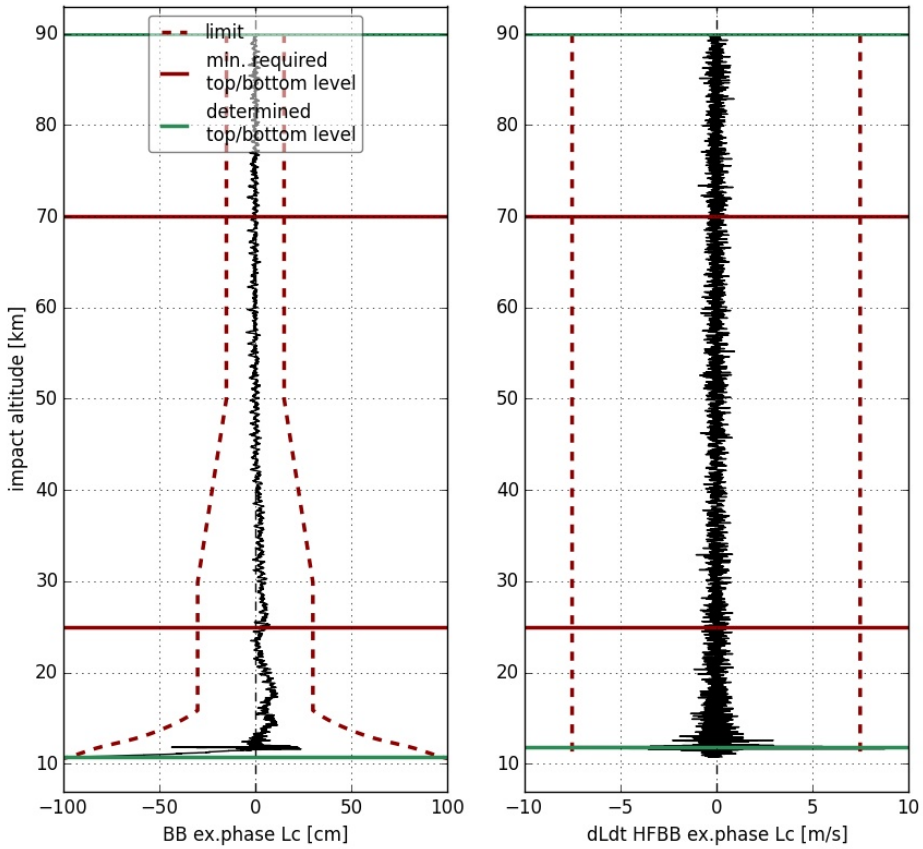

Figure 3.13: Operating principle of bounds and smoothness check. The left panel illustrates the procedure of the bounds check on the BB excess phase Lc, the right panel of the smoothness check on the derivative of the HFBB excess phase Lc. The dashed dark red lines represent the boundary for bound-and smoothness check, the green line the assigned top and bottom levels and the solid dark red line determines the minimum required impact altitude area, within the profiles have to pass the checks. (CHAMP-RO event, 15 July 2008, 00:48:57 UTC)

The boundaries for both checks are defined through moving standard deviation (technically the five-hold of it), height range and the ratio to the top and bottom impact altitude limits.
Figure 3.13 gives an example of the functional principle of the bounds check (left panel) and smoothness check (right panel). The dashed dark red lines represent the certain bounds, whose definition will be explained in the following subsection , the solid dark red lines mark the altitudes, within the profile needs to pass the tests, and the green lines display the determined bottom value of bounds and smoothness check, which are slightly different (for this profile).
When a profile fails somewhere beyond the minimum required altitude range, a new top and/or bottom impact altitude level is set and the failed levels of the profile get a QC flag $\neq 0$.
Otherwise (failing within the minimum required altitudes) a QC flag $\neq 0$ is set for the entire profile and it will be discarded for further processing.
For defining the limits, every setting is a constitution of statistics, analysis and general knowledge. The evaluation is divided in different parts, depending on impact altitude:

- $z_{a\mathrm{MS}}$ within [50,90] km (i.e. Mesosphere (MS))
- $z_{a\mathrm{US}}$ within [30,50] km (i.e. Upper Stratosphere (US))
- $z_{a\mathrm{TLS}}$ within <30 km (i.e. Troposphere and Lower Stratosphere (TLS))
- $z_{a\mathrm{LS}}$ within [15,30] km (i.e. Lower Stratosphere (LS))
- $z_{a\mathrm{TS}}$ <15 km (i.e. Troposphere (TS))

3.6.1 Bounds Check

The bounds check (BC) is a combination of using absolute and relative values as bound, to check the physical plausibility of the BB excess phase Lc, within the before estimated top impact altitude level ($z^{\mathrm{Lc}}_{a\mathrm{Top}}$) and bottom impact altitude level ($z^{\mathrm{Lc}}_{a\mathrm{Bot}} = z^{\mathrm{L2}}_{a\mathrm{Bot}}$).
Depending on the impact altitudes and the limits for the top and bottom impact altitude (ΔL^{Top} and ΔL^{Bot}), the boundary for bounds check changes (e.g. boundary is in high impact altitudes small when compared to high impact altitudes). Therefore the total boundary for the bounds check (ΔL^{BC}) is subdivided in bounds ($\Delta L^{\mathrm{BC}}_{z_{ai}}$), depending on the impact altitude ranges (z_{ai}) which have been introduced in the list in Section 3.6).
The detailed steps are as following:

Box 3.4: The bounds check algorithm

1. Calculation of the .
2. Defining the boundaries for the various impact altitude sections:
   - impact altitude range: $z_a \in [50, 90]$ km:
     bound value $\Delta L^{\mathrm{BC}}_{\mathrm{MS}} = 5 \cdot \Delta L^{\mathrm{Top}} = 15$ cm
   - impact altitude range: $z_a \in [50, 90]$ km:
     bound value $\Delta L^{\mathrm{BC}}_{\mathrm{US}} = k z_a + d$,
     $k = \frac{\Delta L^{50} - \Delta L^{30}}{z_a^{50} - z_a^{30}}$ [m/m] , $d = \frac{z_a^{50} \cdot \Delta L^{30} - z_a^{30} \cdot \Delta L^{50}}{z_a^{50} - z_a^{30}}$ [m]
     where ΔL^{z_a} is the boundary at $z_a \in \{30, 50\}$ km
   - impact altitude range: $z_a \in [0, 30]$ km:
     bound value $\Delta L^{\mathrm{BC}}_{\mathrm{TLS}} = \mathrm{Max}[\Delta L^{\mathrm{BC}}_{\mathrm{TLS,abs}}, \Delta L^{\mathrm{BC}}_{\mathrm{TLS,rel}} \cdot |L_m|]$
     where $\Delta L^{\mathrm{BC}}_{\mathrm{TLS,abs}} = 5 \cdot \mathrm{c}_2 \cdot \Delta L^{\mathrm{Bot}}_{\mathrm{abs}} = 30$ cm is the absolute bound value for $\Delta L^{\mathrm{BC}}_{\mathrm{TLS}}$, with the ratio coefficient $\mathrm{c}_2 = 2$ and $\Delta L^{\mathrm{BC}}_{\mathrm{TLS,rel}} = 0.01 \mathrel{\widehat{=}} 1\,\%$ is the relative bound value for $\Delta L^{\mathrm{BC}}_{\mathrm{TLS}}$
3. Bounds check:
   Check if BB excess phase ($\delta L_{\mathrm{Fcm}}(z_a)$) is in the impact altitude range ($z_a \in [z^{\mathrm{L2}}_{a\mathrm{Bot}}, z^{\mathrm{Lc}}_{a\mathrm{Top}}]$) within the boundary ($\Delta L^{\mathrm{BC}}$):
   $|\delta L_{\mathrm{Fcm}}| < \Delta L^{\mathrm{BC}}$
   - Pass $\rightarrow \mathrm{QC}_{\mathrm{BC}} = 0$
   - Fail
     $\rightarrow$ exceeds boundary exclusively outside of the minimum required area:
     define new top and/or bottom impact altitude level (at the position where profile exceeded boundary first and set $\mathrm{QC}_{\mathrm{BC}} \neq 0$ beyond
     $\rightarrow$ exceeds boundary within the minimum required range:
     set $\mathrm{QC}_{\mathrm{BC}} \neq 0$ for the whole profile and exclude it from further QC

As previously mentioned, the definition of the boundary for the bounds check considers the bound values of the top and bottom assignment. Since the moving standard deviation of the HFBB excess phase (and BB excess phase) has been used to define the bound, it will be compared with the moving standard deviation of the BB excess phase to receive a ratio coefficient, to establish a connection between the processes.

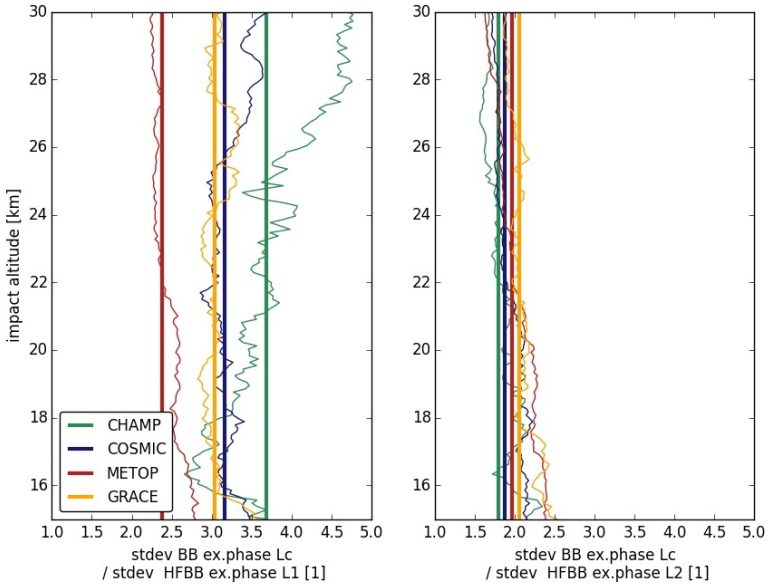

Figure 3.14: Ratio between the stdev of the BB excess phase Lc and stdev of HFBB excess phases L1 (left panel) and L2 (right panel). The different colours, describe the various satellites, the thinner lines are the moving stdevs over all datasets, and the thicker line is the median of the standard deviation in the shown impact altitude range of 15 km to 30 km.

Figure 3.14 illustrates the ratio between the standard deviation of the BB excess phase Lc to HFBB excess phase L1 and L2 in an impact altitude range between 15 km and 30 km. The relation between standard deviation the BB excess phase Lc and standard deviation of the HFBB excess phase L1 is greater than for the HFBB excess phase L2. These proportions demonstrate, that the excess phase L1 has the lowest signal-to-noise ratio, followed by the excess phase L2 and finally the excess phase Lc, which contains a noise summation of the signals.
To achieve an adequate standard deviation level for BB excess phase Lc to the standard deviation level of the HFBB excess phase L1, a division with a factor about three would be necessary; for the standard deviation level of the HFBB excess phase L2, a division with a factor about two. Since the primarily focus is on verifying the bottom impact altitude for excess phase L2 ($z^{\mathrm{L2}}_{a\mathrm{Bot}}$), as described in Section 3.5.2, the average ratio ($\mathrm{c}_2 = 2$) of L2 will be used, which leads to a boundary for this range of:

$$\Delta L^{\mathrm{BC}}_{\mathrm{TLS,abs}} = 5 \cdot \mathrm{c}_2 \cdot \Delta L^{\mathrm{Bot}}_{\mathrm{abs}} = 30\,\mathrm{cm} \tag{3.14}$$

with $\Delta L^{\mathrm{Bot}}_{\mathrm{abs}}$ =3 cm is the absolute bound value of the top impact altitude limit (see Section 3.5.1).

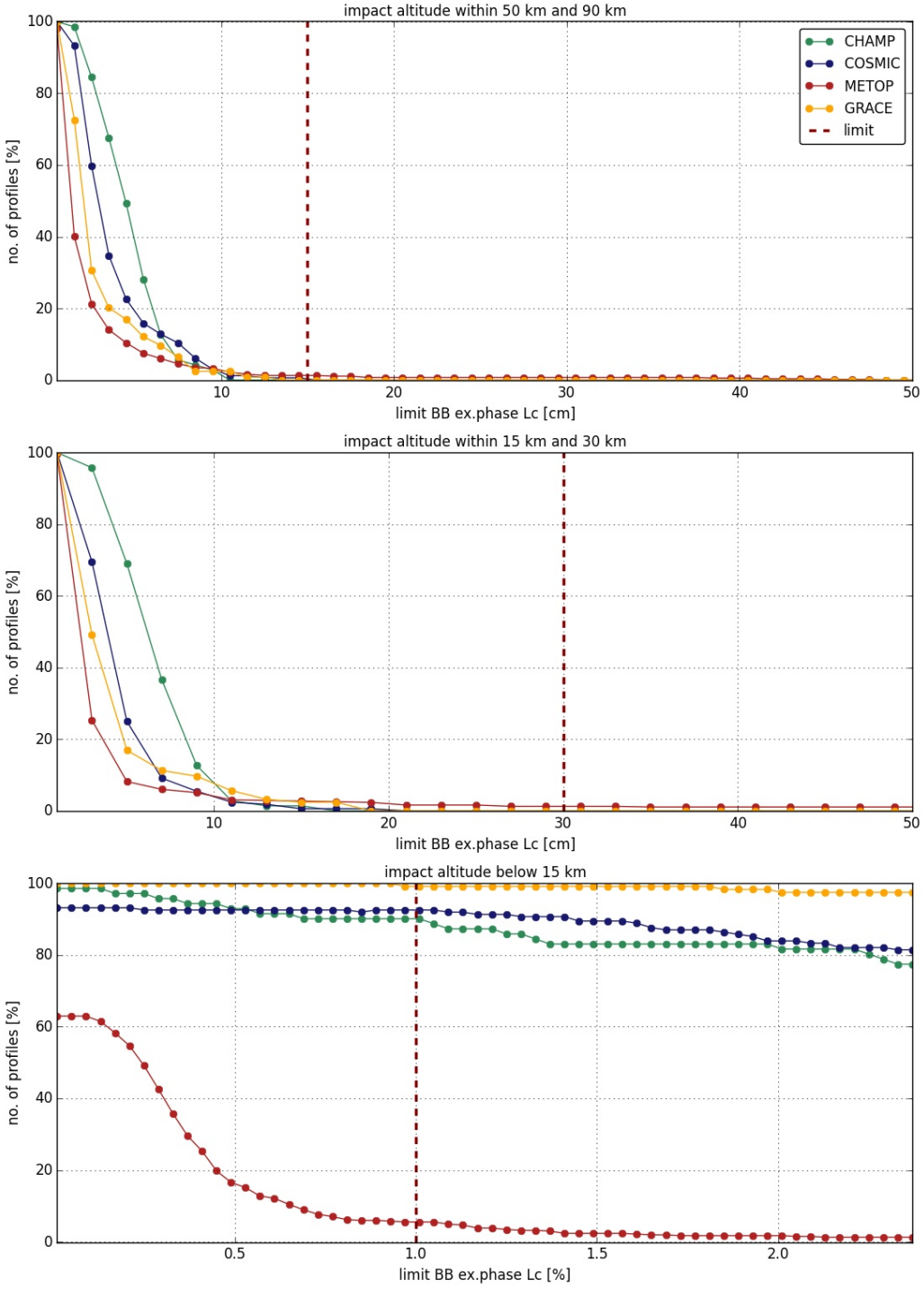

Figure 3.15: Relation between the bound value and the number of profiles, not passing the bounds check. The different colours distinguish between the satellites, the dashed red line marks the chosen bound value in this altitude range. The top panel considered profiles only in an impact altitude range 50 km to 90 km, the middle panel between 15 km and 30 km and the bottom panel in an impact altitude range below 15 km.

Since the top impact altitude level was estimated with BB excess phase Lc too, there is no additional factor needed in an impact altitude range between 50 and 90 km:

$$\Delta L_{\mathrm{MS}}^{\mathrm{BC}} = 5 \cdot \Delta L^{\mathrm{Top}} = 15\,\mathrm{cm} \tag{3.15}$$

with ΔL^{Top} =3 cm is the top impact altitude limit.
In the impact altitude range between 30 km and 50 km a linear fit between those two ($\Delta L_{\mathrm{TLS,abs}}^{\mathrm{BC}}$ and $\Delta L_{\mathrm{MS}}^{\mathrm{BC}}$) is performed.
Analyzing the behavior of BB excess phase Lc in the lowest altitudes, leads to a relative bound value of $\Delta L_{\mathrm{TLS,rel}}^{\mathrm{BC}} = 0.01 \mathrel{\widehat{=}} 1\,\%$.

The three panels in Figure 3.15 represent the relation between the number of profiles (y-axis), that fail at bounds check, corresponding to a certain boundary value (x-axis) in different altitude ranges.
By crosschecking the assigned limit values with the results in Figure 3.15, one can see that for the top and middle panel, the number of profiles is constant or rather almost zero at the chosen limit value (red dotted line). For the relative boundary value (bottom panel), the value seems rather strict, since except for satellite METOP almost all profiles fail at bounds check, because their BB excess phase exceeds the value. This high rate of failure comes from looking at the excess phase in the very lowest impact altitude range. Moreover is the least required impact altitude level at 25 km. Here, the considered phases are checked in an impact altitude lower 15 km checked and by looking at Figure 4.9 in Section 4.3.1 it is observable that the resulting boundary fits nicely to the behavior of the BB excess phase Lc too.

3.6.2 Smoothness Check

The smoothness check is based on the highpass-filtered baseband excess phase Lc, to thoroughly investigate the behavior of the noise. By differentiating the highpass-filtered signal, the level of rapidly raising noise can be located. For derivation, a 5-point derivative is used:

$$\left.\frac{\partial \delta L(t)}{\partial t}\right|_n = \partial L(t)|_n = \frac{-\delta L_{n+2} + 8\delta L_{n+1} - 8\delta L_{n-1} + \delta L_{n-2}}{-t_{n+2} + 8t_{n+1} - 8t_{n-1} + t_{n-2}} \tag{3.16}$$

with n representing a data point of the signal $\delta L(t)$.
The 5-point derivative is symmetrically, more robust than a 3-point derivative and will be also used by further calculations to establish the Doppler shift retrieval in the L1a process.
The range, within the signal is checked, is limited by the top impact altitude level ($z_{a\mathrm{Top}}^{\mathrm{Lc}}$) and bottom impact altitude level ($z_{a\mathrm{Bot}}^{\mathrm{L2}}$), that might have changed during the bounds check. The steps for the smoothness check in detail are:

Box 3.5: The smoothness check algorithm

1. Calculation of the HFBB excess phase Lc (δL_{cHF}):

$$\delta L_{\mathrm{cHF}} = L_{\mathrm{cm}} - L_{\mathrm{Fcm}} \tag{3.17}$$

   with L_{cm} is the BB excess phase, and $L_{\mathrm{Fcm}} = \mathbf{F}^{\mathrm{BWS}} \delta L_{\mathrm{cm}}$ is the LFBB excess phase

2. Calculation of the 5-point derivative of the HFBB excess phase Lc ($\partial L_{\mathrm{cHF}}$) and the 5-point derivative of the excess phase Lm (∂L_{m}) via Equation 3.16:

3. Defining the boundary for the various altitude sections:

   - impact altitude range: $z_a \in [50, 90]\,\mathrm{km}$:
     $\partial L^{\mathrm{SC}}_{\mathrm{abs}} = 5 \cdot \mathrm{c}_1 \cdot \Delta L^{\mathrm{Top}} = 7.5\,\mathrm{m/s}$
     with the ratio coefficent $\mathrm{c}_1 = 50$
   - impact altitude range: $z_a \in [15, 30]\,\mathrm{km}$:
     $\partial L^{\mathrm{SC}}_{\mathrm{abs}} = 5 \cdot \mathrm{c}_2 \cdot \Delta L^{\mathrm{Bot}}_{\mathrm{abs}} = 7.5\,\mathrm{m/s}$
     with the ratio coefficent $\mathrm{c}_2 = 50$
   - impact altitude range: $z_a \in [30, 50]\,\mathrm{km}$:
     $\partial L^{\mathrm{SC}}_{\mathrm{abs}} = k z_a + d$,
     with $k = 0\ \frac{\mathrm{m/s}^2}{m}$, leads to:
     $d = 7.5\,[\mathrm{m/s}] \rightarrow \partial L^{\mathrm{SC}}_{\mathrm{abs}} = 7.5\,[\mathrm{m/s}]$
   - impact altitude range: $z_a \in [0, 90]\,\mathrm{km}$:
     $\partial L^{\mathrm{SC}} = \mathrm{Max}[\partial L^{\mathrm{SC}}_{\mathrm{abs}}\ ,\ \partial L^{\mathrm{SC}}_{\mathrm{rel}} \cdot |\partial L_{\mathrm{m}}|]$
     with $\partial L^{\mathrm{SC}}_{\mathrm{rel}} = 0.75 \mathrel{\widehat{=}} 75\%$ is the relative limit value for ∂L^{SC}

4. Smoothness check:
   Check if the derivative of the HFBB excess phase ($\delta L_{\mathrm{oHF}}(z_a)$) is in the impact altitudes range ($z_a \in [z_{a\mathrm{Bot}}, z_{a\mathrm{Top}}]$) within the boundary ($\partial L^{\mathrm{SC}}$):
   $|\partial L_{\mathrm{cHF}}| < \partial L^{\mathrm{SC}}$

   - Pass $\rightarrow \mathrm{QC}_{\mathrm{SC}} = 0$
   - Fail
     $\rightarrow$ exceeds boundary exclusively outside of the minimum required area:
     define new top and/or bottom impact altitude level at the position where profile exceeded boundary first and set $\mathrm{QC}_{\mathrm{SC}}$ flag $\neq 0$ beyond
     $\rightarrow$ exceeds boundary within the minimum required range:
     set $\mathrm{QC}_{\mathrm{SC}}$ flag $\neq 0$ for the whole profile and exclude it from further QC

Same as for the bounds check, the relations between the moving standard deviation of BB excess phase Lc and HFBB excess phases L1 and L2 to the moving standard deviation of the derivative of HFBB excess phase Lc were studied, to define the boundary. The Figure 3.16 illustrates the ratios between the different signals to the 5-point derivative of the HFBB excess phase Lc in two different impact altitude ranges.
Since the standard deviation of BB excess phase Lc is used to define the top impact altitude level, the standard deviation of the derivative of HFBB excess phase Lc is compared to it in high impact altitudes (left panel).

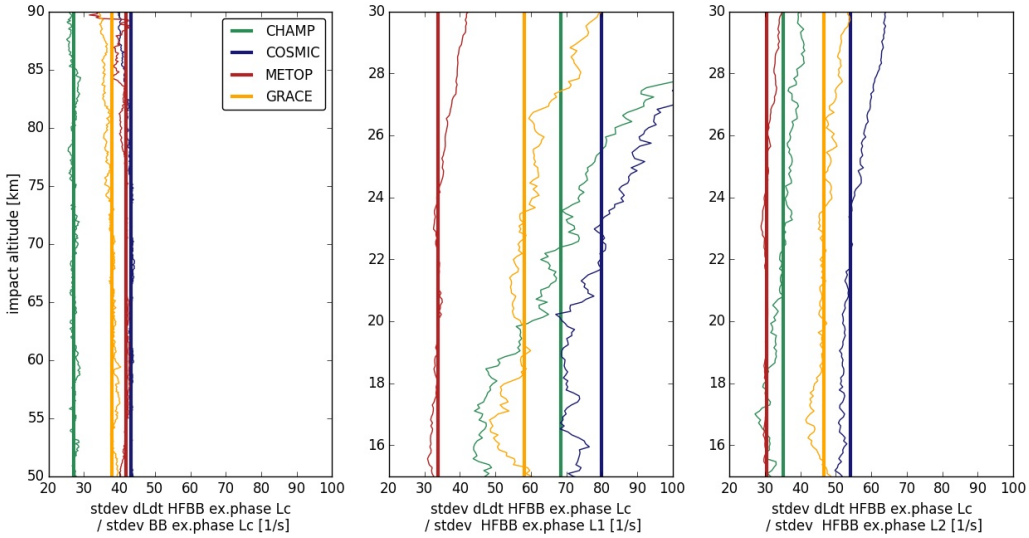

Figure 3.16: Ratio between the standard deviations of the derivative of the HFBB excess phase Lc to the BB excess phase Lc (left panel), of HFBB excess phase L1 (middle panel) and L2 (right panel). The different colours, describe the various satellites, the thinner lines are the moving standard deviations over all datasets for one satellite, and the thicker line is the median of the satellite in the shown impact altitude range of 50 km to 90 km (left panel) and 15 km to 30 km (middle and right panel).

In lower impact altitudes the ratio between moving standard deviation's of HFBB excess phases L1 and L2 to the one of the derivative of HFBB excess phase Lc (middle and right panel) is evaluated.
With differentiating a signal, the signal-to-noise ratio increases, which is clearly shown. Compared to the ratios in Section 3.6.1, the values arise by a factor of about 10.
According to expectations, the ratio between standard deviation of the HFBB excess phase L1 to derivative of HFBB excess phase Lc is higher, than the HFBB excess phase L2 to derivative of HFBB excess phase Lc.
Since the focus is still on verifying the bottom impact altitude for excess phase L2 in lower altitudes, the orientation to find a ratio coeffiecient lies on the results for excess phase L2 (right panel).

In opposite to the BB excess phase, the HFBB excess phase (and also its standard deviation) is almost at a constant level until reaching lowest impact altitude levels. This leads us to use the same boundary value, by multiplying with the factor $c_1 = c_2 = 50\,[1/s]$, before merging into the model-based boundary.
The derivative of excess phase Lm will be multiplied with the relative bound value $\partial L_{\text{rel}}^{\text{SC}} = 0.75 \mathrel{\widehat{=}} 75\%$.
The three panels in Figure 3.15 represent the relation between the number of profiles (y-axes), that fail at smoothness check, corresponding to a certain boundary value (x-axes) in different altitude ranges.
This statistic analysis emphasizes the accuracy of the selected limit values. Same as for the bounds check, the amount of profiles not passing the smoothness check, is in higher impact altitudes very low, which strengthens the choice on focusing on the ratio between the 5-point derivative of HFBB excess phase Lc to the HFBB excess phase L2 (right panel 3.16). An even greater ratio coefficient would have been pointless.

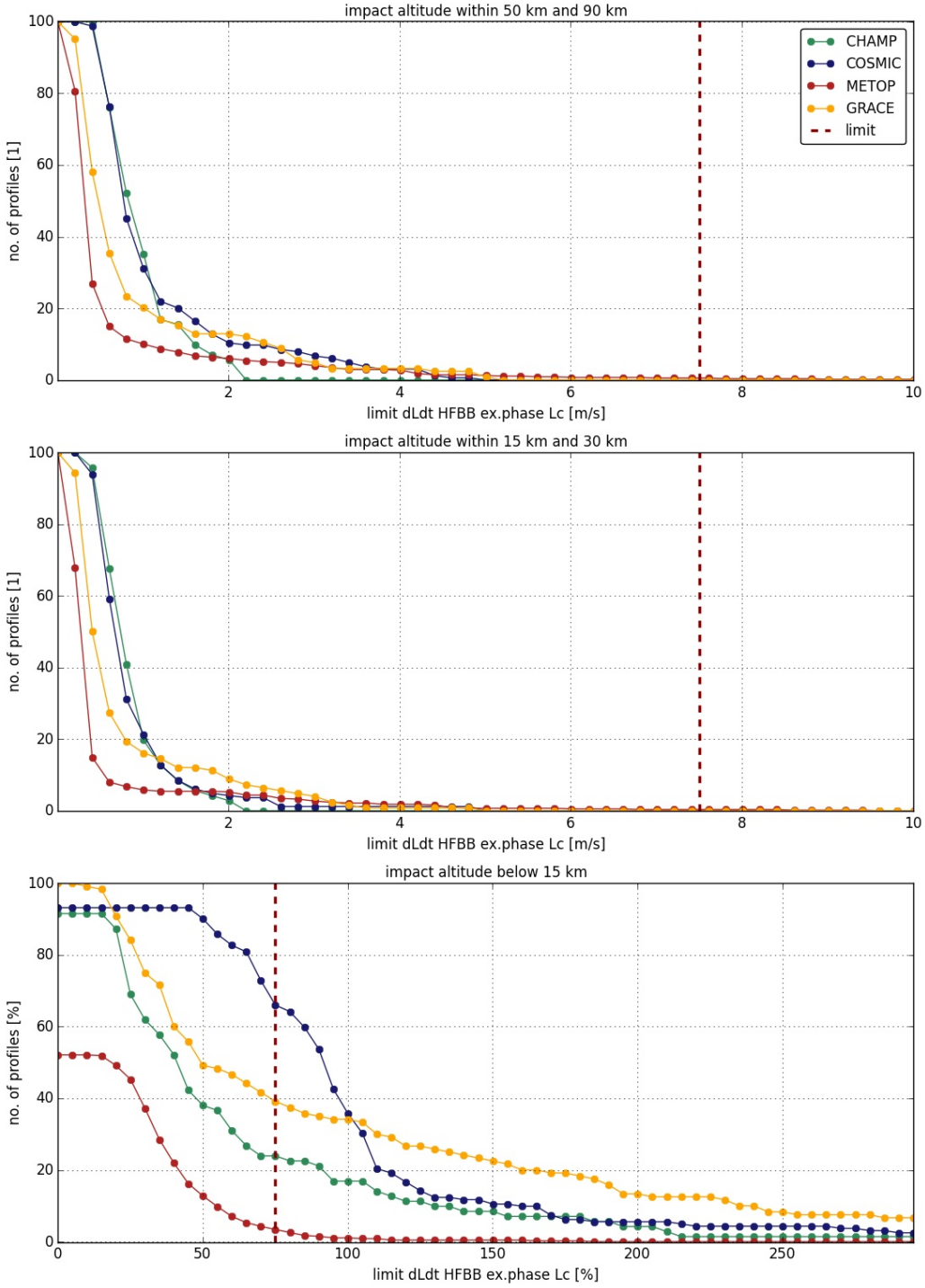

Figure 3.17: Relation between the bound value and the number of profiles, not passing the smoothness check. The different colours distinguish between the satellites, the dashed red lines marks the final chosen limit in this impact altitude range. The top panel considered profiles only in an impact altitude range of 50 km to 90 km, the middle panel between 15 km and 30 km and the bottom panel in an impact altitude range lower 15 km.

3.7 Assignment of Bottom Impact Altitude Level of Excess Phase L1

The previous QC checks reviewed the profiles between the determined top impact altitude level ($z_{a\mathrm{Top}}^{\mathrm{Lc}}$) and bottom impact altitude level ($z_{a\mathrm{Bot}}^{\mathrm{L2}}$) and focused on the review of the bottom impact altitude level of L2 only.
Therefore, the last required step of the QC is the validation of the bottom impact altitude level of L1 ($z_{a\mathrm{Bot}}^{\mathrm{L1}}$). In this section the excess phase L1 itself is used. Due to that, the limits of bounds and smoothness check are adjusted. Because the top impact altitude level of excess phase L1 is already set ($z_{a\mathrm{Top}}^{\mathrm{L1}} = z_{a\mathrm{Top}}^{\mathrm{Lc}}$), only the part of the profiles, where the impact altitude is lower 30 km, is analyzed.
The Figure 3.18 illustrates bounds and smoothness check. One can see in the left panel, that the bounds check boundary has a similar shape as before for BB excess phase Lc. The difference lies in the range of permitted values; before limitations where in a cm-range, whereas now values up to several meters are allowed. Because even after neglecting an offset (between excess phase L1 and excess phase Lm), the difference to model phase dissipates progressively when going downwards. The right panel represents the boundary of smoothness check for L1. In contrast to the smoothness check on the excess phase Lc, the limit for the boundary relaxes into a constant value of 30 m/s in the relative limit impact altitude regime.

The changes of boundary values for excess phase L1 in detail:

- bounds check
  - $\Delta L_{\mathrm{TLS,abs}}^{\mathrm{BC}} = 0.3\,\mathrm{m} \rightarrow \Delta L_{\mathrm{abs}}^{\mathrm{BCL1}} = 2\,\mathrm{m}$
  - $\Delta L_{\mathrm{TLS,rel}}^{\mathrm{BC}} = 0.01\,[1] \rightarrow \Delta L_{\mathrm{rel}}^{\mathrm{BCL1}} = 0.1\,[1]$
- smoothness check
  - $\partial L_{\mathrm{abs}}^{\mathrm{SC}} = 7.5\,\mathrm{m/s} \rightarrow \partial L_{\mathrm{TLS,abs}}^{\mathrm{SCL1}} = 3\,\mathrm{m/s}$
  - $\partial L_{\mathrm{rel}}^{\mathrm{SC}} = \partial L_{\mathrm{TLS,rel}}^{\mathrm{SCL1}} = 0.75\,[1] \mathrel{\widehat{=}} 75\%$,
  - $\partial L_{\mathrm{TS,abs}}^{\mathrm{SCL1}} = 30\,\mathrm{m/s}$

The steps for the verification of the bottom impact altitude level of excess phase L1 are as follows:

Box 3.6: The assignment of the bottom impact altitude level of excess phase L1 algorithm

1. Offset correction of excess phase L1:
   Since focusing and working now on excess phase L1, the offset to the model phase has to be corrected again (before outlier detection, the offset was determined in an impact altitude about 60 km, see Section 3.3). For minimizing the bias here, the median of excess phase L1 and excess phase Lm will be calculated in a certain impact altitude range ($z_a \in [27{,}33]$ km):

   $$L_1 = L_1' - (\bar{L}_{1,[27,33]} - \bar{L}_{\mathrm{m},[27,33]}) \tag{3.18}$$

   with L_1' is the excess phase L1 before, $\bar{L}_{o,[27,33]}$ and $\bar{L}_{\mathrm{m},[27,33]}$ the median of the excess phase L1 and excess phase Lm, respectively.

2. Perform bounds check on BB excess phase L1:
   Check if BB excess phase ($\delta L_{1\mathrm{m}}(z_a)$), in the impact altitude range of $z_a \in [z^{\mathrm{L1}}_{a\mathrm{Bot}}, z^{\mathrm{Lc}}_{a\mathrm{Top}}]$, is within boundary ($\Delta L^{\mathrm{BCL1}}$):
   $|\delta L_{1\mathrm{m}}| < \Delta L^{\mathrm{BCL1}}$
   - Pass → set bottom impact altitude level as: $z^{\mathrm{L1}}_{a\mathrm{Bot,BC}} = z^{\mathrm{L1}}_{a\mathrm{Bot}}$
   - Fail → define new bottom impact altitude level ($z^{\mathrm{L1}}_{a\mathrm{Bot,BC}}$) and set $\mathrm{QC}^{\mathrm{L1}}_{\mathrm{BC}}$ flag $\neq 0$ in ranges below the newly defined $z^{\mathrm{L1}}_{a\mathrm{Bot,BC}}$.

3. Perform smoothness check on derivative of HFBB excess phase L1:
   Check if derivative of HFBB excess phase L1 ($\partial L_{1\mathrm{HF}}(z_a)$)
   is in the range of impact altitude $z_a \in [z^{\mathrm{L1}}_{a\mathrm{Bot}}, z^{\mathrm{Lc}}_{a\mathrm{Top}}]$ within the boundary ($\partial L^{\mathrm{SCL1}}$):
   $|\partial L_{1\mathrm{HF}}| < \partial L^{\mathrm{SCL1}}$
   - Pass → set bottom impact altitude level $z^{\mathrm{L1}}_{a\mathrm{Bot,SC}} = z^{\mathrm{L1}}_{a\mathrm{Bot}}$
   - Fail → define new bottom impact altitude level $z^{\mathrm{L1}}_{a\mathrm{Bot,SC}}$ and set $\mathrm{QC}^{\mathrm{L1}}_{\mathrm{SC}}$ flag $\neq 0$ in ranges below the newly defined $z^{\mathrm{L1}}_{a\mathrm{Bot,SC}}$.

4. Compare $z^{\mathrm{L1}}_{a\mathrm{Bot,BC}}$ with $z^{\mathrm{L1}}_{a\mathrm{Bot,SC}}$:
   Set the one at higher impact altitude as $z^{L1}_{a\mathrm{Bot}}$

5. Compare $z^{\mathrm{L1}}_{a\mathrm{Bot}}$ with $z^{L2}_{a\mathrm{Bot}}$:
   If $z_{a\mathrm{Bot,L2}} < z_{a\mathrm{Bot,L1}} \rightarrow z^{\mathrm{L1}}_{a\mathrm{Bot}} = z^{\mathrm{L2}}_{a\mathrm{Bot}}$

Principally, the excess phase L1 profiles are of higher quality than excess phase

L2 profiles. The profiles, when reaching this part of the QC, already passed the entire tests before, wherefore it will be assumed, that an adequate quality is already proofed. Hence the boundary limits for bounds and smoothness check L1 are chosen more roughly and verify rather logical limits.
The Figures 3.19 and 3.20 show the statistical results for bounds check L1 and smoothness check L1, respectively. The y-axes exhibit the number of profiles, with an exceeding standard deviation in an impact altitude range between 20 km and 30 km (top panel) and for impact altitudes lower 20 km (bottom panel), corresponding to a certain boundary limit (x-axes).
Looking at the top panel of Figure 3.19 one can see, that the saturation occur at about a boundary limit of 0.75 m. Despite of that, the limit $\Delta L_{\text{abs}}^{\text{BCL1}} = 2\,\text{m}$ is set, because the previously done offset correction is in these impact altitude levels not efficiently enough, that it can be guaranteed, that the excess phase L1 will not exceed this boundary due to an natural atmosphere influence.

The bottom panel of Figure 3.19 presents the evaluation of the relative value for the lower regions. Here the saturation is not completely reached, but looking at the results in Chapter 4, Section 4.4, it is shown that the resulting bound value is already chosen bare tolerant, and most of the profiles exceed the limit only in the lowest impact altitudes.
In Figure 3.20 the statistical results for smoothness check L1 are given. It is unequivocal that the chosen boundary limits are again very tolerant. This is also a consequence of the consideration, that ex.phases already reach a wideness of around one kilometer in this low impact altitudes. The 5-point derivative of HFBB excess phase L1 reflects the change of noise within a tenth of a second (in case of $f_s = 50\,\text{Hz}$) and the most bottom bound value of 30 m/s shall be a very rough threshold to avoid a huge rise of noise in the signals.

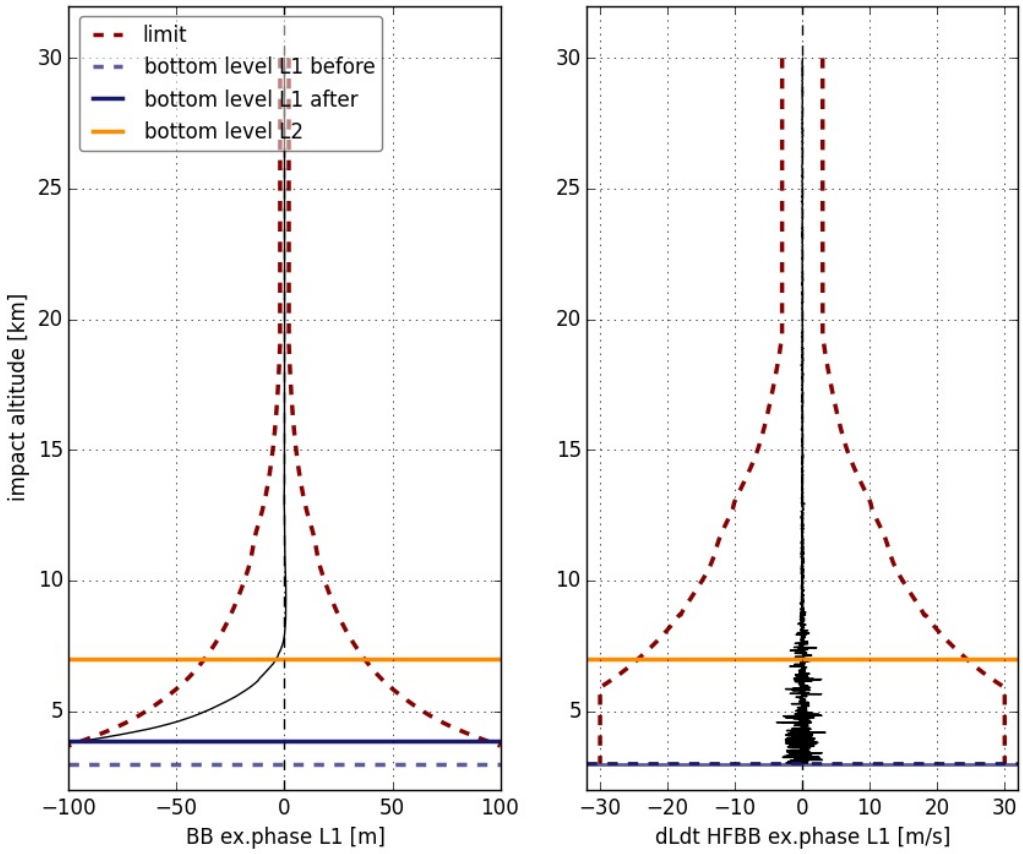

Figure 3.18: Operating principle of bounds and smoothness check L1. The left panel illustrates the procedure of bounds check, the right panel of smoothness check. The yellow line marks the final assigned bottom impact altitude level for excess phase L2, the blue line for excess phase L1 and the dotted blue line marks the impact altitude level, that was estimated at the assignment of bottom impact altitude level before for excess phase L1 (see Section 3.5.2). (CHAMP-RO event, 15 July 2008, 12:26:58 UTC)

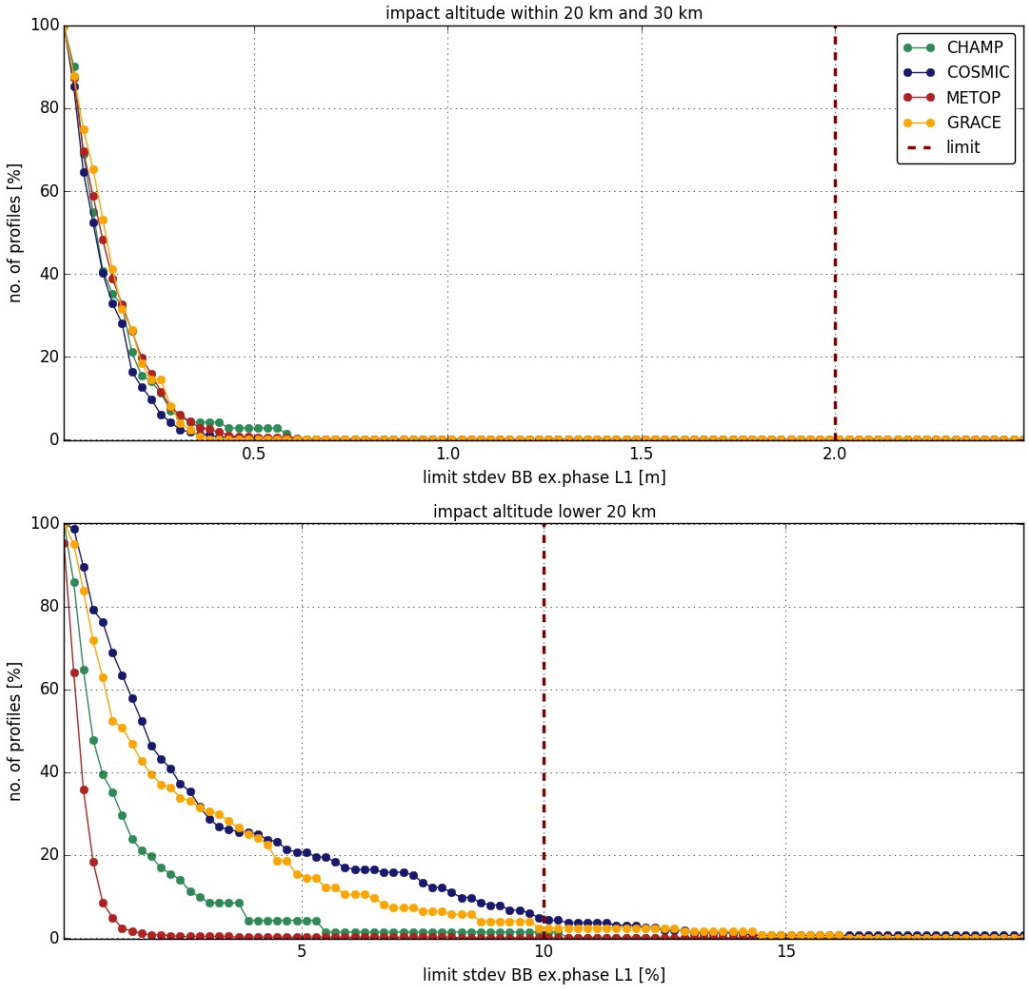

Figure 3.19: Relation between the bound value and the number of profiles, not passing the bounds check L1 for the different satellites. The top panel shows the BB excess phase L1 only in an impact altitude range between 20 km to 30 km, the bottom panel shows the results for the range with impact altitudes lower 20 km.

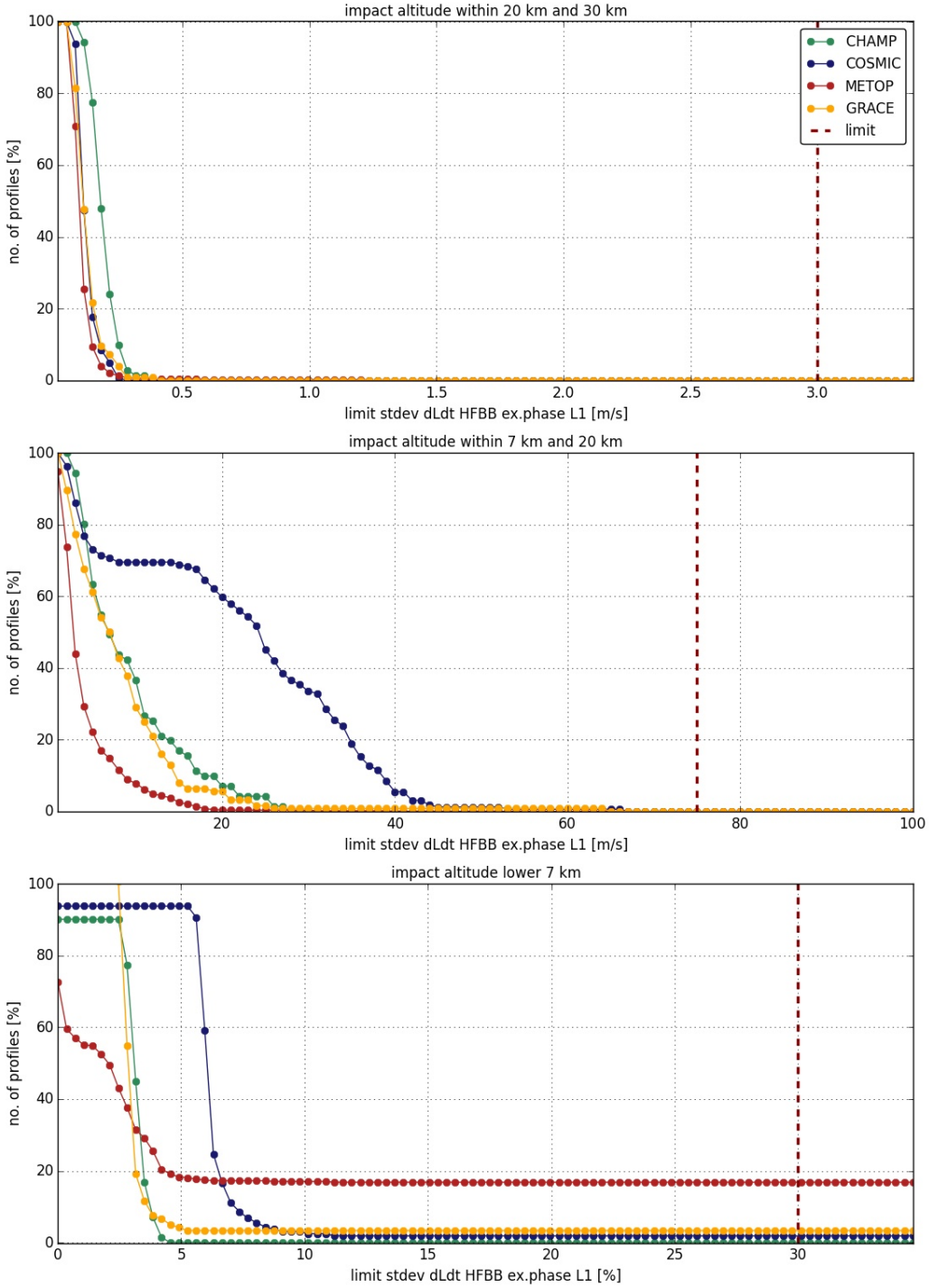

Figure 3.20: Relation between the bound value and the number of profiles, not passing the smoothness check L1 for the different satellites. The top panel shows the HFBB excess phase L1 in an impact altitude range between 20 km to 30 km, the middle one in a range between 7 km and 20 km and the bottom panel shows the phases in a range lower 7 km.

4 Results

Following chapter gives step-wisely and in detail the results of the analyses on the single QC steps as introduced in Chapter 3, where in demonstration plots are given.

4.1 Outlier Detection and Correction

The aim of the outlier correction is the detection and replacement of (non-physical) data values, that are significantly farther apart than the others, to provide a robust basis for an average- and standard deviation-based process.
Following Figures 4.1 and 4.2 illustrate the achievement of the outlier correction. Therefore, one can see the difference between raw exess phases before and after the outlier correction for excess phase L1 and excess phase L2, respectively. The different colors declare the various climate regions. The title displays the amount out of all of profiles, where at least one outlier has been detected, in total and percentage. By comparing the results for excess phase L1 and L2, it is clearly shown, that excess phase L2 hase more detected and corrected outliers than excess phase L1. For ex.phase L1, a few amount of outliers are detected, which are almost exclusively located in very high or low impact altitudes. Whereas for ex.phase L2, a lot more corrections have been done; also in the important impact altitude range between 25 km and 70 km. But it is remarkable, that for the CHAMP profiles, even the excess phase L2 data have rather less detected outliers.
Moreover has to be noted, that in the actual implementation of the QC in the rOPS after the L1a process, the profiles will be checked only in an impact altitude range below 90 km. Therefore, even less outlier are situated in the profiles.

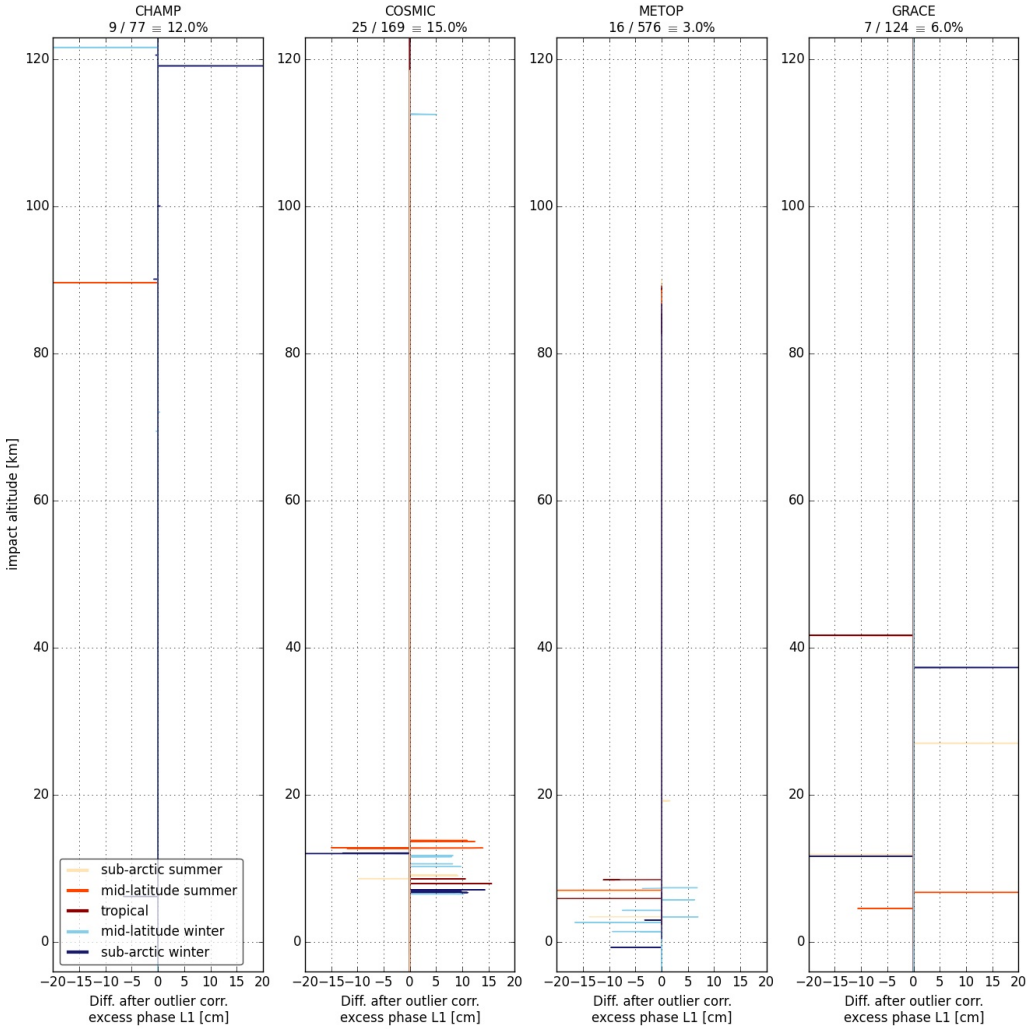

Figure 4.1: Difference between raw excess phase L1 and outlier corrected excess phase L1 for the four satellites. The title presents the amount of profiles, where at least one outlier has been detected, the different colors illustrate the various climate ranges.

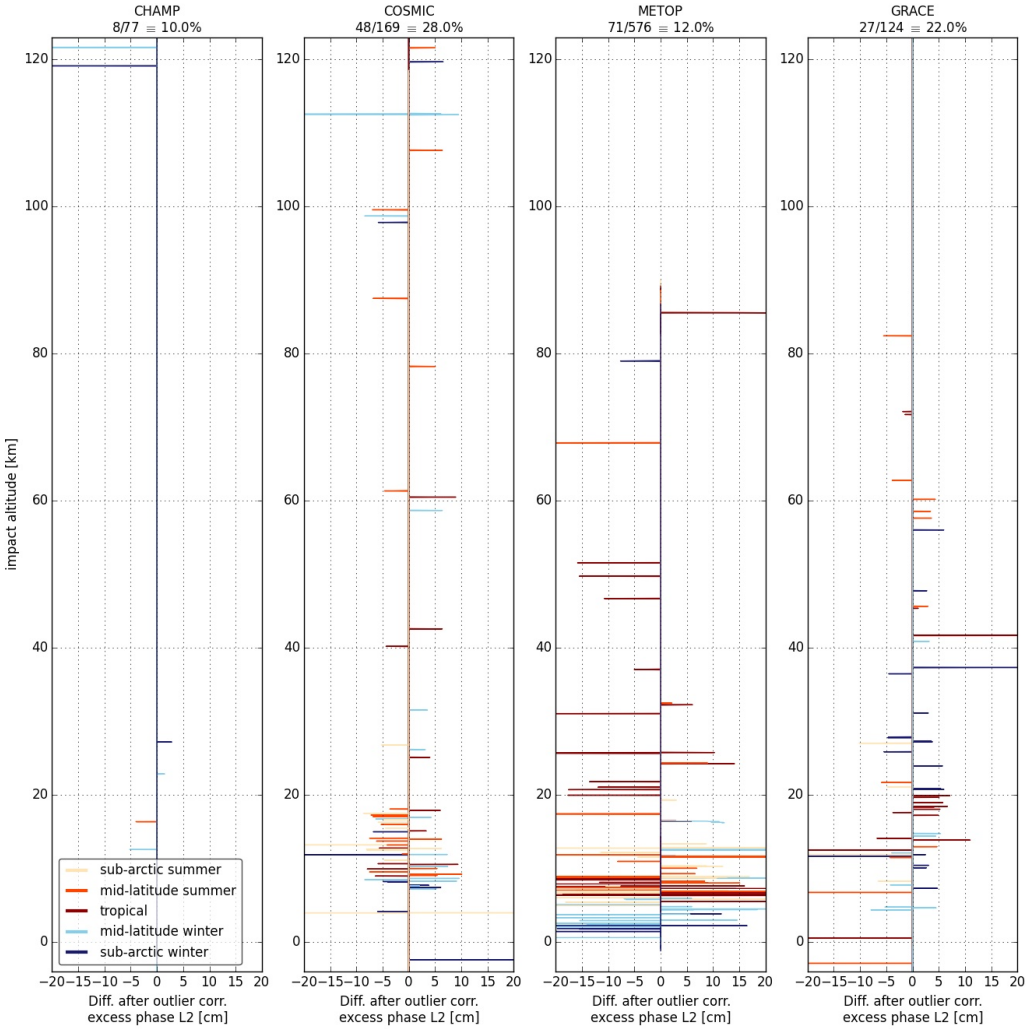

Figure 4.2: Difference between raw excess phase L2 and outlier corrected excess phase L2 for the four satellites. The title presents the amount of profiles, where at least one outlier has been detected, the different colors illustrate the various climate ranges.

4.2 Assignment of Impact Altitude Range

Following section exhibits the results of the estimation of the top impact altitude level ($z_{a\mathrm{Top}}$) and bottom impact altitude level ($z_{a\mathrm{Bot}}$). The aim of this routine is to evaluate the profiles in the highest and lowest impact altitudes and set a new top and bottom level, to truncate the parts of the profiles, where the data's quality is not sufficient. In the subsequent Section 4.3, the profiles will be checked only within these impact altitude levels.

4.2.1 Assignment of Top Impact Altitude Level

The assignment of the top impact altitude level ($z_{a\mathrm{Top}}$) is done on the moving standard deviation of the BB excess phase Lc and will be adopted for the excess phase L1 and L2.

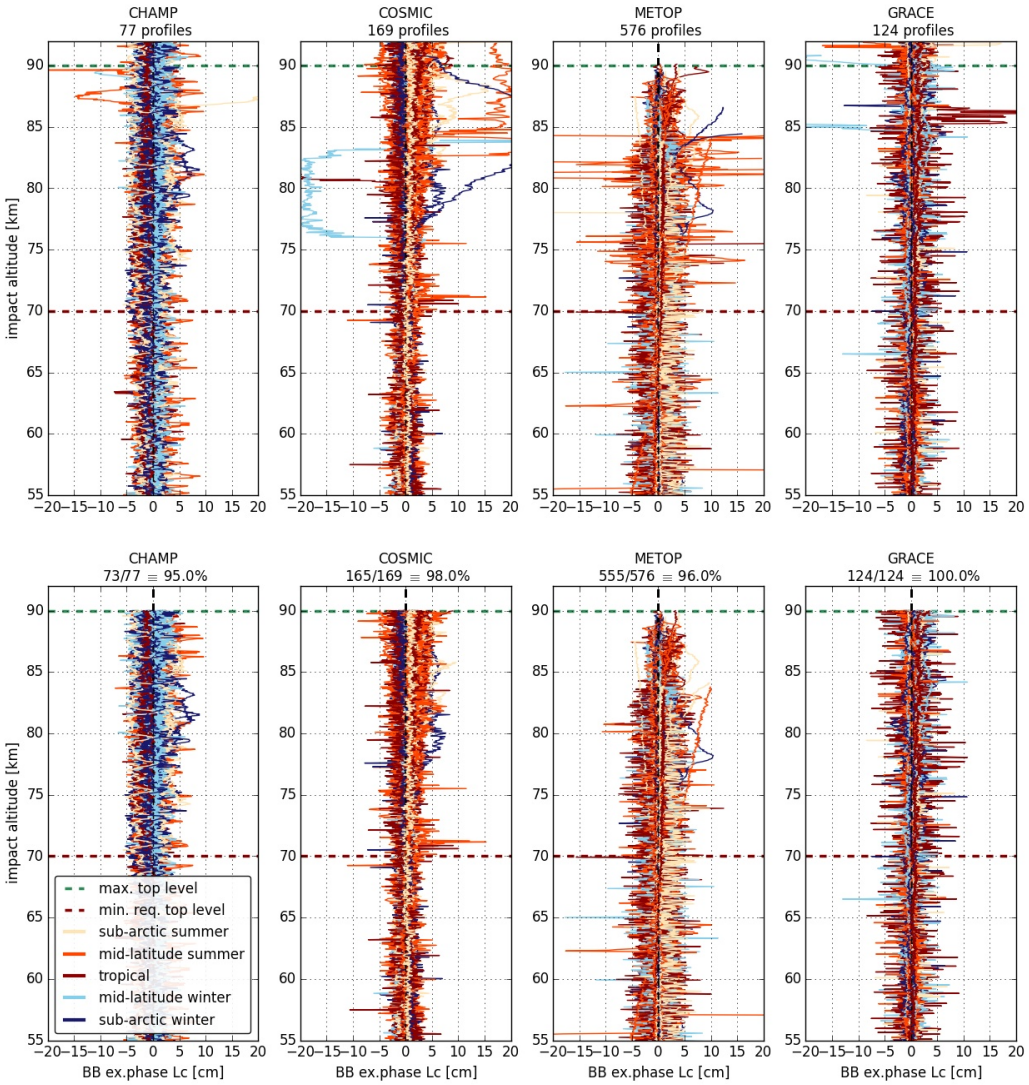

Figure 4.3: BB excess phase Lc before (top panel) and after (bottom panel) the assignment of the top impact altitude level. The green line marks the highest possible impact altitude level and the red line the minimum required one that has to be reached. The different colours illustrate the diverse climate regions. The title shows the total amount of profiles, the ratio in bottom panel's title, illustrates how many files passed the check out of all profiles in total and percentage.

Figure 4.3 shows the fairly unbiased BB signals of Lc before (top row) and

after (bottom row) setting a new top impact altitude level. The highest permitted altitude level is at an impact altitude of 90 km, although plenty of profiles have an adequate high quality above.
Comparing these two graphs, demonstrates how efficient the estimation, by checking the moving standard deviation works. The profiles with a readjusted top impact altitude level do not exhibit any remarkable outstanding deviations. Also profiles with a bias jump, (for example light blue line in second panel of Figure 4.3) have been detected and removed.

The amount of profiles, which have been rejected, due to an assigned top impact altitude level lower than the minimum required one ($z_{a\mathrm{Top}}^{\mathrm{min}} = 70\,\mathrm{km}$), is in general very small; for satellite GRACE it is in fact zero.
Figure 4.4 shows the related moving stdevs of the BB excess phase Lc before (top row) and after (bottom panel) the assignment. The behavior of the stdev after the readjustment of the top impact altitude level of the profiles is highly satisfying. The majority of profiles have a standard deviation below 1 cm. Only in the third panel of the second row (satellite METOP), some values strongly increase at the bottom of the graph. They have been undetected, due to the limited observation range of impact altitudes between 60 km and 90 km.
This demonstrates, the importance of the following QC checks (see Section 4.3), to check the profiles within the assigned top and bottom impact altitudes levels to ensure continuous qualitative excess phase profiles.

4.2.2 Assignment of Bottom Impact Altitude Level

Instead of using excess phase Lc, excess phase L1 and L2 have been used to determine the bottom impact altitude level ($z_{a\mathrm{Top}}$). As already mentioned in Section 3.5.2, the phase delay strongly increase with decreasing impact altitude and increase its noise at about an impact altitude between 10 and 15 km, which can be also seen in Figures 4.7 and 4.8, which displays the moving standard deviations of the HFBB excess phase L1 and L2. Furthermore the difference in quality between HFBB excess phase L1 and L2 is evident (see Figure 4.5 and 4.5).

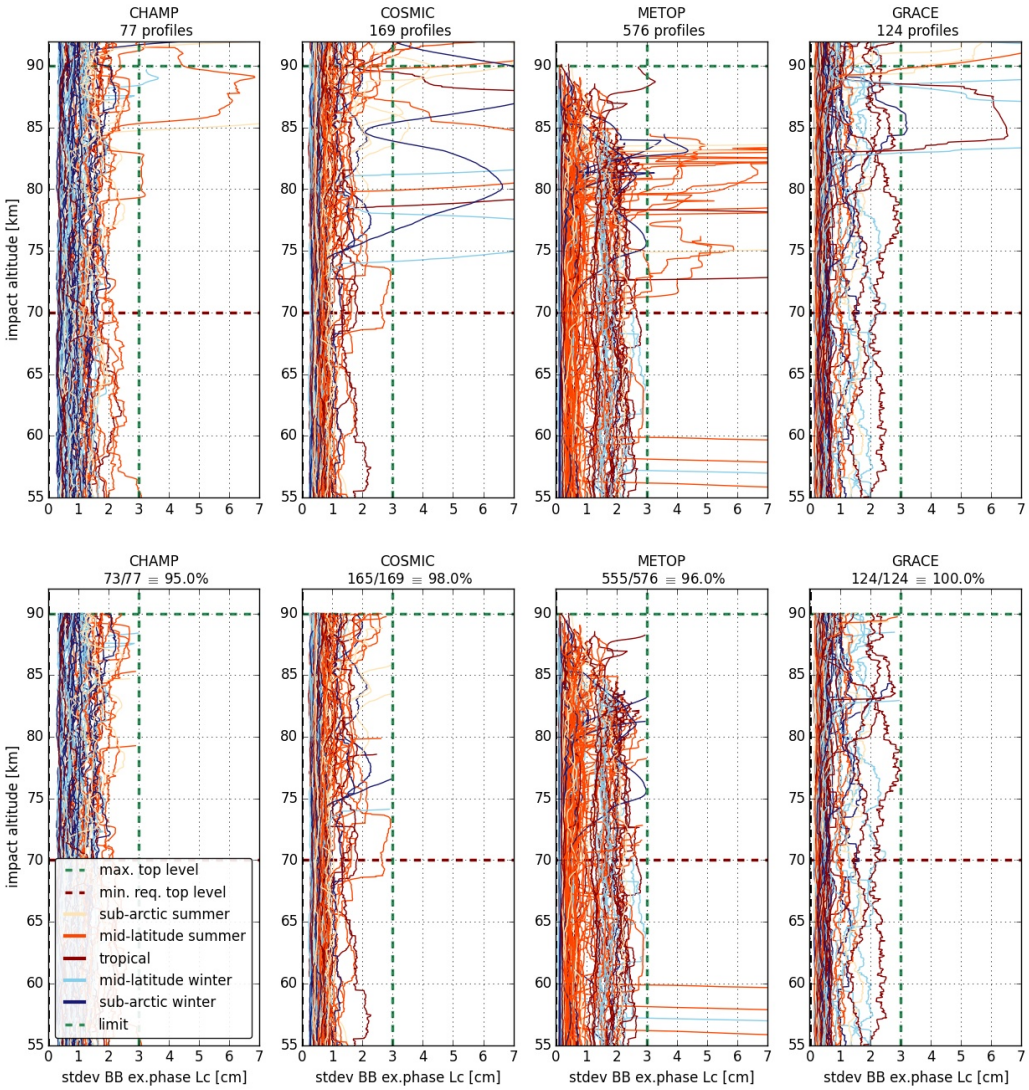

Figure 4.4: Moving standard deviation of BB excess phase Lc before (first row) and after (second row) the assignment of the top impact altitude level. The vertical green line (vertical) marks the chosen limit of 3 cm for the stdev, the horizontal green line marks the highest possible impact altitude level, the horizontal red line (horizontal) marks the minimum required one and the different colours illustrate the diverse climate regions. The title shows the total amount of profiles, the ratio in bottom panel's title, illustrates how many files passed the check out of all profiles in total and percentage.

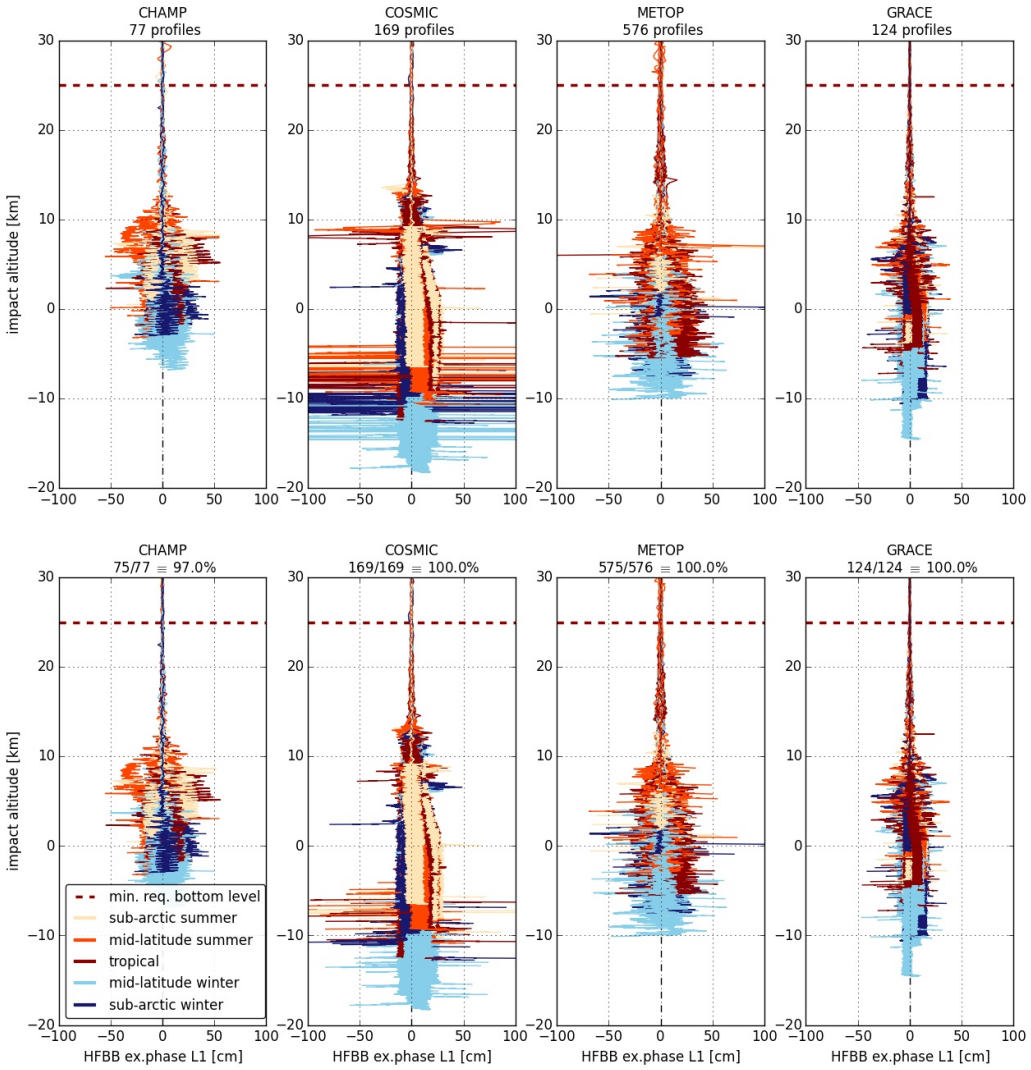

Figure 4.5: HFBB excess phase L1 before (first row) and after (second row) the assignment of the bottom impact altitude level. The red dashed line marks the minimum required bottom impact altitude level, the different colours illustrate the diverse climate regions. The title shows the total amount of profiles, the ratio in bottom panel's title, illustrates how many files passed the check out of all profiles in total and percentage.

For HFBB excess phase L1, the signal-to-noise ratio increases rather fast up to an certain level, but stays afterwards fairly constant. In contrast to ex.phase L2, which gets larger and larger by going towards bottom. As a result, the excess phase L1 achieves lower impact altitudes for the bottom impact altitude level than excess phase L2.

When comparing the various satellite excess phase L1 profiles with each other, it is noticeable, that except for COSMIC in the most lowest impact altitudes, all signals are without big variations. For the derivative of HFBB excess phase L2, the performance of satellite METOP profiles seems to be the best.

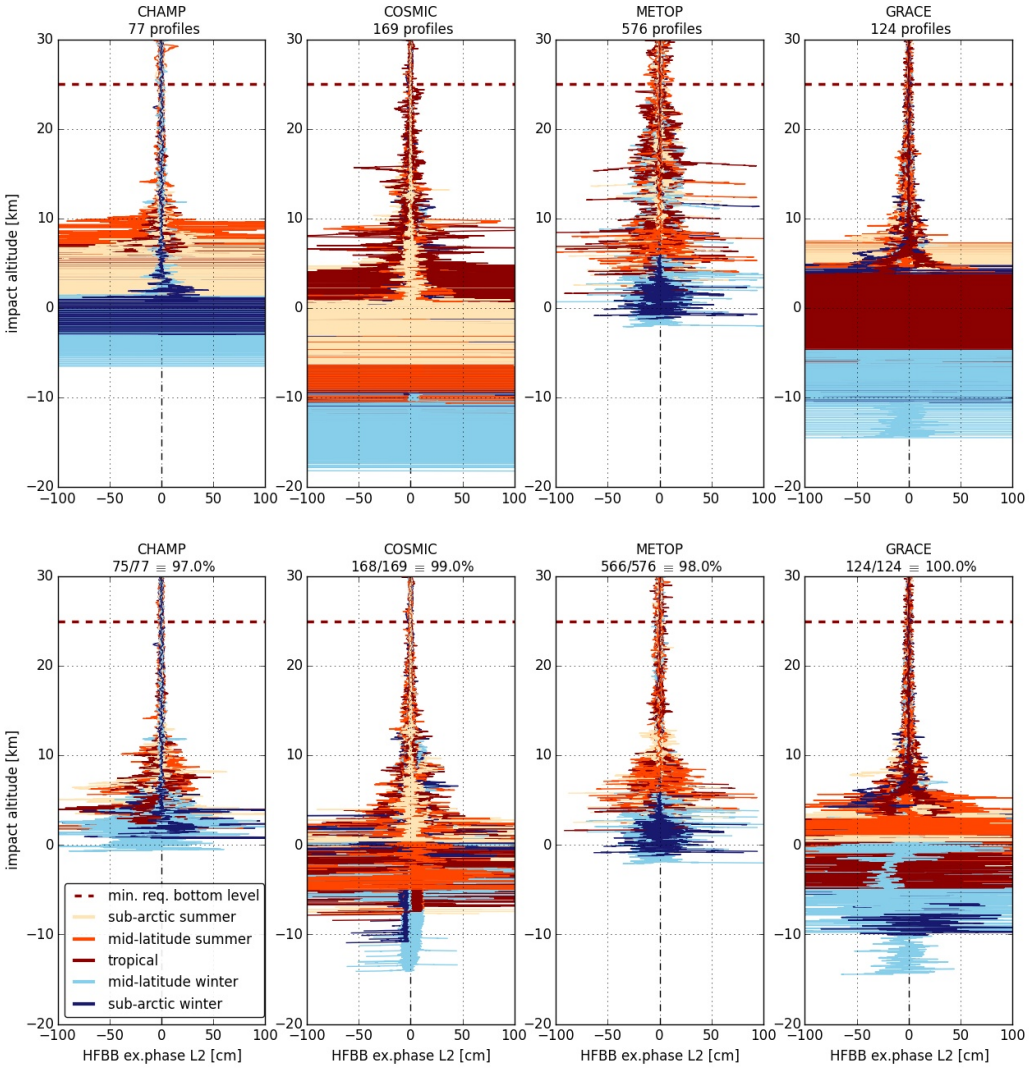

Figure 4.6: HFBB excess phase L2 before (first row) and after (second row) the assignment of the bottom impact altitude level. The red dashed line marks the minimum required impact altitude level, the different colours illustrate the diverse climate regions. The title shows the total amount of profiles, the ratio in bottom panel's title, illustrates how many files passed the check out of all profiles in total and percentage.

The Figures 4.7 and 4.8 presenting the moving standard deviation of the HFBB excess phase L1 and L2 and emphasize the difference between the various climate regions. Profiles in the sub-arctic (winter) regions have a remarkable lower standard deviation than profiles from tropics. The excess phase Lm take this into account, by exhibiting larger values for tropics than for colder areas. Therefore the choice of combining an absolute with an relative value (which corresponds to the excess phase Lm) as boundary limit is strengthen, since all profiles are so quantitatively treaten equally.

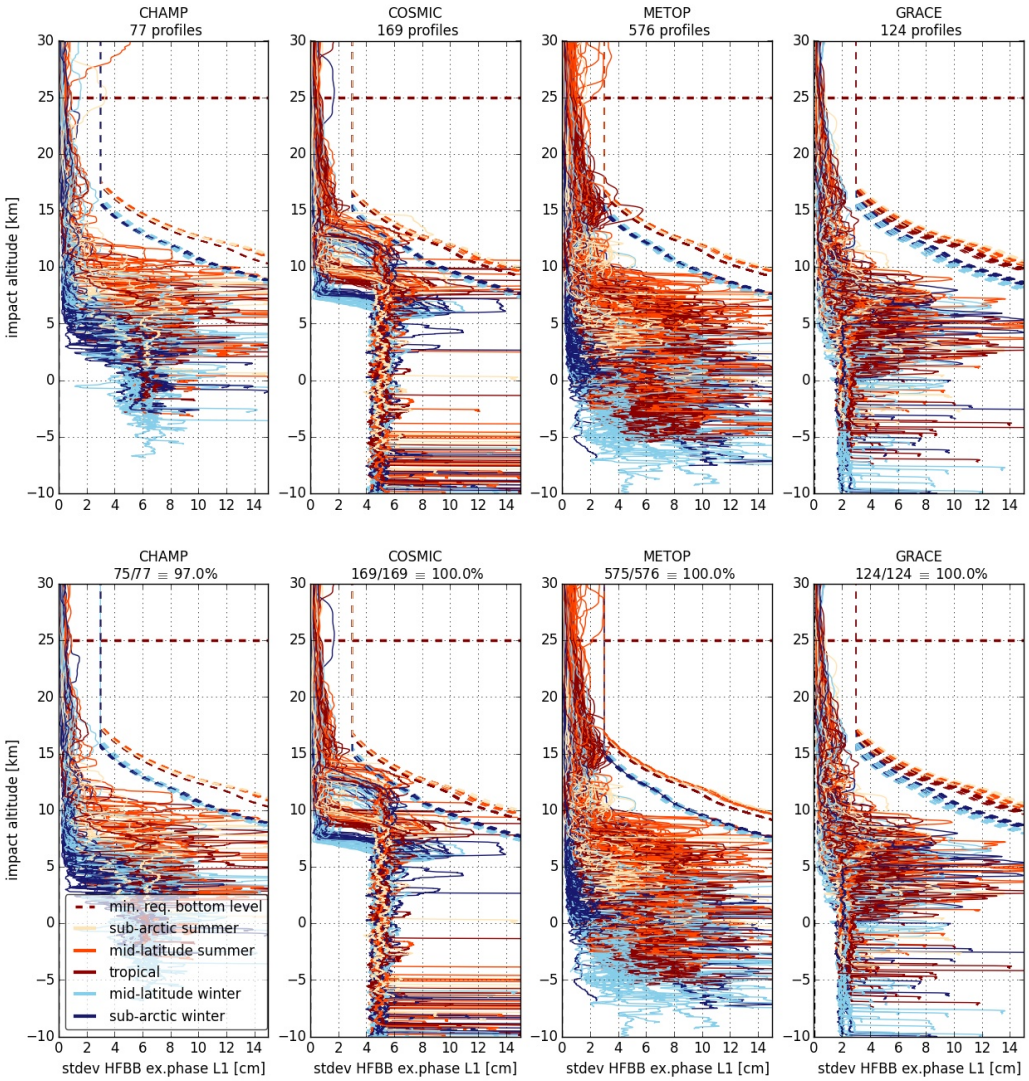

Figure 4.7: Moving standard deviation of HFBB excess phase L1 before (first row) and after (second row) the assignment of the bottom impact altitude level. The red dashed line marks the minimum required impact altitude level, the different colours illustrate the diverse climate regions, the corresponding dashed lines mark the limit for the moving standard deviation depending on the particular climate region of the profile. The title shows the total amount of profiles, the ratio in bottom panel's title, illustrates how many files passed the check out of all profiles in total and percentage

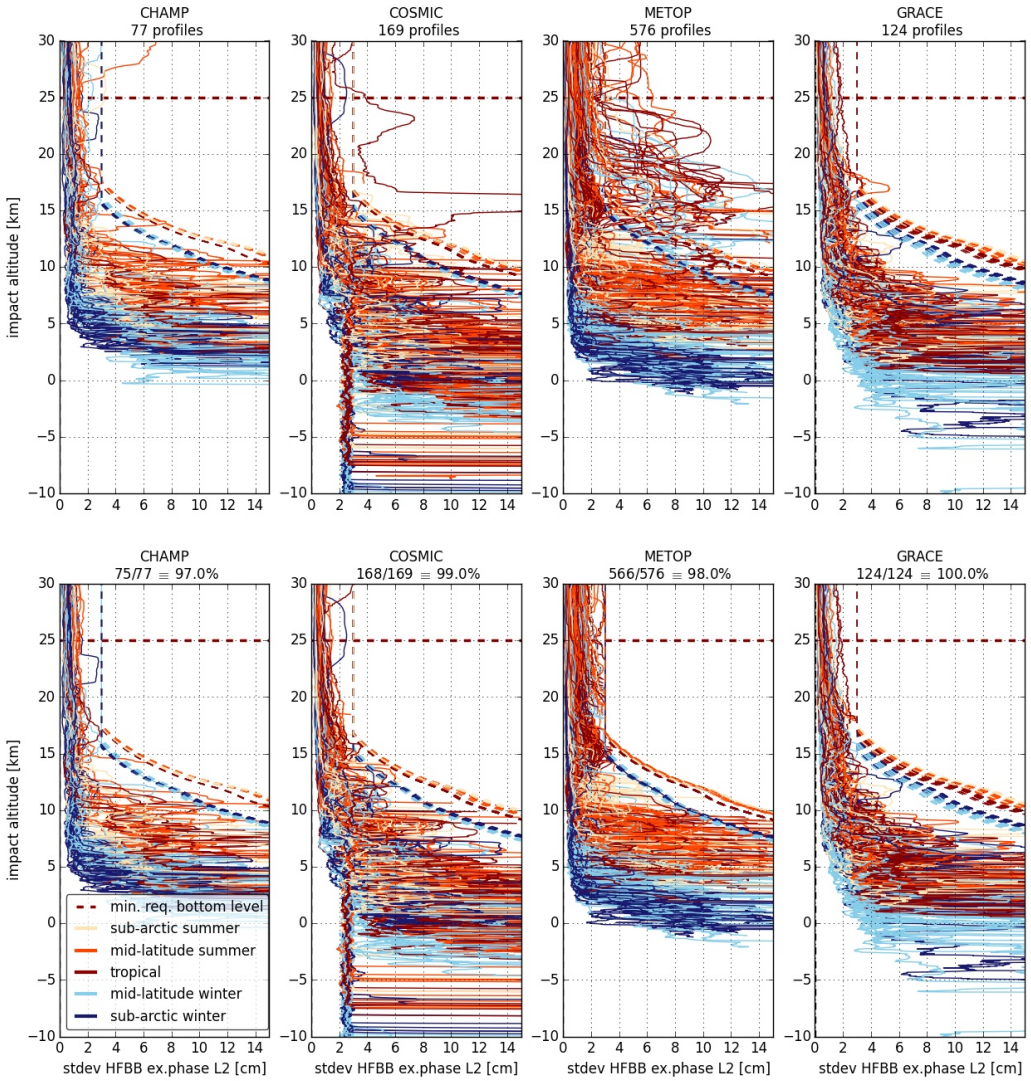

Figure 4.8: Moving standard deviation of HFBB excess phase L2 before (first row) and after (second row) the assignment of the bottom impact altitude level. The red dashed line marks the minimum required impact altitude level, the different colours illustrate the diverse climate regions, the corresponding dashed lines mark the limit for moving standard deviation depending on the particular climate region of the profile. The title shows the total amount of profiles, the ratio in bottom panel's title, illustrates how many files passed the check out of all profiles in total and percentage

4.3 Quality Check of Data Values

In this section, the results for bounds and smoothness check are illustrated.
The validation of these two checks are performed on the excess phase Lc within the previously determined top impact altitude level ($z^{\mathrm{Lc}}_{a\mathrm{Top}}$) and bottom impact altitude level ($z^{\mathrm{Lc}}_{a\mathrm{Bot}}$=$z^{\mathrm{L2}}_{a\mathrm{Bot}}$).
The checks are sucessive; if a profile does not pass the bounds check it will be not further processed to the smoothness check.
Each of the following Figures contains in the title, the name of the specific satellite and a ratio. For the Figures 4.9 and 4.12, the ratio presents the amount of profiles that passed the check.
The number in brackets, depicts the amount of profiles, where top and/or bottom impact altitude level has been readjusted to pass the check. For the other figures, the ratio displays the amount of profiles that did not pass.

4.3.1 Bounds Check

In following Figures 4.9, 4.10 and 4.11) the BB excess phases Lc, with included bounds check-boundaries are shown.

Figure 4.9 presents the profiles, which passed the bounds check. Except for satellite METOP (third panel), all profiles passed. But as it can be seen at the numbers in brackets, almost all profiles have a readjusted top and/or bottom impact altitude level, which will be discussed in Section 4.3.3.
The BB excess phases that are mapped in Figure 4.10 are those profiles, which failed the check. All of these profiles have a big bias jump, that justifies the decision of setting the quality flag QC $\neq 0$. Incidentally these profiles are the ones, which had also a big increase in their standard deviation at about an impact altitude of 55 km (see in Figure 4.4). This clarifies the importance of a first determination of top and bottom impact altitude level and the following check of the range within this impact altitude levels via bounds and smoothness check.

In Figure 4.11 the profiles, that already did not pass the altitude check at the assignment of the top and/or bottom impact altitude level (because impact altitude level $z^{\mathrm{Lc}}_{a\mathrm{Top}}/z^{\mathrm{Lc}}_{a\mathrm{Bot}}$ is lower/higher than 70 km/25 km) are shown.
This illustration is intended for the purpose of explanation only, since the profiles would not have been further processed with a quality flag $\mathrm{QC}_{\mathrm{Top}} \neq 0$ or $\mathrm{QC}_{\mathrm{Bot}} \neq 0$. Here, the decision of discarding these profiles gets strengthen because all profiles do not reach the minimum of signal length and exhibit anomalies somewhere in the signal as well.

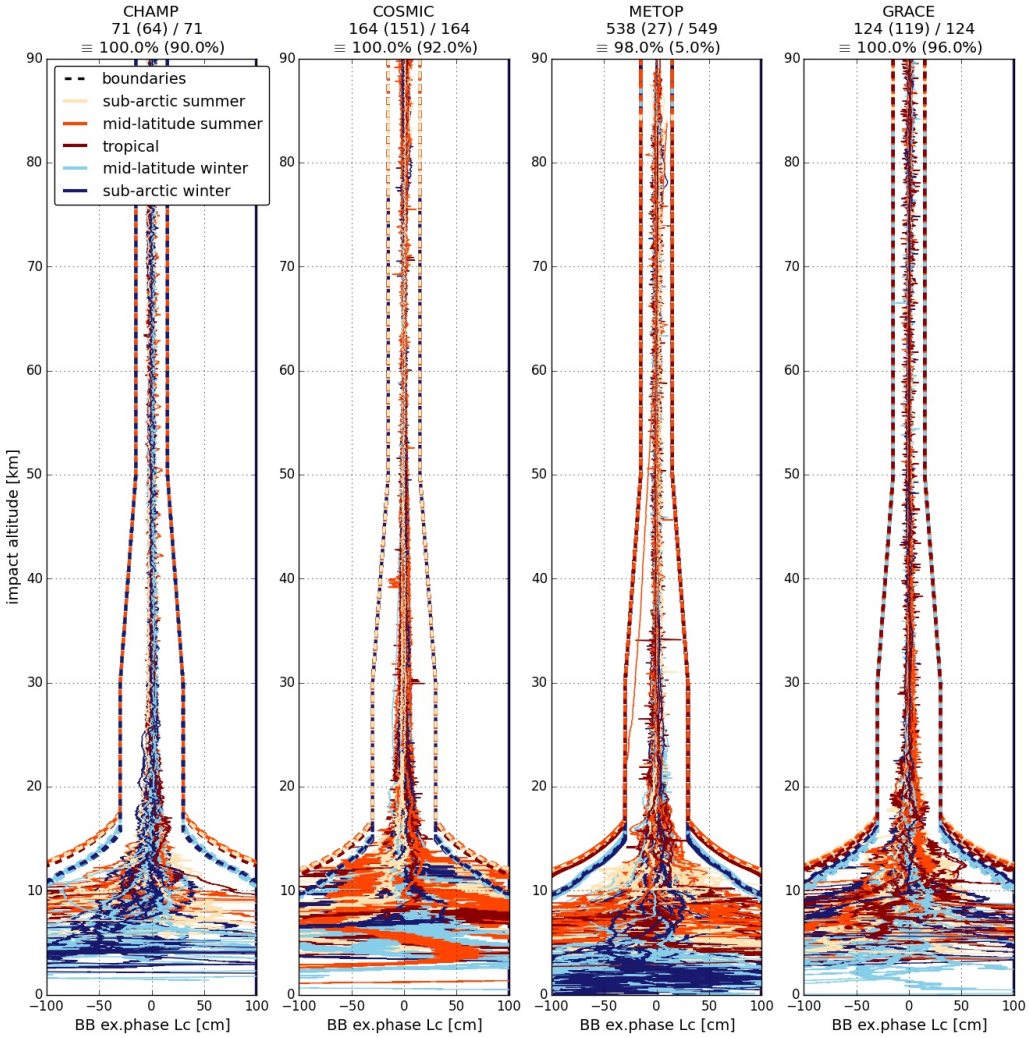

Figure 4.9: BB excess phases of Lc, that passed the bounds check The dashed lines, mark the limit for baseband ex.phases depending on the particular climate region of the profile. At top one can see the number of profiles, that passed the check in total and percentage. The amount in brackets, illustrates the number of profiles that passed only, by re-setting the top and/or bottom impact altitude level.

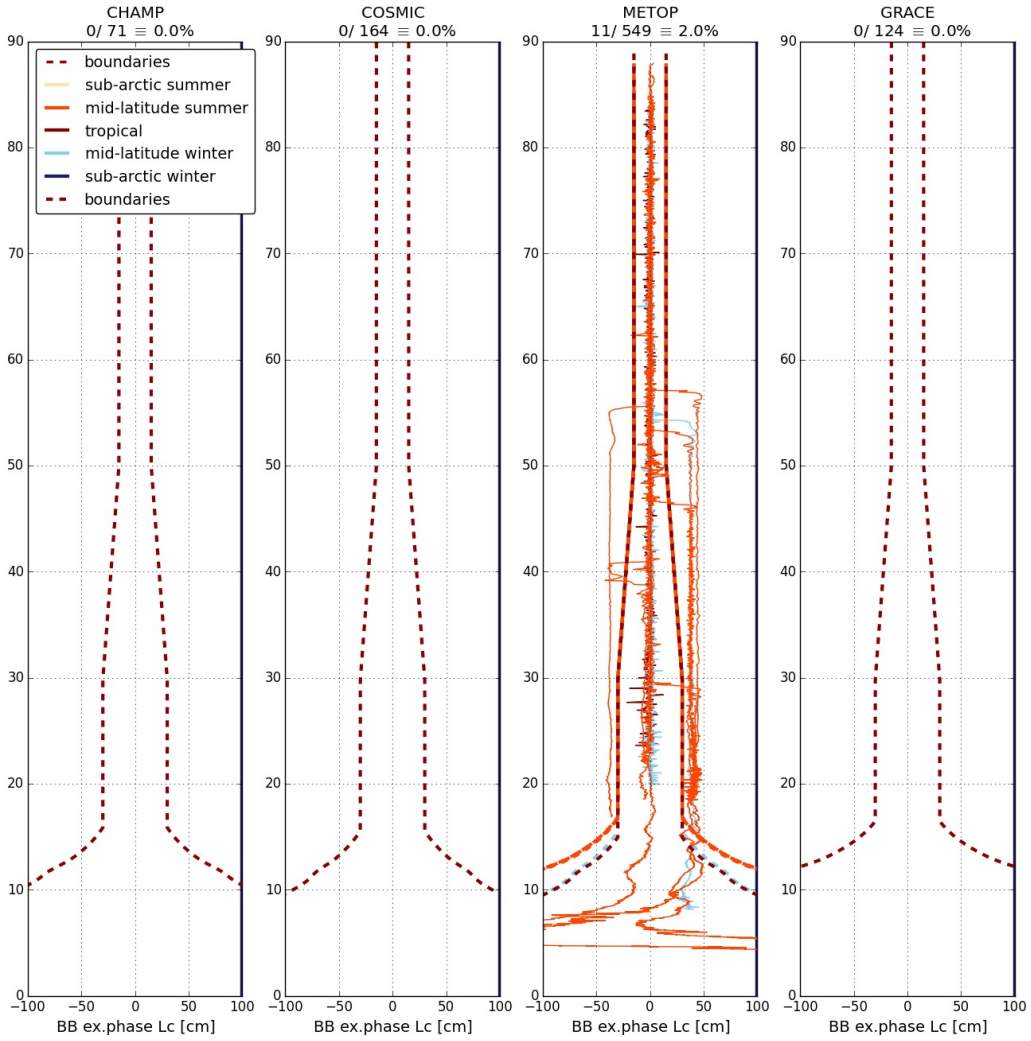

Figure 4.10: BB excess phases of Lc, that did not pass the bounds check. The red dashed line, marks the boundary limit for the BB excess phases. At top one can see the number of profiles, that did not pass the check in total and percentage.

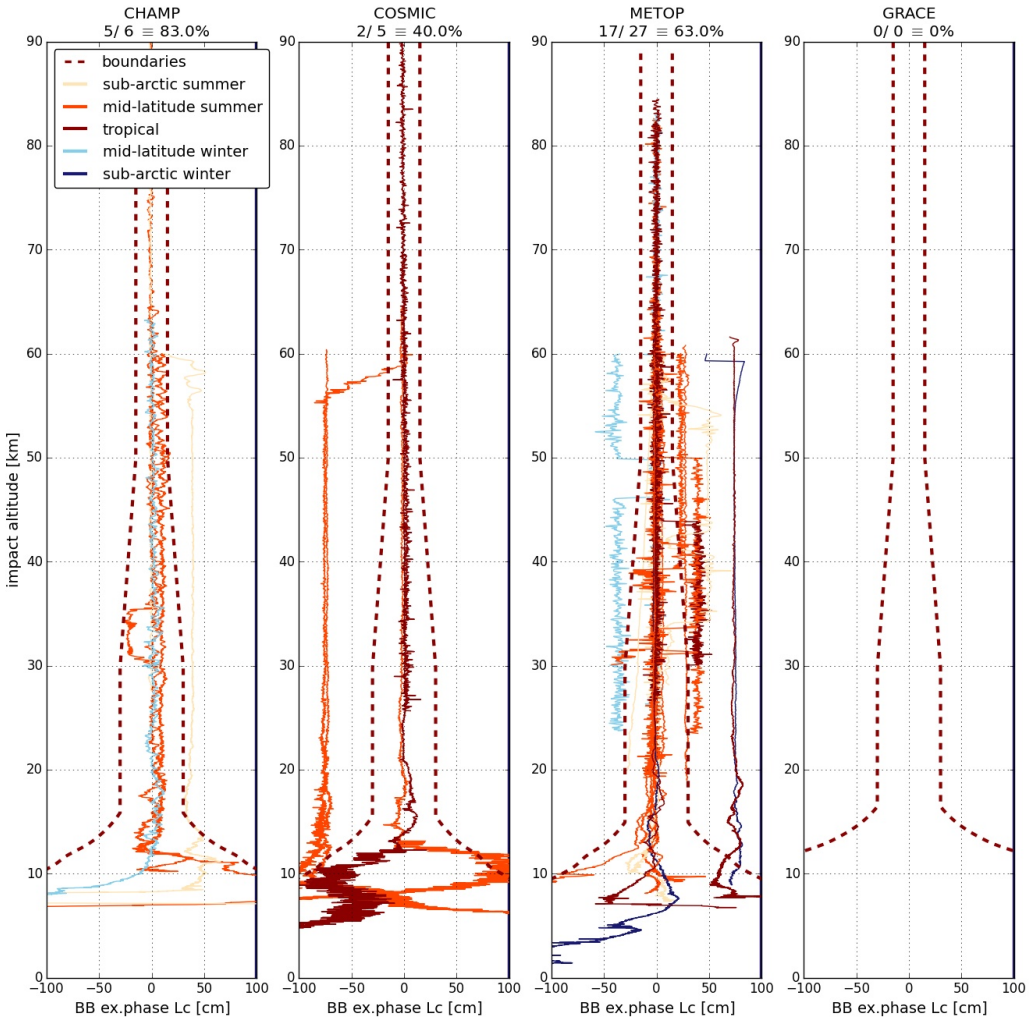

Figure 4.11: BB excess phases of Lc, that did not pass the altitude check at the assignment of the impact altitude levels. The red dashed line, marks the boundary limit for the BB excess phase. At top one can see the number of profiles, that did not pass the altitude check in total.

4.3.2 Smoothness Check

In following Figures 4.12, 4.13 and 4.14, the 5-point derivative of the HFBB excess phases Lc, with included boundaries are illustrated.
Again, except for satellite METOP (third panel) all profiles, after passing bounds check, passed also the smoothnesss-check (see Figure 4.9). As opposed to bounds check, the amount of profiles, with a readjusted top and/or bottom impact altitude (number in brackets in Figure 4.12) to pass the check, is fewer.

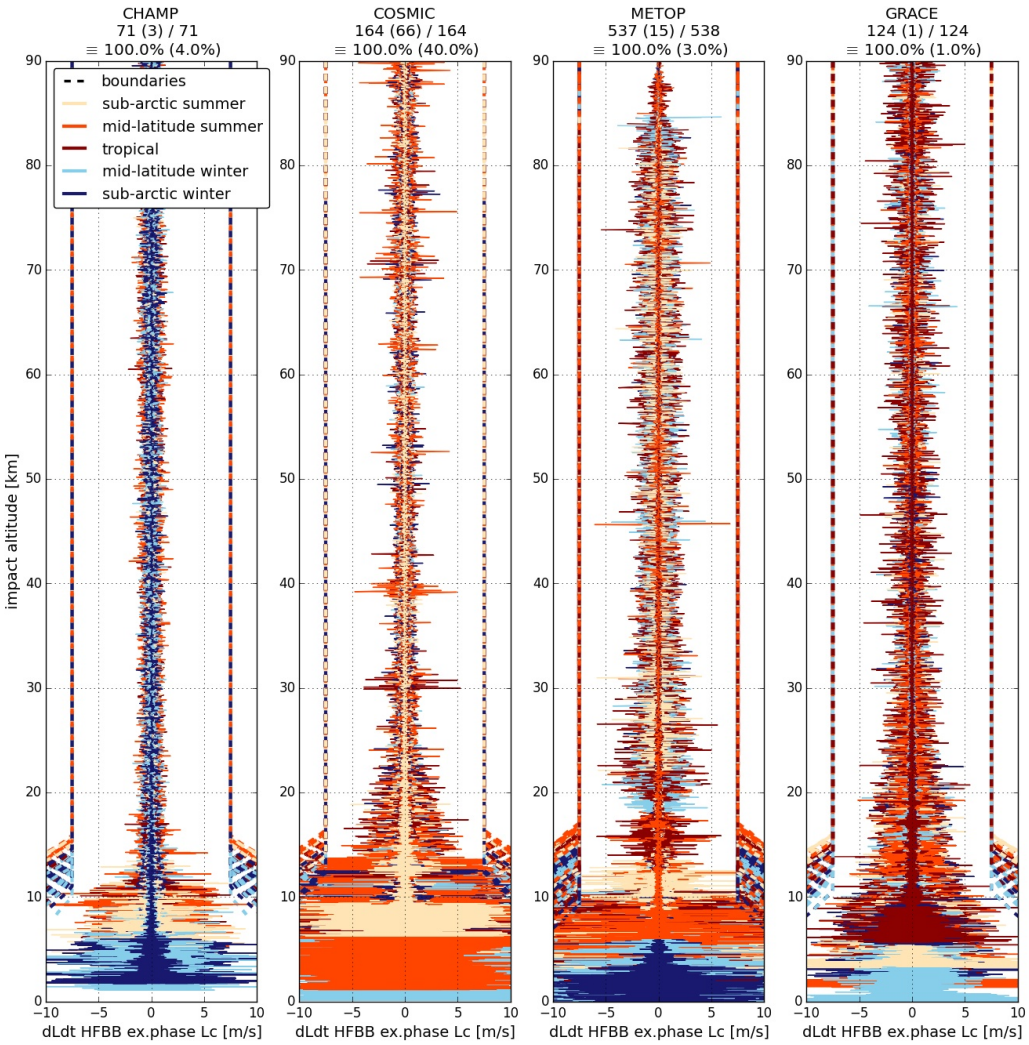

Figure 4.12: Derivative of HFBB excess phases of Lc, that passed the smoothness check for the various sattelites. The dashed lines, mark the boundary limit for derivatives depending on the particular climate region of the profile. At top one can see the number of profiles, that passed the check in total and percentage. The count in the brackets, illustrates the amount of profiles that passed, after a readjustment of the top and/or bottom impact altitude level.

The reason for the smaller amount of failing profiles is on the one hand, that the top/bottom impact altitude levels of many profiles have been already readjusted at the bounds check before the smoothness check. And on the other hand, the relative boudnary value is not as strict as it is for the bounds check (see Figure 4.12).

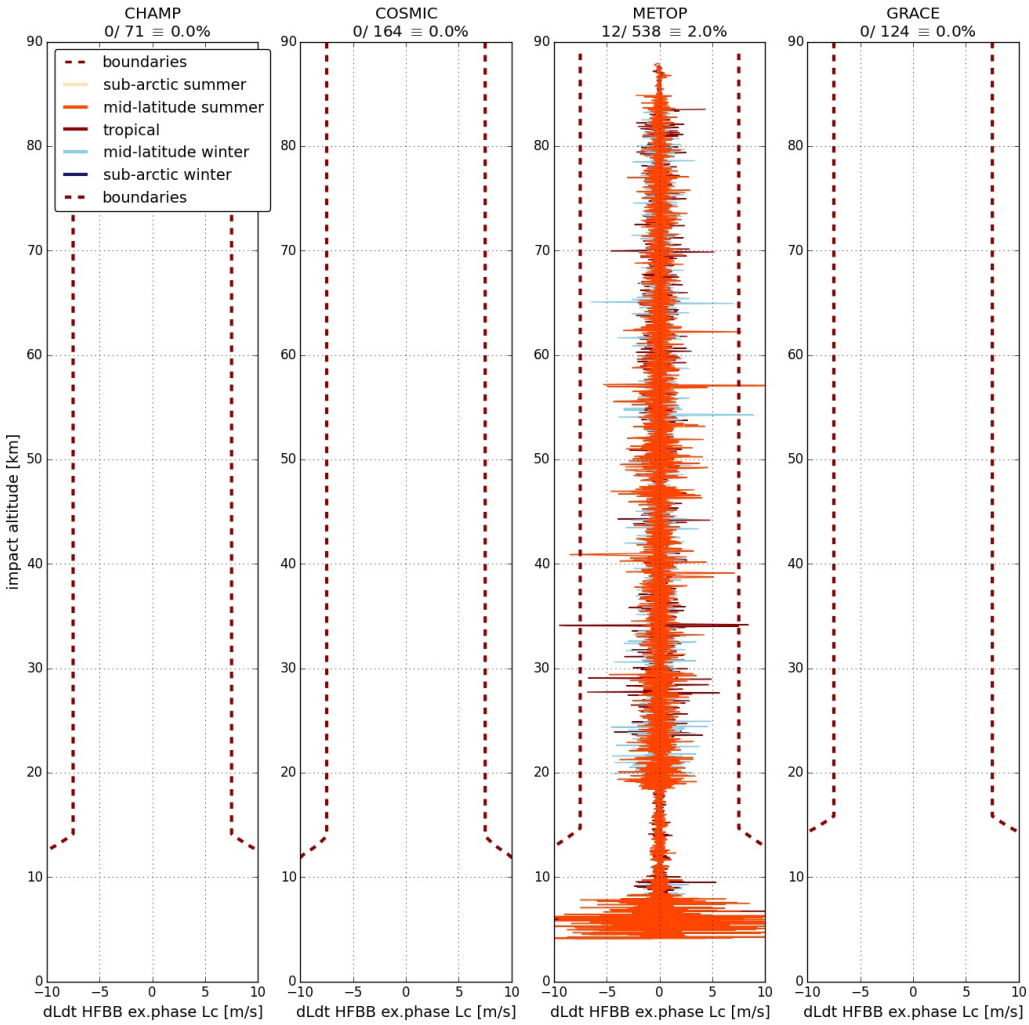

Figure 4.13: Derivative of HFBB excess phases of Lc, that did not pass the smoothness check for the various sattelites. The dashed lines, mark the boundary limit for derivatives depending on the particular climate area of the profile. At top one can see the number of profiles, that failed the check in total and percentage.

The derivatives of the HFBB excess phase Lc that are mapped in Figure 4.13 is of those profiles, which did not pass the smoothness check, due to the high rise in its derivative.
In Figure 4.14 the profiles, that already would have been discarded at the altitude

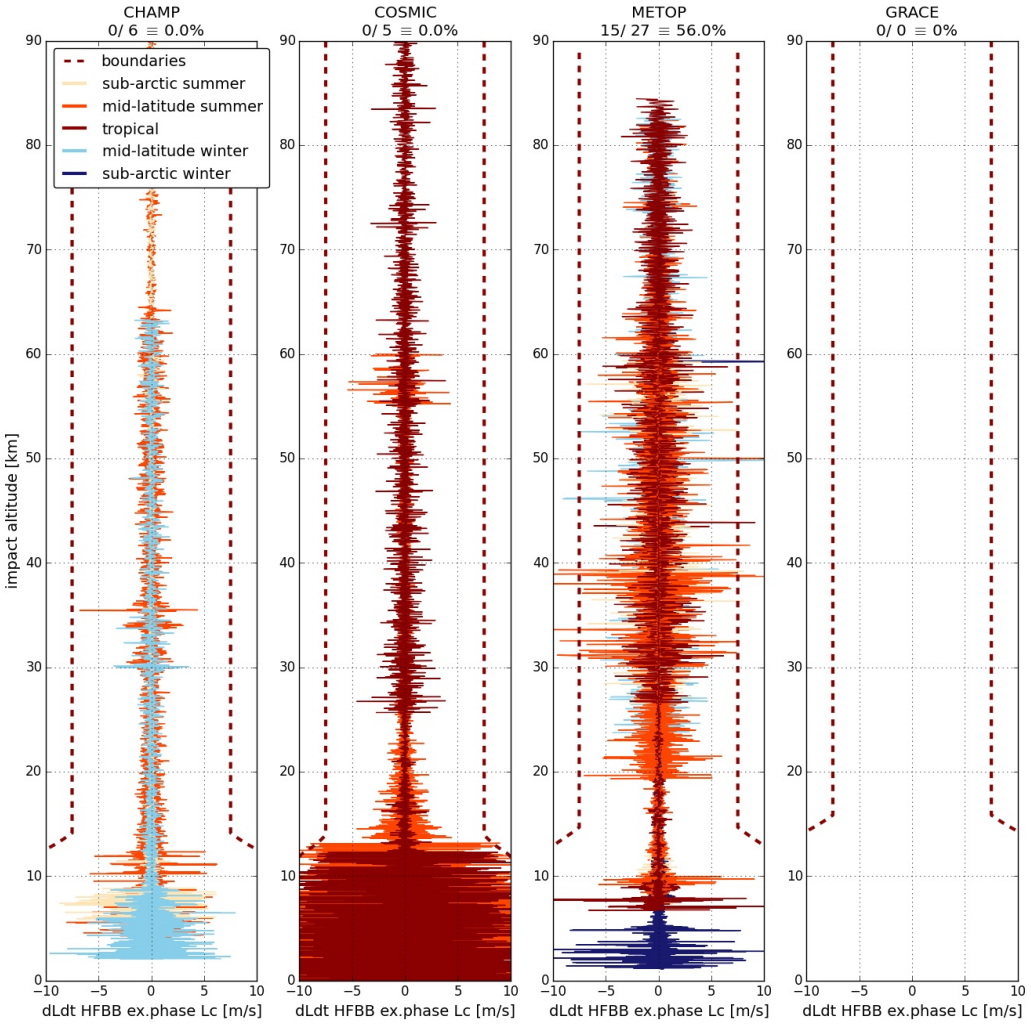

Figure 4.14: Derivative of HFBB excess phases of Lc, that did not pass the altitude check at the assignment of the impact altitude levels for the various sattelites. The dashed lines,mark the boundary limit for the derivatives, depending on the particular climate area of the profile. At top one can see the number of profiles, that did not pass the smoothness check in total and percentage.

check (because assigned impact altitude level $z^{\mathrm{Lc}}_{a\mathrm{Top}}/z^{\mathrm{Lc}}_{a\mathrm{Bot}}$ is lower/higher than 70/25 km) are shown. Here the Figure confirms again, that profiles not got unfairly flagged, since the profiles mostly exhibit striking values.

4.3.3 Comparison of Impact Altitude Levels of Excess Phase Lc

The following histograms in Figure 4.15 and 4.16 shall give an overview how the top and bottom impact altitude levels change through the process of the QC for the various satellite profiles. The ratio besides the QC task in the legend presents for the assignment of impact altitude levels, how many profiles passed the altitude check (AC) out of all profiles, for bounds check (BC) and smoothness check (SC) the ratio displays, the amount of profiles, passing the test in the specific impact altitude range (for top impact altitude level between 60 km and 90 km and for bottom impact altitude below 30 km) and the number in brackets illustrates the number of profiles, where the top/bottom impact altitude level has changed to pass the certain check.

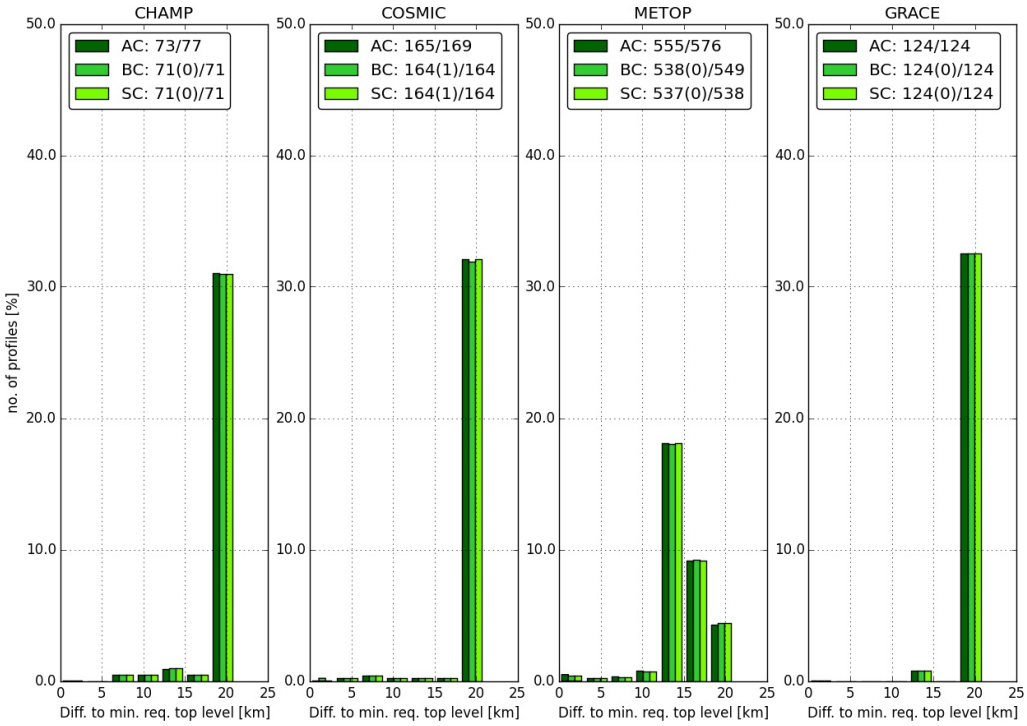

Figure 4.15: Overview of the distribution of the top impact altitude level, after different QC steps. The legend displays the amount of profiles that passed the altitude check (AC), the bounds check (BC) and the smoothness check (SC), respectively. The number in brackets illustrates the amount of profiles, which passed only after a readjustment of the top impact altitude level

By looking at the various bars in Figure 4.15, it is observable how far the top impact altitude level is away from the minimum required one ($z_{a\mathrm{Top}}^{\mathrm{min}} = 70\,\mathrm{km}$). The higher the difference the better; by providing profiles with impact altitude ranges until the maximum reachable impact altitude level at 90 km (which correspond to an altitude difference $\Delta z_a = 20\,\mathrm{km}$).

Except for satellite METOP the majority of the profiles has impact altitude levels at an impact altitude about 90 km. The reason for METOP, not largely reaching top impact altitude levels of 90 km, is not because of poorer quality. The measurements provided by satellite METOP starting in impact altitudes at about 90 km instead of the other satellites, where data is sometimes available from impact altitudes higher than 120 km. This indicates the high quality of METOP by providing sufficient accurate data right after the start of the measurement.
The top impact altitude level changed through further QC only for one profile of satellite COSMIC, which indicates, that the provided ex.phases are in general of good quality in high altitude ranges.

In Figure 4.16 the bars present the height distribution of the bottom impact altitude levels. As before, the assigned difference indicates the gap between reached and minimum required bottom impact altitude level ($z_{a\mathrm{Bot}}^{\mathrm{min}} = 25\,\mathrm{km}$).
By achieving differences of $\Delta z_a > 25\,\mathrm{km}$, yields to impact altitudes lower 0 km, which is due to the calculation of the impact altitudes with an inter- and extrapolation (see Section 3.3).
Nevertheless it is clearly observable, that coherently to the top level, the bottom impact altitude level of the profiles changes during the QC. For satellite METOP, the differences are fairly small, whereas for the other satellites especially the lowest achievable impact altitudes change. After the altitude check (AC) at the assignment of bottom impact altitude level, about 15% of COSMIC's profiles have bottom levels, with a difference between assigned and minimum required top impact altitude level greater than 30 km. In final, the majority of COSMIC profiles has a difference $\Delta z_a = 20 \pm 5\,\mathrm{km}$, which suits well for the other satellites too.

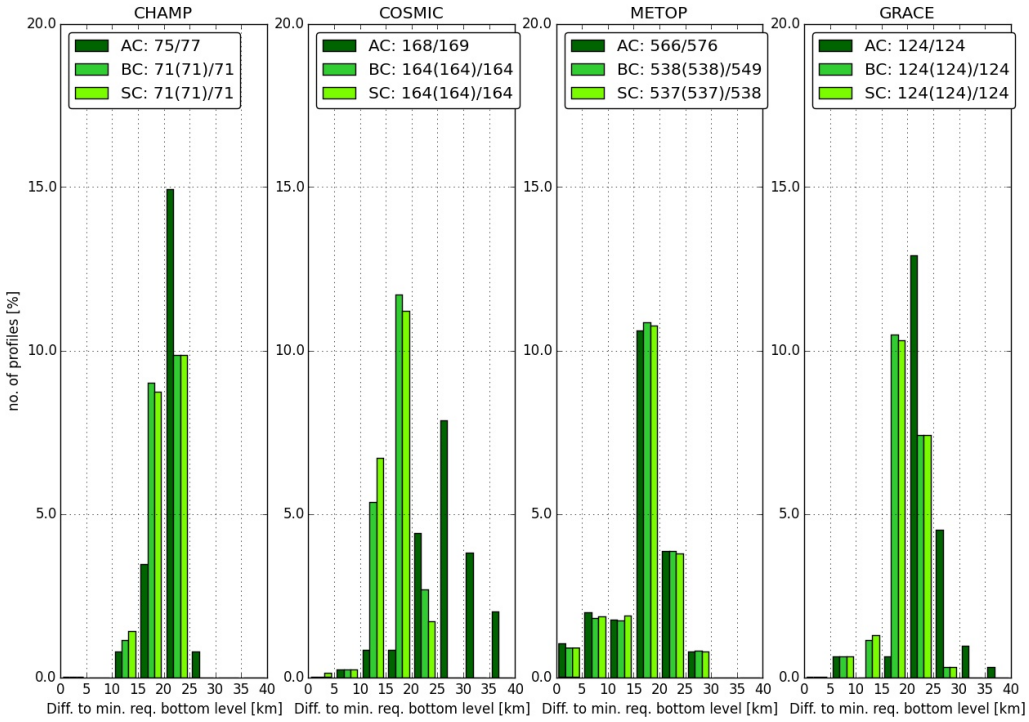

Figure 4.16: Overview of the distribution of the bottom impact altitude level, after different QC steps. The legend displays the amount of profiles that passed the altitude check (AC), the bounds check (BC) and the smoothness check (SC), respectively. The number in brackets illustrates the amount of profiles, which passed only after a readjustment of the bottom impact altitude level

4.4 Assignment of Bottom Impact Altitude Level of Excess Phase L1

In this section the results of the assignment of the bottom impact altitude level of L1 are discussed. Compared to the bounds and smoothness check based on the excess phase Lc, the checks on the excess phase L1 are independent of each other. Afterwards the determined bottom impact altitude levels of both tests are compared with each other. As final step, the higher impact altitude level will be chosen for the new bottom impact altitude level of L1. Furthermore the chosen limits for bounds and smoothness check for excess phase L1 are more gentle than before, which leads to a broaded threshold.

4.4.1 Bounds Check of Excess Phase L1

Figure 4.17 represents the results for bounds check L1. As one can see in the title of each panel, all excess phase L1 profiles passed the check.

The number in brackets gives the number of profiles, where a readjustment of the top and/or bottom impact altitude level has been done to pass the check. All satellites have a rate of readjustment nearby 50 %, except for METOP, where only 10 % of the bottom impact altitude levels have to be re-determined. By comparing the BB excess phases L1 of METOP with the other satellites, it is noticeable, that the deviation between ex.phase L1 and excess phase Lm (i.e the BB excess phase L1) is longer at a constant value. Foremost, the broadening of BB excess phase begins in impact altitudes below 7 km, whereas for the other satellites the

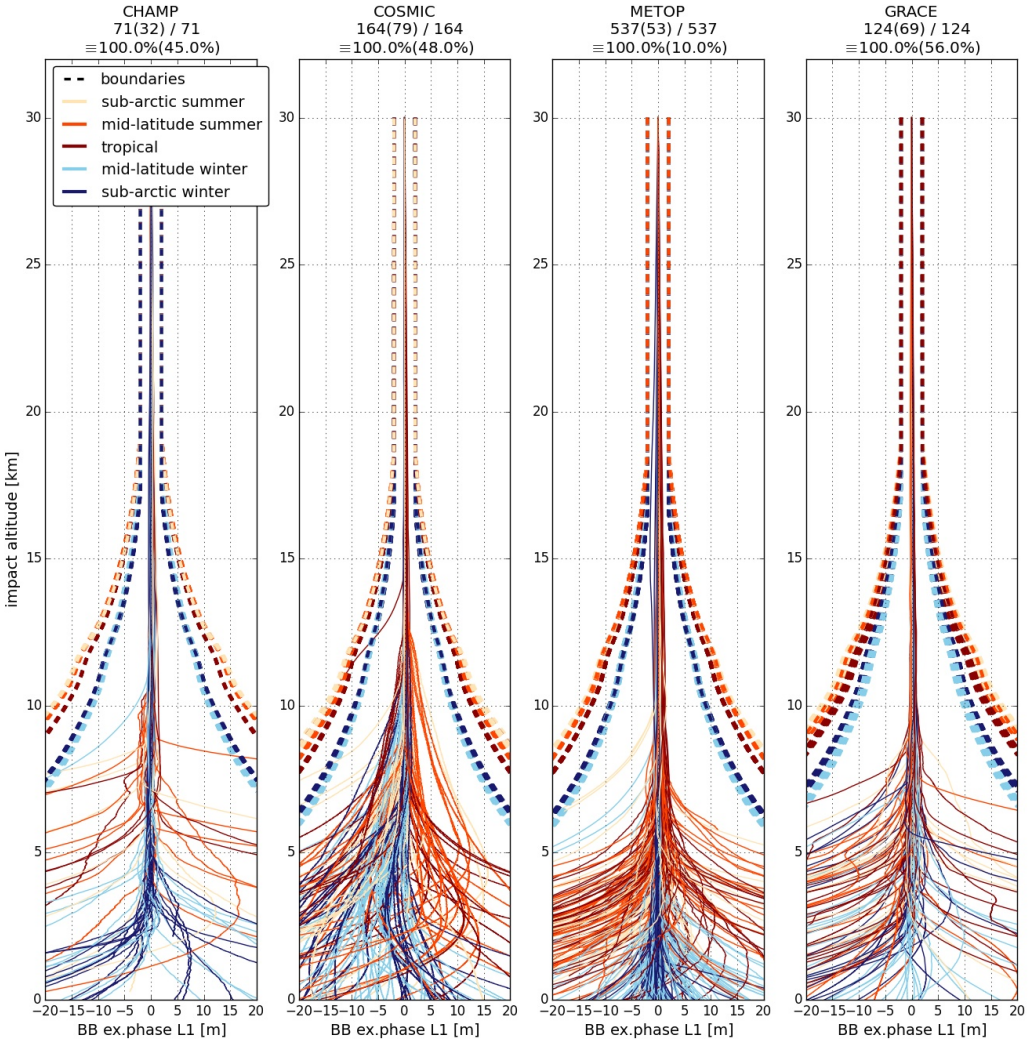

Figure 4.17: BB excess phases L1, including the boundaries of bounds check for the various satellites. The dashed lines, mark the boundary limit depending on the particular climate region of the profile. At top one can see the number of profiles, that passed the check in total and percentage. The count in the brackets, gives the number of profiles that passed, after a readjustment of the top and/or bottom impact altitude level.

broadening starts at impact altitudes between 10 km and 15 km.
It is also clearly visible that the boundary is looser, than for BB excess phase Lc, (see in Figure 4.9). On the one hand, the absolute value of the boundary is in the meter range, despite of the centimeter range for the ex.phase Lc, which comes particularly from the fact that the ex.phase Lc's offset is very little, compared to the ex.phase L1. And on the other hand, changed the relative value from 0.01 [1] to 0.1 [1], leading to a transition between constant and relative limit in higher impact altitudes and results in a more loose boundary.

4.4.2 Smoothness Check of Excess Phase L1

The following Figure 4.18 illustrates the results for the smoothness check L1. As one can see in the title of each panel; all profiles passed the check, without changing the bottom impact altitude level.

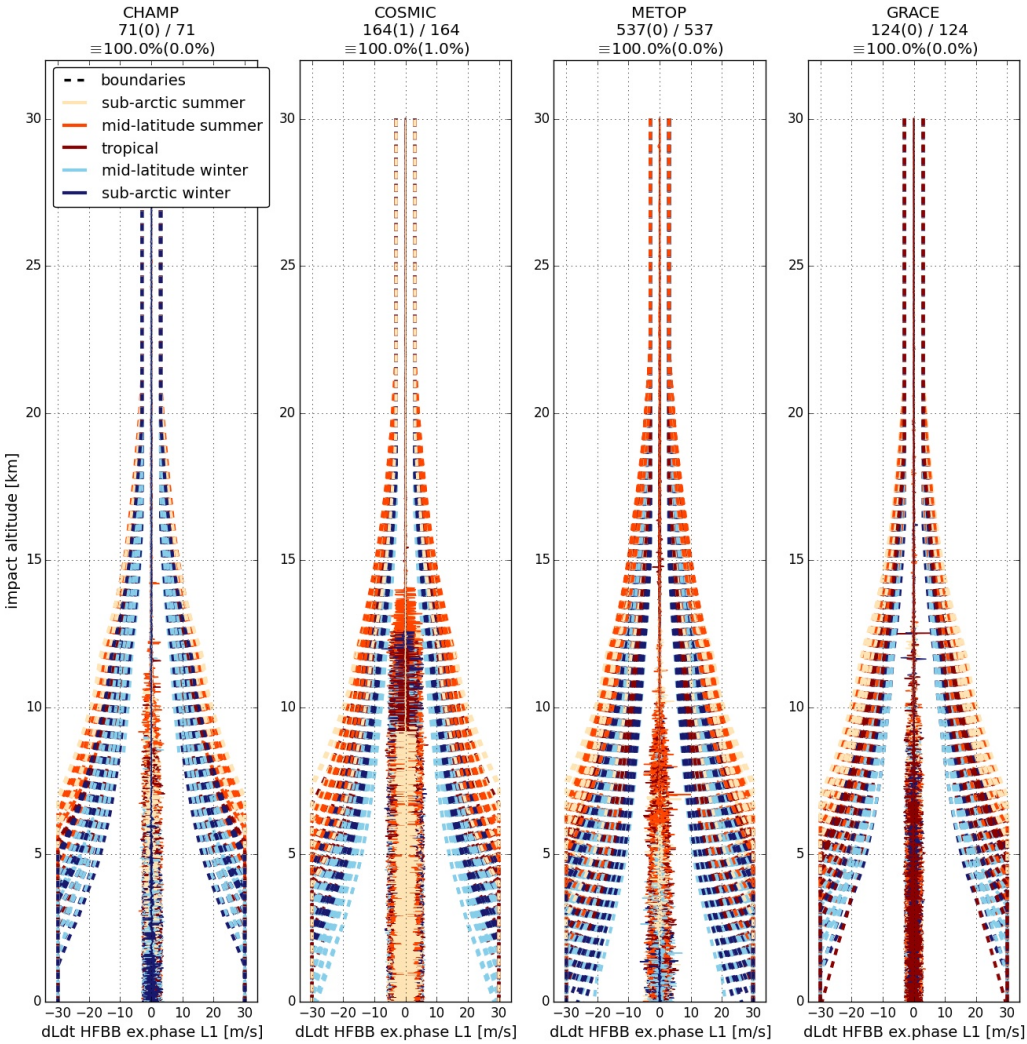

Figure 4.18: Derivative of HFBB ex.phase L1, including the boundaries of smoothness check for the various satellites. The dashed lines, mark the limit for baseband ex.phases depending on the particular climate region of the profile. At top one can see the number of profiles, that passed the check in total and percentage. The count in the brackets, gives the number of profiles that passed, after a readjustment of the top and/or bottom impact altitude level

It is observed that the derivative of HFBB excess phase L1 is quite different to the derivative of HFBB excess phase Lc (see in Section 4.3.2). In contrast to Lc, the noise of the derivative stays fairly constant after a small jump at an impact altitude z_a within $[10, 15]$ km.
But despite of this, the boundaries remain almost the same and are visibly looser than before. The new implemented lowest limit of 30 m is far from being reached.

4.4.3 Comparison of Impact Altitude Levels of Excess Phase L1

The blue bars in Figure 4.19 shows the distribution of the shift of the bottom impact altitude levels after the various QC steps for L1 to the minimum required impact altitude bottom level. Furthermore the distribution of the shift of the bottom impact altitude level L2 (yellow bar) to the minimum required bottom level is mapped. The difference displays how far the bottom levels are away from the minimum required impact altitude level ($z_{a\mathrm{Bot}}^{\mathrm{min}} = 25\,\mathrm{km}$).
It is evident, that bottom impact altitudes levels of L2 are closer to the minimum required level, than the bottom levels of L1. This emphasizes that the ex.phase of L1 has a better quality than L2, even at lower impact altitude ranges.
Moreover it can be seen that the distribution of the bars for the estimation (dark blue) and the smoothness check (light blue) are nearly the same (the slightly difference comes from the different number of profiles, caused that some profiles, which passed the estimation range, failed at the bounds or smoothness check). This is not unexpected, since the results in Figure 4.18 show, that all profiles passed the test without the need for a readjustment of the impact altitude level.
The distribution of the bottom impact altitude level after the bounds check shifted slightly in direction of minimum required bottom level. This leads to the assumption, that the bounds check of L1 will in general set the bottom impact altitude level of L1. Unless this bottom level L1 is lower than for excess phase L2. In this case the bottom level for L1 is adopted from L2.

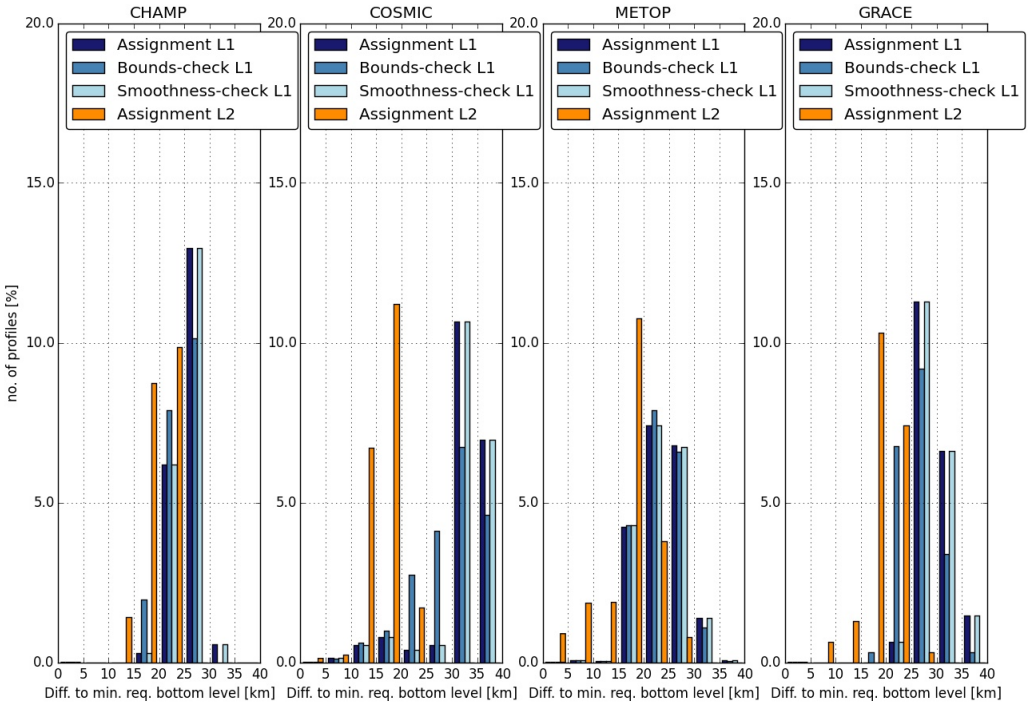

Figure 4.19: Overview of the distribution of bottom impact altitude level of excess phase L1, after the first assignment (dark blue bars), after the bounds check L1 (blue bars) and after the smoothness check L1 (light blue bars) and the final assigned bottom impact altitude level of excess phase L2 after QC (yellow bars).

4.5 Final Results

The following Figures provide a summary of the several QC tasks by showing the BB excess phase Lc, which makes it easier to compare between the various profiles, since the ionospheric influence is corrected.

The amount of profiles, that did not pass the QC is for all satellite missions is less than 10 %. For satellite GRACE actually all profiles passed (see Figure 4.23). Those profiles convince with their small deviations all along the altitude range. Uncommon behavior occurs only in impact altitudes higher 90 km, and is easy to detect. the only disadvantage are two outliers in an impact altitude around 45 km (see first panel in Figure 4.23), whereas for the other satellites, outlier exclusively appear in impact altitudes $z_a > 100$ km (for example: CHAMP outlier occur at an impact altitude at about 120 km in Figure 4.20, COSMIC outlier at an impact altitude about 110 km in Figure 4.21).
METOP has various profiles with bias jumps in the important impact altitude range between 25 km and 70 km (see Figure 4.22) while for the other satellites, jumps primarly occur in impact altitudes above 70 km.

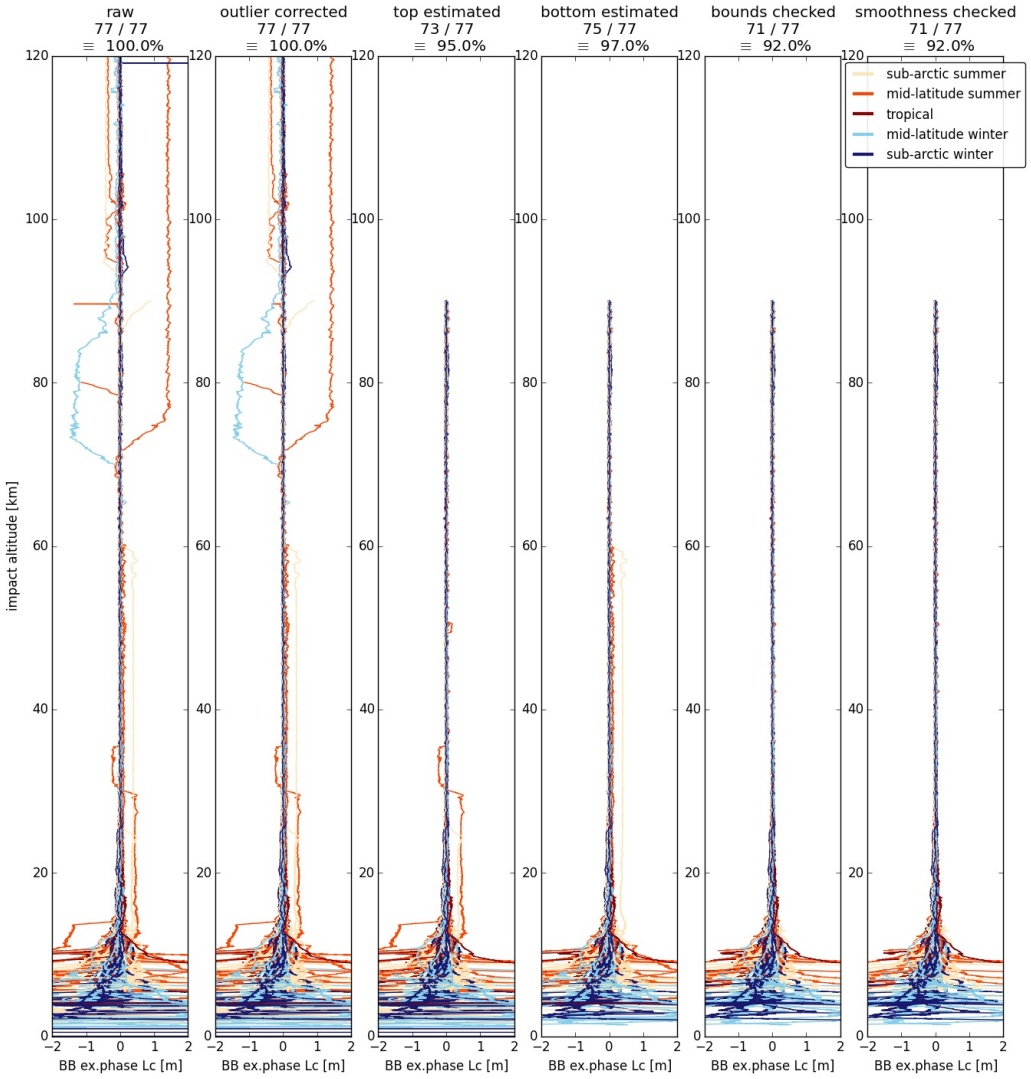

Figure 4.20: Overview of the various QC tasks, based on BB excess phase Lc profiles of satellite CHAMP. First panel shows the raw excess phase, the second the excess phase after outlier correction, the third after the top impact altitude estimation, the fourth after the bottom impact altitude level estimation, the fifth after passing the bounds check and the sixth panel shows the excess phase after passing the smoothness check. On top one can see, the number of profiles that passed the prior checks and the different colors present the various climate regions

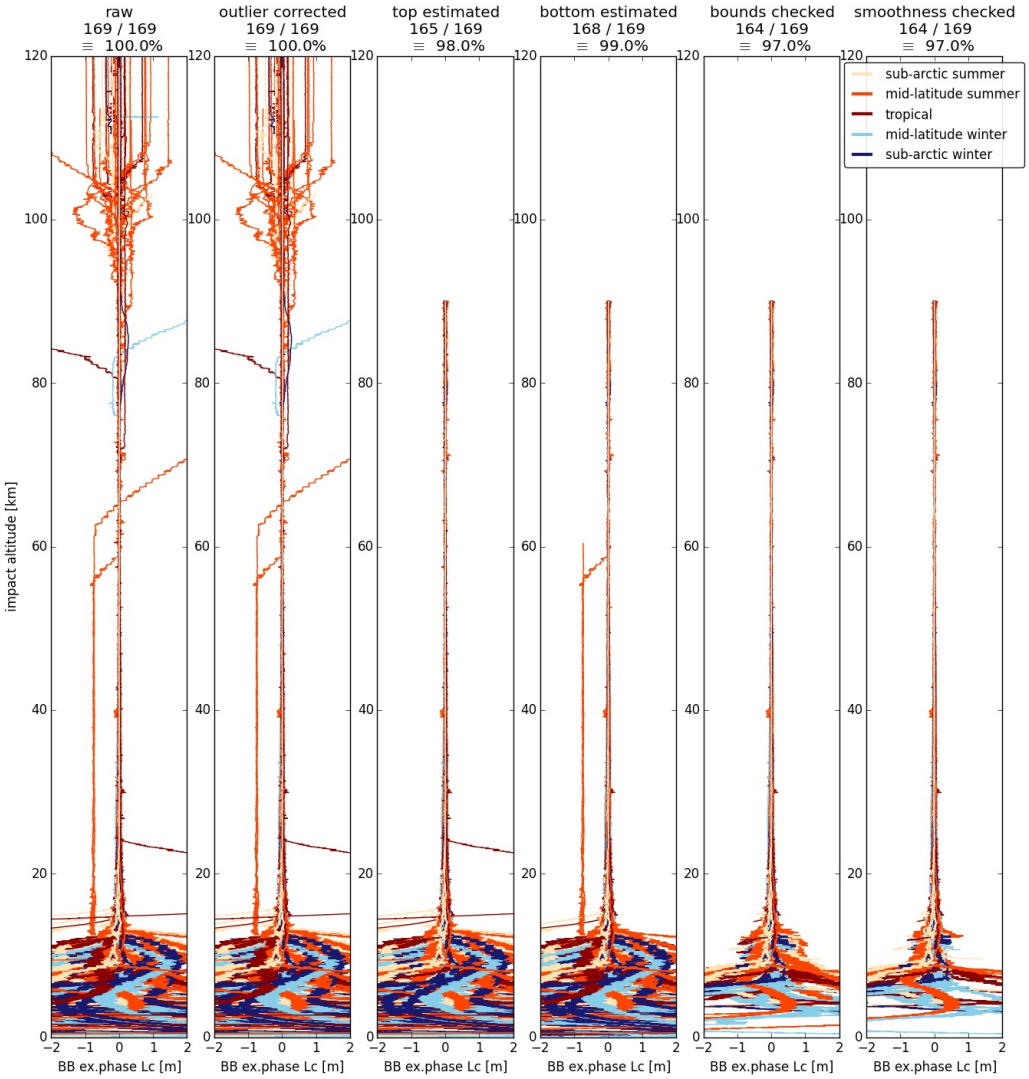

Figure 4.21: Overview of the various QC tasks, based on BB excess phase Lc profiles of satellite COSMIC. First panel shows the raw excess phase, the second the excess phase after outlier correction, the third after the top impact altitude estimation, the fourth after the bottom impact altitude level estimation, the fifth after passing the bounds check and the sixth panel shows the excess phase after passing the smoothness check. On top one can see, the number of profiles that passed the prior checks and the different colors present the various climate regions

It must be noted, that these expressions are only valid for the specific test day 2008-07-15, and METOP provides three times more profiles than the other satellite missions, whereas it cannot be ruled out that the other satellite missions will not have to face this problems as well.

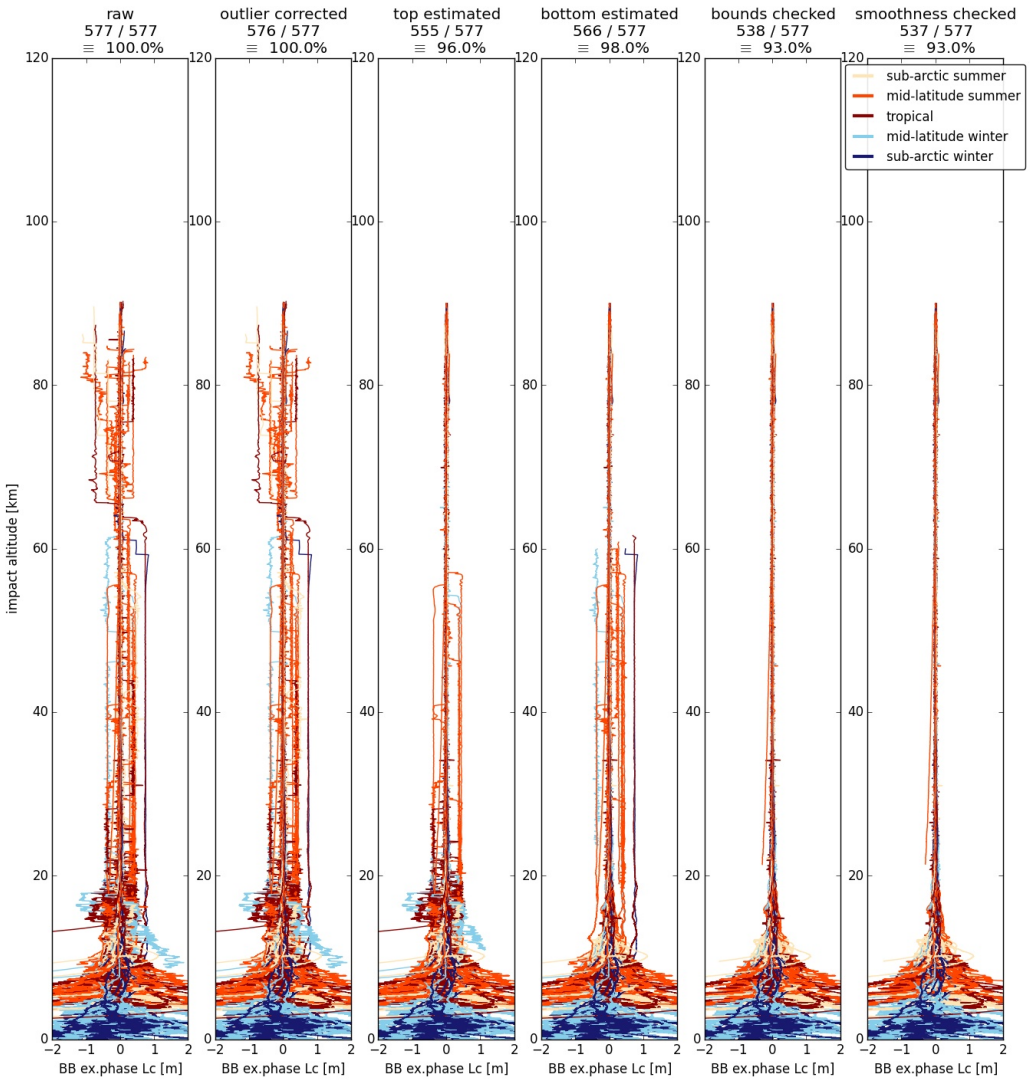

Figure 4.22: Overview of the various QC tasks, based on BB excess phase Lc profiles of satellite METOP. First panel shows the raw excess phase, the second the excess phase after outlier correction, the third after the top impact altitude estimation, the fourth after the bottom impact altitude level estimation, the fifth after passing the bounds check and the sixth panel shows the excess phase after passing the smoothness check. On top one can see, the number of profiles that passed the prior checks and the different colors present the various climate regions

When concerning the various climate regions, it points out, that the hotter regions have a higher noise level than the colder ones, due to denser and moister medium up to the highest impact altitudes. All together the here introduced raw-excess phase-based QC is very efficient and monitors all profiles equally, independent of their satellite source and climate region, which makes the processing with the rOPS robust for L1a input data and the QC code very effective and simple.

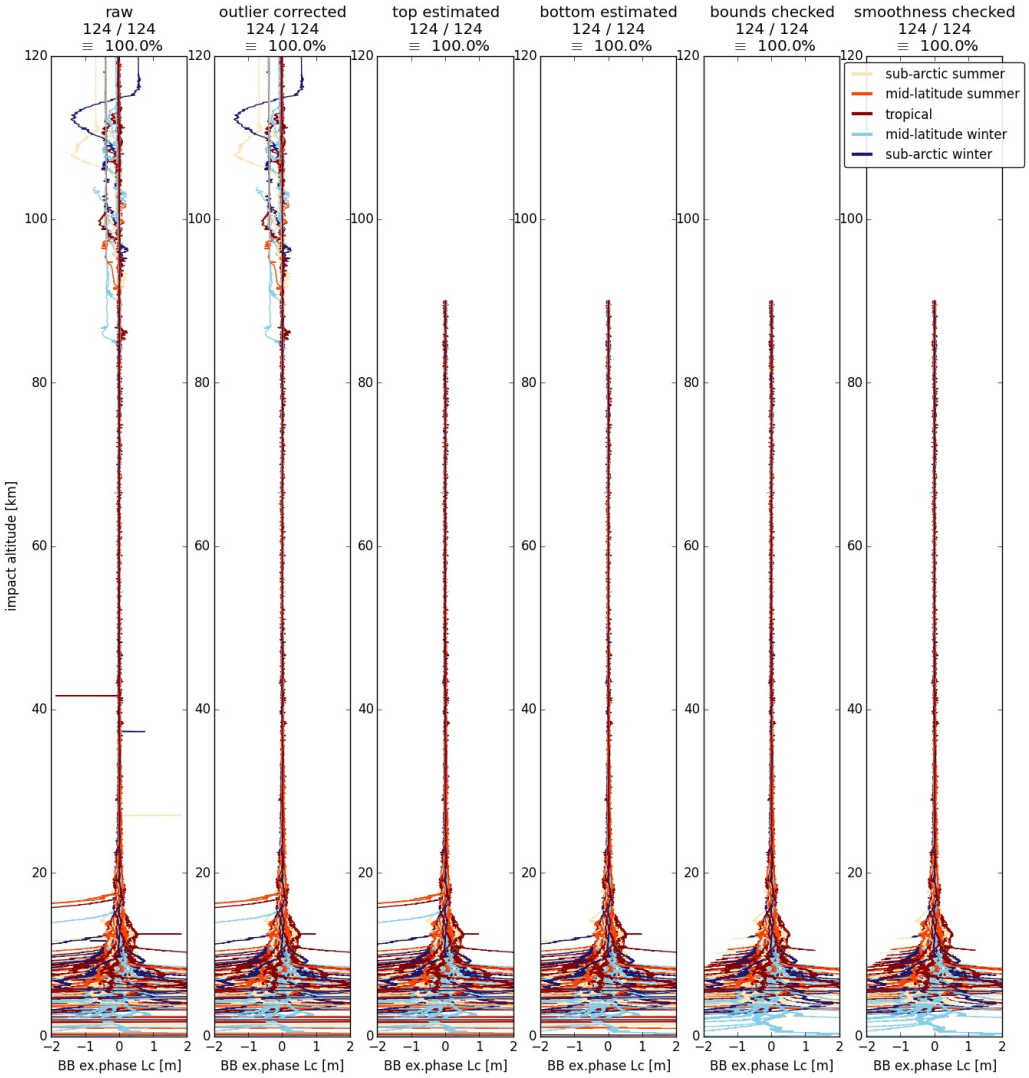

Figure 4.23: Overview of the various QC processing steps, based on BB excess phase Lc profiles of satellite GRACE. First panel shows the raw excess phase, the second the excess phase after outlier correction, the third after the top impact altitude estimation, the fourth after the bottom impact altitude level estimation, the fifth after passing the bounds check and the sixth panel shows the excess phase after passing the smoothness check. On top one can see, the number of profiles that passed the prior checks and the different colors present the various climate regions

5 Summary and Conclusions

The implementation of the QC, subsequently to the L1a raw processing and before the actual retrieval of atmospheric profiles, has a significant impact on the quality of the output from rOPS. Working on the near-raw excess phase data enables to reject profiles with inadequate quality early enough in the processing chain. Also, by setting QC top and bottom levels and flags provides great benefit for the later atmospheric profiles retrieval to perform reliably.
The key results and parameter settings of the full QC algorithm system are concisely summarized below. For explanation of the acronyms and symbols used in this summary see the list of Acronyms and the list of Symbols below.

Fundamental plausibility check. The performance of a fundamental plausibility check is strictly necessary to secure detection and elimination of unphysical profiles right at beginning, since further calculations assume data which are basically plausible. Table 5.1 summarizes the respective bound-settings.

Table 5.1: Settings for the fundamental plausibility check

Checked Variable	Bound value [m]	Range [km]
BB ex.phase L1, L2	$\Delta L^{\text{basic}} = \text{L}_\text{m} \pm 50$ [a]	< 90

[a] for UCAR derived profiles: $\Delta L^{\text{basic}} = \text{L}_\text{m} \pm 500$, see Section 3.3

Outlier detection and correction. The task of the detection and correction of outliers identifies and replaces values that deviate nonphysically strong from the average of the neighboring data, without adjusting values that tend to appear still caused by a physical natural influence. It is ensured that the corrected outlier values are statistically set within a defined bound of $\pm 3 \cdot \sigma$. For detailed parameter settings see Table 5.2.

Table 5.2: Settings for the outlier detection and correction

Checked Variable	Bound value [m][a]	Range [km]
BB ex.phase L1, L2	$\Delta L_{\downarrow}^{\text{out}} = p_{50;L_\text{o}} - 5 \cdot (p_{50;L_\text{o}} - p_{16;L_\text{o}})$	< 90
BB ex.phase L1, L2	$\Delta L_{\uparrow}^{\text{out}} = p_{50;L_\text{o}} + 5 \cdot (p_{84;L_\text{o}} - p_{50;L_\text{o}})$	< 90
BB ex.phase L1, L2	$\Delta L^{\text{corr}} = L_\text{o} \pm 3\sigma_{L_\text{o}}$	< 90

[a] with $p_{i;L_\text{o}}$ being the ith-percentile and σ_{L_o} the stdev of the observed excess phase L_o with $\text{o} \in \{1, 2\}$ and $i \in \{16, 50, 84\}$

Assigning top and bottom altitude levels. Setting a top impact altitude level prevents further processing from input data with a high noise level. The bottom impact altitude level crops the low altitude data to a level below which it can not be expected that profiles are accurate enough to enable appropriate quality of thermodynamic profiles.
For the top impact altitude level an absolute value suited best, for the bottom a combination of relative and absolute values turned out to work best. For the detailed parameter settings see Table 5.3.

Table 5.3: Settings for assigning top and bottom impact altitude levels

Checked Variable	Bound value [m]	Range [km]
stdev BB ex.phase Lc	$\Delta L^{\text{Top}} = 0.03$	60 – 90
stdev HFBB ex.phase L1, L2	$\Delta L^{\text{Bot}} =$ $\text{Max}\,[\,\Delta L_{\text{abs}}^{\text{Bot}},\, \Delta L_{\text{rel}}^{\text{Bot}} \cdot \lvert L_\text{m} \rvert]$ [a]	< 30

[a] $\Delta L_{\text{abs}}^{\text{Bot}} = 0.03\,[\text{m}]$ is the absolute bound value and $\Delta L_{\text{rel}}^{\text{Bot}} = 0.001\,[1]$ is the relative bound value for ΔL^{Bot}; the higher one of the two values is always assigned

Bounds and smoothness checks. The bounds and smoothness checks are the core of the QC. The bounds check uses a combination of an absolute and relative boundary, which is used to check whether the observed profiles have a plausible difference to the forward-modeled excess phase profile, by performing the test on the BB excess phase test variable. By broadening the bound while going down in impact altitude, the downward BB excess phase increase is taken into account.
The smoothness check focuses on the noise in the profiles. Data will be flagged whenever the derivative of the HFBB excess phase test variable exceeds the defined

smoothness boundary. Same as for the bounds check, higher values are tolerated at lower impact altitudes. Detailed settings can be seen in Table 5.4.

Table 5.4: Settings for the bounds and smoothness check

Checked Variable	Bound value [m] (∂L^{SC} [m/s])	Range [km]
BB ex.phase Lc	$\Delta L^{\mathrm{BC}}_{\mathrm{MS}} = \pm 0.15$	50 - 90
BB ex.phase Lc	$\Delta L^{\mathrm{BC}}_{\mathrm{US}} = \pm(k \cdot z_a + d)$ [a]	30 - 50
BB ex.phase Lc	$\Delta L^{\mathrm{BC}}_{\mathrm{TLS}} =$ $\pm\mathrm{Max}\left[\Delta L^{\mathrm{BC}}_{\mathrm{TLS,abs}},\ \Delta L^{\mathrm{BC}}_{\mathrm{TLS,rel}} \cdot \lvert L_m \rvert\right]$ [b]	< 30
dLdt HFBB ex.phase Lc	$\partial L^{\mathrm{SC}} =$ $\pm\mathrm{Max}\left[\partial L^{\mathrm{SC}}_{\mathrm{abs}},\ \partial L^{\mathrm{SC}}_{\mathrm{rel}} \cdot \frac{\partial}{\partial t}\lvert L_{\mathrm{m}} \rvert\right]$ [c]	< 90

[a] $k = \frac{\Delta L^{50} - \Delta L^{30}}{z_a^{50} - z_a^{30}}$ [m/m] , $d = \frac{z_a^{50}\Delta L^{30} - z_a^{30}\Delta L^{50}}{z_a^{50} - z_a^{30}}$ [m]
where ΔL^{z_a} is the boundary at $z_a \in \{30, 50\}$ km

[b] $\Delta L^{\mathrm{BC}}_{\mathrm{TLS,abs}} = 0.3$ [m] is the absolute bound value for and
$\Delta L^{\mathrm{BC}}_{\mathrm{TLS,rel}} = 0.01$ [1] is the relative bound value for $\Delta L^{\mathrm{BC}}_{\mathrm{TLS}}$

[c] $\partial L^{\mathrm{SC}}_{\mathrm{abs}} = 7.5$ [m/s] is the absolute bound value and
$\partial L^{\mathrm{SC}}_{\mathrm{rel}} = 0.75$ [1] is the relative bound value for $\partial L^{\mathrm{SC}}_{\mathrm{abs}}$

Assigning final bottom impact altitude level of excess phase L1. In the final task of the QC the before-estimated bottom impact altitude level of excess phase L1 is checked and optionally re-determined. The boundaries serve as a rough but plausible threshold. For the detailed parameter settings see Table 5.5.

Table 5.5: Settings for the checks for assigning the final L1 bottom altitude level

Checked Variable	Bound [m] ($\partial L^{\mathrm{SCL1}}$ [m/s])	Range [km]
BB ex.phase L1	$\Delta L^{\mathrm{BCL1}} =$ $\pm\mathrm{Max}\left[\Delta L^{\mathrm{BCL1}}_{\mathrm{abs}},\ \Delta L^{\mathrm{BCL1}}_{\mathrm{rel}} \cdot \lvert \mathrm{L_m} \rvert\right]$ [a]	< 30
dLdt HFBB	$\partial L^{\mathrm{SCL1}}_{\mathrm{TLS}} =$	10 - 30
ex.phase L1	$\pm\mathrm{Max}\left[\partial L^{\mathrm{SCL1}}_{\mathrm{TLS,abs}}, \partial L^{\mathrm{SCL1}}_{\mathrm{TLS,rel}} \cdot \frac{\partial}{\partial t}\lvert L_{\mathrm{m}} \rvert\right]$ [b]	
dLdt HFBB	$\partial L^{\mathrm{SCL1}}_{\mathrm{TS}} =$	< 10
ex.phase L1	$\pm\mathrm{Min}\left[\ \partial L^{\mathrm{SCL1}}_{\mathrm{TLS}},\ \partial L^{\mathrm{SCL1}}_{\mathrm{TS,abs}}\right]$	

[a] $\Delta L^{\mathrm{BCL1}}_{\mathrm{abs}} = 2$ [m] is the absolute bound value and
$\Delta L^{\mathrm{BCL1}}_{\mathrm{rel}} = 0.1$ [1] is the relative bound value for ΔL^{BCL1}

[b] $\partial L^{\mathrm{SCL1}}_{\mathrm{TLS,abs}} = 3$ [m/s] is the absolute bound value and
$\partial L^{\mathrm{SCL1}}_{\mathrm{TLS,rel}} = 0.75$ is the relative bound value for $\partial L^{\mathrm{SCL1}}_{\mathrm{TLS}}$ and
$\partial L^{\mathrm{SCL1}}_{\mathrm{TS,abs}} = 30$ [m/s] is the absolute bound value for $\partial L^{\mathrm{SCL1}}_{\mathrm{TS}}$

For the used test datasets the QC is found highly efficient, although no strict separation between climate region, excess phase L1 and L2, or satellite mission

was done. The checks are simple in the implementation but nevertheless ensured to be robust by using moving medians, averages and percentile as found most appropriate.
For the future fully developed rOPS system that will be run in re-processing mode over years of multi-satellite RO data, an adjustment of some bound value settings could be required, since the here used L1a data were provided by UCAR. However, the modifications are expected to be small, because the L0 data sources are identical.
Overall we find this innovative QC algorithm system highly effective in detecting and discarding bad-quality parts of the RO data across multiple RO missions and all climate regions globally. The result is a set of data that enables to provide high quality thermodynamic profiles of temperature, density and pressure for climate monitoring and research.

Acronyms

excess phase Lc ionosphere corrected excess phase.

excess phase Lm forward-modeled excess phase.

BB excess phase baseband excess phase.

BC bounds check.

ECMWF European Centre for Medium-Range Weather Forecasts.

ex.phase excess phase.

GNSS Global Navigation Satellite System.

GPS Global Positioning System.

GPS/MET Global Positioning System/Meteorology [experiment].

HFBB excess phase highpass-filtered baseband excess phase.

L0 Level 0 [data product].

L1a Level 1a [data product].

L1b Level 1b [data product].

L2a Level 2a [data product].

L2b Level 2b [data product].

LEO Low Earth Orbit.

LFBB excess phase lowpass-filtered baseband excess phase.

LS Lower Stratosphere.

MS Mesosphere.

MSL Mean Sea Level.

QC Quality Control.

RO Radio Occultation.

rOPS Reference Occultation Processing System.

SC smoothness check.

SLTP Straight Line Tangent Point.

stdev standard deviation.

TLS Troposphere and Lower Stratosphere.

TS Troposphere.

UCAR University Corporation for Atmospheric Research.

US Upper Stratosphere.

UTLS Upper Troposphere–Lower Stratosphere.

WEGC Wegener Center for Climate and Global Change [University of Graz].

Symbols

ΔL^{BCL1} boundary for the bounds check L1.

$\Delta L^{\mathrm{BCL1}}_{\mathrm{abs}}$ absolute value of the boundary for the bounds check L1.

$\Delta L^{\mathrm{BCL1}}_{\mathrm{rel}}$ relative bound value of the boundary for the bounds check L1.

ΔL^{BC} boundary for the bounds check.

$\Delta L^{\mathrm{BC}}_{\mathrm{MS}}$ bound value for bounds check in the Mesosphere.

$\Delta L^{\mathrm{BC}}_{\mathrm{TLS,abs}}$ absolute bound value of the boundary for bounds check in the Troposphere and Lower Stratosphere.

$\Delta L^{\mathrm{BC}}_{\mathrm{TLS,rel}}$ relative bound value of the boundary for bounds check in the Troposphere and Lower Stratosphere.

$\Delta L^{\mathrm{BC}}_{\mathrm{TLS}}$ boundary for bounds check in the Troposphere and Lower Stratosphere.

$\Delta L^{\mathrm{BC}}_{\mathrm{US}}$ boundary for bounds check in the Upper Stratosphere.

ΔL^{Bot} boundary for bottom the impact altitude check.

$\Delta L^{\mathrm{Bot}}_{\mathrm{abs}}$ absolute bound value for the bottom impact altitude check.

$\Delta L^{\mathrm{Bot}}_{\mathrm{rel}}$ relative bound value for the bottom impact altitude check.

ΔL^{Top} bound value for the top impact altitude check.

$\Delta L^{\mathrm{basic}}$ boundary value for the plausibility check.

ΔL^{corr} boundary for the corrected data value at outlier check.

$\Delta L^{\mathrm{out}}_{\downarrow}$ low boundary for the outlier check.

$\Delta L^{\mathrm{out}}_{\uparrow}$ high boundary for the outlier check.

δL_{cHF} HFBB excess phase Lc.

δL_{cm} BB excess phase Lc.

δL_{oHF} HFBB excess phase Lo.

$\partial L^{\mathrm{SCL1}}$ boundary for the smoothness check.

$\partial L^{\mathrm{SCL1}}_{\mathrm{TLS,abs}}$ absolute bound value of boundary for the smoothness check L1 in the Troposphere and Lower Stratosphere.

$\partial L^{\mathrm{SCL1}}_{\mathrm{TLS,rel}}$ relative bound value of the boundary for the smoothness check L1 in the Troposphere and Lower Stratosphere.

$\partial L^{\mathrm{SCL1}}_{\mathrm{TLS}}$ boundary for the smoothness check L1 in the Troposphere and Lower Stratosphere.

$\partial L^{\mathrm{SCL1}}_{\mathrm{TS,abs}}$ absolute value of the boundary for the smoothness check L1 in the Troposphere.

$\partial L^{\mathrm{SCL1}}_{\mathrm{TS}}$ boundary for the smoothness check L1 in the Troposphere.

∂L^{SC} boundary for the smoothness check.

$\partial L^{\mathrm{SC}}_{\mathrm{abs}}$ absolute bound value of the boundary for the smoothness check.

$\partial L^{\mathrm{SC}}_{\mathrm{rel}}$ relative bound value of the boundary for the smoothness check.

z_a impact altitude.

$z_{a\mathrm{Bot}}$ bottom impact altitude level.

$z^{\mathrm{L1}}_{a\mathrm{Bot}}$ bottom impact altitude level of ex.phase L1.

$z^{\mathrm{L2}}_{a\mathrm{Bot}}$ bottom impact altitude level of ex.phase L2.

$z^{\mathrm{Lc}}_{a\mathrm{Bot}}$ bottom impact altitude level of ex.phase Lc.

$z_{a\mathrm{Top}}$ top impact altitude level.

$z^{\mathrm{L1}}_{a\mathrm{Top}}$ top impact altitude level of ex.phase L1.

$z^{\mathrm{L2}}_{a\mathrm{Top}}$ top impact altitude level of ex.phase L2.

$z^{\mathrm{Lc}}_{a\mathrm{Top}}$ top impact altitude level of ex.phase Lc.

List of Figures

List of Tables

List of Algorithm Boxes

Bibliography

Anthes, R. A. (2011). "Exploring Earth's atmosphere with radio occultation: contributions to weather, climate, and space weather". *Atmos. Meas. Tech.* 4, pp. 1077–1103. DOI: 10.5194/amt-4-1077-2011.

Blewitt, G. (1989). "Carrier phase ambiguity resolution for the Global Positioning System applied to geodetic baselines up to 2000 km". *J. Geophys. Res.* 94.8, pp. 0187–10203. DOI: 10.1256/wea.74.04.

Dixon, T. H. (1991). "An introduction to the Global Positioning System and some geological applications". *Rev. Geophys.* 29.2, pp. 249–276.

Gorbunov, M. E. and G. Kirchengast (2015). "Uncertainty propagation through wave optics retrieval of bending angles from GPS radio occultation: Theory and simulation results". *Radio Sci.* 50, RS6001. DOI: 10.1002/2015RS005730.

– (2018). "Wave-optics uncertainty propagation and regression-based bias model in GNSS radio occultation bending angle retrievals". *Atmos. Meas. Tech.* 11, pp. 111–125. DOI: 10.5194/amt-11-111-2018.

Hajj, G. A., E. R. Kursinski, L. J. Romans, W. I. Bertiger, and S. S. Leroy (2002). "A technical description of atmospheric sounding by GPS occultation". *J. Atmos. Solar-Terr. Phys.* 64.4, pp. 451–469. DOI: 10.1016/S1364-6826(01)00114-6.

Hofmann-Wellenhof, B., H. Lichtenegger, and E. Wasle (2008). *GNSS—Global Navigation Satellite Systems*. Wien New York: Springer. 516 pp.

Innerkofler, J., C. Pock, G. Kirchengast, M. Schwärz, C. Marquardt, Y. Andres, and J. Schwarz (2018). "GNSS radio occultation excess phase processing with integrated uncertainty estimation for climate applications". *Atmos. Meas. Tech.* in preparation.

IPCC (2013). *Climate Change 2013: The Physical Science Basis. Contribution of Working Group I to the Fifth Assessment Report of the Intergovernmental Panel on Climate Change*. Ed. by T. F. Stocker, D. Qin, G.-K. Plattner, M. Tignor, S. K. Allen, J. Boschung, A. Nauels, Y. Xia, V. Bex, and P. M. Midgley. Cambridge, United Kingdom and New York, NY, USA: Cambridge University Press. 1535 pp.

Kirchengast, G., M. Schwärz, J. Schwarz, J. Ramsauer, J. Fritzer, B. Scherllin-Pirscher, J. Innerkofler, V. Proschek, T. Rieckh, and J. Danzer (2016a). *Reference OPS DAD – Reference Occultation Processing System (rOPS) Detailed Algorithm Description*. WEGC/UniGraz Technical Report for ESA and FFG No. 3/2016, Doc-Id: WEGC–rOPS–2016–TR02, Issue 1.5. Wegener Center, University of Graz.

Kirchengast, G., M. Schwärz, J. Schwarz, J. Ramsauer, J. Fritzer, B. Scherllin-Pirscher, J. Innerkofler, V. Proschek, T. Rieckh, J. Danzer, and C. Pock (2017).

Reference OPS DAD—Reference Occultation Processing System (rOPS) Detailed Algorithm Description. Tech. Rep. for ESA and FFG No. 1/2017, Doc-Id: WEGC–rOPS–2017–TR01, Issue 1.7. Wegener Center, Univ. of Graz.

Kirchengast, G., M. Schwärz, J. Schwarz, B. Scherllin-Pirscher, C. Pock, J. Innerkofler, V. Proschek, A. K. Steiner, J. Danzer, F. Ladstädter, and U. Foelsche (2016b). *The reference occultation processing system approach to interpret GNSS radio occultation as SI-traceable planetary system refractometer*. Presentation at OPAC-IROWG International Workshop 8–14 September 2016, Seggau/Leibnitz, Austria, available online at http://wegcwww.uni-graz.at/opacirowg2016 > Scient. Programme > Mon, Sep 12.

Kuo, Y.-H., T.-K. Wee, S. Sokolovskiy, C. Rocken, W. Schreiner, D. Hunt, and R. A. Anthes (2004). "Inversion and error estimation of GPS radio occultation data". *J. Meteor. Soc. Japan* 82.1B, pp. 507–531.

Kursinski, E. R., G. A. Hajj, J. T. Schofield, R. P. Linfield, and K. R. Hardy (1997). "Observing Earth's atmosphere with radio occultation measurements using the Global Positioning System". *J. Geophys. Res.* 102.D19, pp. 23429–23465. DOI: 10.1029/97JD01569.

Melbourne, W. G., E. S. Davis, C. B. Duncan, G. A. Hajj, K. R. Hardy, E. R. Kursinski, T. K. Meehan, L. E. Young, and T. P. Yunck (1994). *The application of spaceborne GPS to atmospheric limb sounding and global change monitoring*. Tech. rep. Pasadena, California, USA: Jet Propulsion Laboratory, NASA. 147 pp.

Pirscher, B. (2010). *Multi-satellite climatologies of fundamental atmospheric variables from radio occultation and their validation (Ph.D. thesis)*. Sci. Rep. 33-2010. Austria: Wegener Center Verlag Graz. ISBN: 978-3-9502940-3-3.

Rocken, C., R. Anthes, M. Exner, D. Hunt, S. Sokolovskiy, R. Ware, M. Gorbunov, W. Schreiner, D. Feng, B. Herman, Y.-H. Kuo, and X. Zuo (1997). "Analysis and validation of GPS/MET data in the neutral atmosphere". *J. Geophys. Res.* 102.D25, pp. 29849–29866. DOI: 10.1029/97JD02400.

Schwarz, J. C., G. Kirchengast, and M. Schwaerz (2018). "Integrating uncertainty propagation in GNSS radio occultation retrieval: from excess phase to atmospheric bending angle profiles". *Atmos. Meas. Tech.* 11, pp. 2601–2631. DOI: 10.5194/amt-11-2601-2018.

Smith, S. W. (1999). *The Scientist and Engineer's Guide to Digital Signal Processing*. 2nd ed. San Diago, CA, USA: California Technical Publishing.

Steiner, A. K. (1998). "High resolution sounding of key climate variables using the radio occultation technique". PhD thesis. University of Graz, Austria: IGAM.

Steiner, A. K., B. C. Lackner, F. Ladstädter, B. Scherllin-Pirscher, U. Foelsche, and G. Kirchengast (2011). "GPS radio occultation for climate monitoring and change detection". *Radio Sci.* 46, RS0D24. DOI: 10.1029/2010RS004614.

Syndergaard, S. (1999). *Retrieval analysis and methodologies in atmospheric limb sounding using the GNSS radio occultation technique (PhD thesis)*. DMI Sci Rep 99-6. Danish Meteorological Institute, Copenhagen, Denmark, p. 131.

– (2000). "On the ionosphere calibration in GPS radio occultation measurements". *Radio Sci.* 35.3, pp. 865–883.

Trenberth, K. E. and J. T. Fasullo (2013). "An apparent hiatus in global warming?" *Earth's Future* 1, pp. 19–32. DOI: 10.1002/2013EF000165.

Ware, R., M. Exner, D. Feng, M. Gorbunov, K. Hardy, B. Herman, Y.-H. Kuo, T. Meehan, W. Melbourne, C. Rocken, W. Schreiner, S. Sokolovskiy, F. Solheim, X. Zou, R. Anthes, S. Businger, and K. Trenberth (1996). "GPS sounding of the atmosphere from low Earth orbit: Preliminary results". *Bull. Amer. Meteor. Soc.* 77.1, pp. 19–40. DOI: 10.1175/1520-0477(1996)077<0019:GSOTAF>2.0.CO;2.

Yunck, T. P., C.-H. Liu, and R. Ware (2000). "A History of GPS Sounding". *Terr. Atmos. Ocean. Sci.* 11.1, pp. 1–20.